Pharmacological BACE1 inhibitor treatment during early progression of β-amyloid pathology maximizes therapeutic efficacy

Dissertation der Fakultät für Biologie
der Ludwig-Maximilians-Universität München

vorgelegt von
Finn Peters
geboren in Hamburg

München, 2017

Erklärung

Diese Dissertation wurde angefertigt unter der Leitung von Prof. Dr. Jochen Herms am Zentrum für Neuropathologie und Prionforschung der Ludwig-Maximilians-Universität und wurde vertreten von Prof. Dr. Rainer Uhl.

Eidesstattliche Versicherung

Ich versichere hiermit an Eides statt, dass meine Dissertation selbständig und ohne unerlaubte Hilfsmittel angefertigt worden ist. Die vorliegende Dissertation wurde weder ganz, noch teilweise bei einer anderen Prüfungskommission vorgelegt. Ich habe noch zu keinem früheren Zeitpunkt versucht, eine Dissertation einzureichen oder an einer Doktorprüfung teilzunehmen.

München, 21.03.2018

Finn Peters

Erstgutachter:	Prof. Dr. Rainer Uhl
Zweitgutachterin:	Prof. Dr. Anja Horn-Bochtler
Tag der Abgabe:	21.09.2017
Tag der mündlichen Prüfung:	14.02.2018

Table of Contents

Summary............ VI

Zusammenfassung VIII

1. Introduction............ 1

1.1 Alzheimer’s disease............ 1

1.1.1 Clinical symptoms and disease etiology 1

1.1.2 Neuropathological characteristica............ 2

1.1.3 Amyloid plaques 3

1.1.4 Tangles............ 4

1.1.5 Synaptic failure 5

1.1.6 Molecular biology............ 6

1.1.7 Proteolytic processing of APP 7

1.1.8 Amyloid cascade hypothesis 9

1.2 BACE1............ 11

1.2.1 Physiological function 12

1.2.2 Pathophysiology of BACE1 in AD............ 14

1.3 Therapeutic approaches 15

1.3.1 Pharmacological inhibition of BACE1 16

1.3.2 Mechanism-based side effects of BACE1 inhibition 18

1.4 Intravital microscopy 19

1.4.1 Fluorescence microscopy 19

1.4.2 *In vivo* two-photon microscopy 22

1.5 VGLUT1^{Venus} mouse model 24

2. Results 26

2.1 NB-360 reduces soluble Aβ levels 26

2.2 Concurrent imaging of β-amyloid deposition and synaptic pathology 27

2.3 BACE1 inhibition slows down β-amyloid deposition 28

2.4 BACE1 inhibition most effectively lowers formation of new plaques . 30

2.5 BACE1 inhibition reduces plaque growth irrespective of plaque size 32

2.6 Formation of new plaques is enhanced in vicinity to pre-existing plaques 34

2.7 BACE1 inhibition fails to prevent BACE1 accumulation in peri-plaque dystrophies 36

2.8 BACE1 inhibition mitigates progression of presynaptic pathology 37

2.9 BACE1 inhibition fails to prevent plaque-associated bouton loss 41

3. Discussion 42

3.1 Amyloid plaque kinetics 42

3.2 Synaptic Aβ pathology 43

3.3 BACE1 inhibitor dosage 43

3.4 Timing of pharmacological BACE1 inhibition 45

3.5 Conclusion 47

4. **Materials and Methods 50**

4.1 BACE1 inhibitor 50

4.2 Transgenic mice 50

4.3 Statistical Analysis 51

4.4 Plasma and brain homogenization and extraction 51

4.5 Aβ quantification 52

4.6 Cranial window implantation 52

4.7 Immunohistochemistry 55

4.8 Microscopy 55

4.8.1 Confocal microscopy 55

4.8.2 Chronic two-photon *in vivo* imaging 56

4.9 Data analysis of 3D microscopical data 57

4.10 Software 60

4.11 VGLUT1^{Venus} signal segmentation 60

5. **List of Figures 70**

6. **List of Tables 71**

7. **Reference 72**

8. **Abbreviations 96**

9. **Curriculum Vitae 98**

10. **List of Publications 102**

11. **Acknowledgements 104**

Summary

Alzheimer's disease (AD) is a chronic neurodegenerative disease of the central nervous system (CNS) characterized by progressive cognitive decline. AD is the most common cause of all dementia cases worldwide, and as a result of demographic aging the number of affected individuals grows at an alarming rate. The amyloid hypothesis of Alzheimer's disease (AD) emphasizes amyloid-β peptide (Aβ) as primary cause of the disease, with toxic effects on synapses leading to cognitive decline and memory impairments. Beta site amyloid precursor protein cleaving enzyme 1 (BACE1) as the rate-limiting enzyme of amyloidogenic processing of amyloid precursor protein (APP), is one of the prime drug targets for the treatment of AD. However, despite the development of potent and selective small-molecule BACE1 inhibitors, so far all human clinical trials have failed to rescue the cognitive decline in AD patients. Recent findings indicate that treatment has to be commenced before AD symptoms arise, since in symptomatic patients β-amyloid deposition has already reached a plateau. Moreover, several studies have described dose-dependent adverse effects in animal models. Therefore, it is a central requirement to develop a treatment strategy that is therapeutically effective and at the same time avoids excessive interference with physiological function of BACE1.

In this study, transgenic AD mice were treated at an early stage of β-amyloid pathology with the potent, blood brain barrier penetrating BACE1 inhibitor NB-360. Longitudinal *in vivo* two-photon imaging was performed to repeatedly monitor individual amyloid plaques, presynaptic boutons and axonal dystrophies in living mice. In APPPS1 mice pharmacological BACE1 inhibition fails to revert but significantly reduces the progressive amyloid deposition and mitigates presynaptic pathology. Notably, the data show that plaque seed formation, rather than the subsequent phase of gradual plaque growth, is most sensitive to BACE1 inhibition. These results imply, that preventive BACE1 inhibitor treatment is required to achieve therapeutic efficacy. For clinical therapy, to exploit the particular susceptibility of plaque formation to BACE1 inhibition, a dosage has to be empirically determined that effectively halts formation of new plaques rather than aiming at halting plaque growth. This strategy might optimally balance potential mechanism-based adverse effects and efficacious reduction of β-amyloid deposition.

Zusammenfassung

Morbus Alzheimer ist eine chronische neurodegenerative Erkrankung des zentralen Nervensystems und äußert sich in progressivem Verlust kognitiver Funktionen und Gedächtnisleistung. Die Erkrankung ist die weltweit häufigste Ursache für Demenz und aufgrund demografischer Alterung in den Industrieländern, nimmt die Zahl der Alzheimer Patienten stetig zu. Der Amyloid-Kaskaden-Hypothese zufolge, wird die Alzheimer Erkrankung durch pathologische Akkumulation und Aggregation des Aβ-Peptids (Aβ) ausgelöst. Aβ wird durch sequentielle enzymatische Spaltung des Amyloid-Vorläuferproteins APP produziert. Die β-Sekretase BACE1 initiiert den ersten Schritt dieses sogenannten amyloiden Prozessierungswegs und ist somit eines der aussichtsreichsten Wirkstoffziele zur Senkung des Aβ-Spiegels. Im Verlauf der letzten Jahre wurden sehr wirksame und zugleich selektive BACE1 Inhibitoren hergestellt, doch bislang sind klinische Studien daran gescheitert, den progressiven Gedächtnisverlust aufzuhalten. Neueste Erkenntnisse weisen darauf hin, dass die Behandlung bereits vor dem Auftreten der ersten Symptome begonnen werden muss, da in symptomatischen Patienten die Ablagerung von Aβ in den meisten Fällen bereits abgeschlossen ist. Hinzu kommt, dass in den letzten Jahren vermehrt negative Begleiterscheinungen der Behandlung mit BACE1 Inhibitoren in Mäusen bekannt geworden sind. Die entscheidende Herausforderung ist somit, eine Behandlungsstrategie zu entwickeln, welche einerseits die physiologische Funktion von BACE1 nicht zu stark beeinträchtigt, aber zugleich therapeutische Effizienz gewährleistet.

In der vorliegenden Studie wurden transgene Alzheimer Mäuse in einem frühen Stadium der β-amyloiden Pathologie mit dem potenten BACE1 Inhibitor NB-

360 behandelt. Mittels chronischer *in vivo* Mikroskopie konnten einzelne β-amyloide Plaques, präsynaptische Boutons und axonale Dystrophien in lebenden Mäusen verfolgt werden. Die Behandlung erbrachte zwar keinen Rückgang der Aβ Ablagerung, konnte jedoch deren Fortschreiten verringern, sowie die progressive axonale Pathologie abschwächen. Insbesondere zeigten unsere Daten, dass die BACE1 Inhibitor Behandlung einen wesentlich größeren Einfluss auf die Bildung neuer β-amyloider Plaques, als auf deren Wachstum hatte. Diese Ergebnisse weisen darauf hin, dass die Behandlung mit BACE1 Inhibitoren präventiv erfolgen muss. Für die klinische Anwendung könnte man sich die besondere Anfälligkeit der Neubildung von Plaques zu Nutze machen und über empirische Versuche einen Dosisbereich bestimmen, welcher ausreicht, die Neubildung von Plaques zu unterdrücken. Diese Strategie könnte zu einer ausgewogenen Behandlung führen, welche die progressive Aβ Ablagerung verzögert und gleichermaßen das Auftreten von Nebenwirkungen verhindert.

1. Introduction

1.1 Alzheimer’s disease

Alzheimer’s disease (AD) is a chronic neurodegenerative disease of the central nervous system (CNS) characterized by progressive cognitive decline (1). AD is the most common cause of all dementia cases (2) and the fourth leading cause of death after cardiovascular diseases, cancer and stroke. Currently, about 36 million people are affected worldwide, and as a result of demographic aging the number of affected individuals grows at an alarming rate (3,4). Due to the immense economical and emotional burden for patients, their family and the whole society, it will be one of the main challenges of this century to develop a therapy for AD. To date, more than 100 years after the first description of AD by Alois Alzheimer (5) no medication has proven to delay or halt the progression of the disease in human patients (6). Given the current lack of an effective treatment there is an urgent need in developing and evaluating disease-modifying therapies.

1.1.1 Clinical symptoms and disease etiology

AD etiology can be subdivided into three stages (7):

1. The early stage is characterized by impaired episodic memory – the capability to memorize autobiographical incidents. These deficits are probably due to progressive degeneration of the medial temporal lobe and the hippocampus (8).

2. In the advanced stage, memory function progressively declines and patients require support from other people. Notably, a rapid deterioration of episodical and semantic memory occurs. The latter includes the whole factual knowledge, like the meaning of words and their relationships in abstract form. In conjunction there is a change in the emotional state and personality of patients.
3. In the final stage, the cognitive capabilities are massively affected. Patients lose the capability to communicate and are physically strongly restricted. In many cases muscles stiffen and reflexes are lost. The most common cause of death is pneumonia, which results from problems to regulate the larynx that leads to swallowing of liquids and food.

The mean lifespan after onset of symptoms is seven years with strong inter-individual variations (9). However, the neurodegenerative process already starts long before the symptomatic stage. In biomarker studies, pathological changes could be detected already 25 years before symptom onset in patients with inherited AD (1).

1.1.2 Neuropathological characteristica

On the macroscopic level AD is characterized by progressive cortical atrophy, mainly affecting medial temporal lobe and associated brain regions. This process can be detected quite early during clinical pathological progression by applying magnetic resonance imaging (MRI) and manifests as dilation of the lateral ventricles (10). On the microscopic level AD is characterized by the presence of intracellular neurofibrillary tangles composed of hyperphosphorylated tau and extracellular cerebral amyloid plaques composed of the 40 – 42 amino acid β-amyloid peptide (11–13). These lesions are thought to be the primary cause for degeneration of synapses, neuron loss (14) and inflammation (15–17).

1.1.3 Amyloid plaques

The term “amyloid” plaques was coined by the German pathologist Rudolf Virchow and originates from the Latin translation of starch “*amylum*”. In 1854, Virchow was the first to detect plaques, by applying a iodine staining which labels starch (18). Even though it was shown later that amyloid plaques are composed mainly of protein (19,20), the term was maintained for historical reason.

Amyloid plaques arise from aggregation of β-amyloid (Aβ) that is produced from sequential proteolytic cleavage of the amyloid precursor protein (APP) (21,22). Plaques are typically of spheric morphology, with a diameter ranging up to 200 µm (23). Generally two types of amyloid plaques can be distinguished. Neuritic plaques have a compact core, composed of amyloid fibrils with characteristic parallel beta-pleated sheet conformation (24). Typically, neuritic plaques are surrounded by reactive astrocytes, activated microglia and dystrophic neurites (25,26). Diffuse plaques are amorphous structures and have no sharply defined outer boundary. These plaques lack a dense core, and instead, Aβ deposition is evenly distributed throughout the whole plaque (26). Unlike neuritic plaques, diffuse plaques are not detrimental to the neuropil. They are not considered as pathological criterium for diagnosis of AD (27), since they are frequently found in cognitively unaffected aged humans.

The β-amyloid pathology typically initiates locally at specific sites and then gradually disperses into adjoining unaffected regions (28–33). The sequential order in which distinct brain regions are affected can be divided in five phases

(33). (1) isocortex, (2) entorhinal cortex and hippocampus, (3) striatum and diencephalon, (4) different nuclei of the brainstem, (5) cerebellum. While neuritic plaques are clearly detrimental to surrounding neuropil, clinical studies have shown that cognitive decline in Alzheimer patients does not correlate well with plaque density nor the total plaque burden (34–36).

1.1.4 Tangles

Neurofibrillary tangles develop due to hyperphosphorylation, misdistribution and ultimate intracellular aggregation of the protein tau (37,38). Native tau has no rigid three-dimensional structure but can adopt different conformations (39). Even though it is difficult to experimentally retrace the conformational changes of tau during the process of aggregation, there is a general consensus about the initiation of tau aggregation. Tau has a lysine-rich subdomain that can bind and thereby stabilize the negatively charged β-tubulin subunit of microtubules (40–44). Due to this characteristic, tau plays an important role in formation of cell protrusions (45), cell polarity (11,46) and regulation of axonal transport (47). Under pathological conditions, the tau protein is hyperphosphorylated (48,49) and binding to microtubules is reduced (50). As a consequence, axonal transport is impaired (51) and tau is aberrantly distributed into the somatodendritic compartment (52,53). Enrichment of tau in the cytosol causes a conformational change into the Alz50-conformation (a specific epitope is detected by antibody Alz50) that promotes aggregation of tau (54). Subsequent postranslational modifications cause formation of paired helical filaments with β-sheet structure similar to amyloid fibrils (55). These intraneuronal aggregates are designated neurofibrillary tangles and even remain as extracellular deposits after the neuron has perished (52,56). Hyperphosphorylated tau aggregates also develop in dystrophic neurites in proximity to neuritic plaques and are called neuropil threads (57). Similar to sequential spreading of amyloid pathology, tau pathology also proceeds in temporally and spatially defined manner. The german neuropathologist Heiko Braak divided the progression of tau pathology in six stages (58): (stage I and II) trans-entorhinal and entorhinal cortex, (stage III and IV) hippocampus, (stage V and VI) isocortex. Since tau pathology more reliably correlates with cognitive decline than amyloid pathology (59), this classification by Braak is used as standard for clinical *post mortem* diagnosis for AD (58).

1.1.5 Synaptic failure

AD is characterized by progressive degeneration of synapses and neurons which manifests *post mortem* as strong atrophy of the brain (60,61). The most severely affected brain regions are the hippocampus and anatomically adjoining entorhinal, parietal and frontal cortex (62–64). Loss of presynaptic boutons was revealed by immunohistochemical studies in which a reduction of the presynaptic marker synaptophysin could be detected (65) and is most pronounced in close proximity to amyloid plaque deposits (66–74). In the AD brain, plaques are typically surrounded by swollen, dystrophic neurites (Figure 1) (25,75) and the majority of these peri-plaque dystrophies is presynaptic or axonal in origin (76–81). However, while dendrites rarely form dystrophies, dendritic spines are particularly reduced around plaques (82). Numerous studies have shown that synapses are a structural correlate for learning and memory (83–85). Indeed, the progressive cognitive decline correlates better with synapse loss than any other neuropathological phenotypes (86–88).

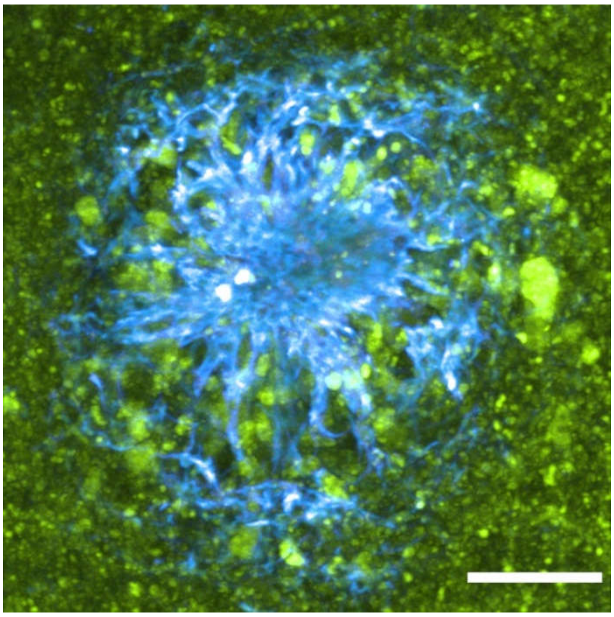

Figure 1. Aβ plaques are surrounded by axonal dystrophies. Microscopic image of a neuritic plaque from a 7 months old APPPS1xVGLUT1^{Venus} mouse (89,90). β-amyloid fibrils were stained with the dye Methoxy-X04 (cyan) and VGLUT1-positive boutons and axonal dystrophies are labelled due to endogenous expression of VGLUT1^{Venus} (green). Scale bar represents 10 µm.

1.1.6 Molecular biology

Due to methodological progress in molecular biology and genetics, knowledge on the pathological mechanisms underlying AD could be greatly expanded in the last three decades. In 1984, for the first time, the biochemists George Glenner and Philip Wong purified and sequenced the main constituent of amyloid plaques – the Aβ peptide (91). Only three years later, APP was identified as the precursor protein for Aβ generation (92). In the majority of patients, AD occurs idiopathically without identifiable cause, and only approximately 5% of cases suffer from inherited autosomal dominant type (93). Genetic studies have shown that some patients suffering from inherited AD have point mutations in the APP gene (94,95), which facilitate generation and aggregation of Aβ and thereby the formation of Aβ plaques (96,97). These observations lead to the ’Amyloid cascade hypothesis’, which states that excessive generation and subsequent deposition of Aβ in the brain is the causal initiator of a cascade of pathological events that ultimately lead to AD (98).

1.1.7 Proteolytic processing of APP

APP is a ubiquitously expressed transmembrane glycoprotein of type 1 (95). In mammals, APP together with homologous amyloid precursor like proteins 1 and 2 (APLP1 and APLP2) constitute the APP-protein family. However, only APP contains the Aβ domain necessary for Aβ plaque formation (99–101). In humans, the APP gene is localized on chromosome 21 (92,102–104) and is present in three different splice variants of 695, 751 or 770 amino acids. While APP751 and APP770 are expressed in almost all tissues, the variant APP695 is primarily expressed by neurons and localizes to synapses, dendrites and axons (105–109). After initial translation, APP traffics along the secretory pathway and matures by posttranslational modifications, including glycosylation, phosphorylation and sulfation (110). Subsequently, the APP holoprotein is proteolytically cleaved either along the amyloidogenic pathway or the non-amyloidogenic pathway (111).

In the non-amyloidogenic pathway, APP is initially cleaved by the metalloprotease ADAM10 (a disintegrin and metalloproteinase 10) within the Aβ domain between amino acids 16 and 17 (112). This cleavage generates the soluble ectodomain sAPPα (113,114) and the membrane bound carboxy-terminal fragment, αCTF (C83). αCTF is further processed by γ-secretase, (115) yielding the amyloid precursor protein intracellular domain (AICD) and a series of short hydrophobic peptides including Aβ17–40 and Aβ17–42, which are collectively called p3 fragments (116). Outside the CNS, APP is preferentially cleaved by α-secretase (117–119).

The amyloidogenic pathway (Figure 2), leads to the generation of Aβ and is initiated by proteolytic cleavage of APP by β-site APP cleaving enzyme 1 (BACE1). BACE1 processing of APP takes place in endosomes, since their acidic environment offers optimal conditions for enzymatic activity of BACE1 with an optimal pH of approximately 5 (120,121). Proteolytic cleavage of APP by BACE1 is the rate-limiting step in the cascade and results in the generation of a large soluble extracellular fragment commonly referred to soluble APP-β (sAPPβ) which is released into the extracellular space and a membrane anchored C-terminal fragment (CTFβ or C99). CTFβ is finally cleaved by the γ-secretase complex. γ-secretase is a multi-subunit aspartyl protease that consists of nicastrin, the stabilizing factor APH-1, presinilin-enhancer 2 and the catalytic subunits presinilin-1 and presinilin-2 (122). γ-secretase cleaves APP-CTFβ and many other type I transmembrane proteins within their transmembrane domains (123–125). CTFβ processing results in the generation of the membrane-anchored nuclear-localizing fragment AICD and Aβ-peptide which is released into the extracellular space (110,126).

The initial cleavage by γ-secretase takes place within the transmembrane domain close to the cytoplasmic border of the membrane and releases AICD. Subsequently, the remaining long Aβ fragment is successively cut producing Aβ-peptides ranging from 37 to 43 amino acids (127). Mutations in γ-secretase and APP destabilize the intermediary enzyme-substrate complex, leading to enhanced dissociation and thereby release of longer and more amyloidogenic peptides (128). Thus, sequential cleavage of APP by γ-secretase is a key determining feature that can increase an individual's risk of developing AD. The different Aβ species have different conformational characteristics (129). In comparison to the most abundant variant $A\beta_{40}$, the variant $A\beta_{42}$ has a tendency to aggregate into amyloid fibrils (130,131). Indeed, the main constituent of fibrillar Aβ in neuritic plaques is $A\beta_{42}$ (132). In contrast, shorter Aβ peptides including the predominant Aβ40 species, inhibit Aβ aggregation and deposition (133,134).

1.1.8 Amyloid cascade hypothesis

Accumulation of Aβ in protein aggregates triggers numerous pathophysiological changes that ultimately lead to cognitive dysfunction (135). The amyloid cascade hypothesis is the prevailing theory that describes the sequence of pathological changes that lead to AD (98,136,137) and was postulated in 1991 by John Hardy and Dennis Selkoe. The amyloid cascade hypothesis puts forward the accumulation of Aβ as initial and causative event. The aggregation of Aβ has detrimental effect on synapses and causes gliosis as well as hyperphosphorylation of tau, leading to generation of intracellular tau fibrils. Finally, the cascade results in progressive synaptic and neuronal degeneration and thereby culminates in dementia with characteristic plaque and tangle pathology (138).

The observation that Aβ is the main constituent of β-amyloid plaques and cerebral angiopathies (91,139) does not causally link Aβ pathology to AD. However, genetic studies provide strong indications for a clear correlation. In Down syndrome patients the chromosome 21, which contains the APP gene, is present three times, resulting from a chromosome aberration. In these patients, Aβ production and thereby β-amyloid deposition are enhanced. Almost all cases develop clinical symptoms of AD until 55 years of age (136,140–142). Up to now, all mutations linked with the inherited form of AD are related to the cellular machinery implicated in Aβ production (143) and either occur in the APP-gene (95,144) or in catalytical subunits of PS1 and PS2 of the γ-secretase complex (145). In addition, mutations within the β-cleavage site of APP that reduce the production of Aβ confer protection against cognitive decline in the elderly (146) and knockout of the *Bace1* gene abrogates amyloid pathology in AD mice (147). The only genetic risk factor for AD identified so far is Apolipoprotein E4 (ApoE4). The protein is secreted by glia and is essentially involved in binding and clearance of Aβ from the CNS (148). Recently, it was shown that ApoE4 exacerbates neuronal Aβ production via a signal transduction pathway whereby ApoE activates a non-canonical mitogen-activated protein (MAP) kinase cascade that enhances APP transcription and thereby Aβ production (149).

The amyloid cascade hypothesis is based on the assumption that the occurrence of tau pathology is a consequence of β-amyloid deposition. This notion is supported by results from patients with frontotemporal dementia, a neurodegenerative disease characterized by massive tau pathology despite lack of β-amyloid pathology (150,151). This indicates that pathological accumulation of tau *per se* is neurotoxic but cannot initiate Aβ pathology (136,152). Conversely, in tau overexpressing mouse models, tau pathology is aggravated by coexpression of mutated human APP (153). Further evidence on the interplay between Aβ and tau pathology was obtained from experiments in transgenic mouse models and cell culture. Genetic knockout of tau ameliorates Aβ induced learning deficits, reduced long-term potentiation (LTP) and nerve cell loss (154–156). The molecular mechanisms of tau induced synaptotoxicity of Aβ are still under investigation. Aβ aggregation triggers hyperphosphorylation of tau via the CAMKK2-AMPK signaling cascade (calcium/calmodulin-dependent protein kinase kinase 2, 5´ adenosine monophosphat-activated protein kinase) and thereby causes mislocalization of tau to the dendritic compartment (157). Aberrant localization of tau in dendritic spines has been claimed to lead via kinase Fyn to hyperphosphorylation of NMDA-receptors (N-Methyl-D-Aspartat). Subsequently, excessive release of neurotransmitter glutamate results in excitotoxicity and degeneration of synaptic terminals (158,159).

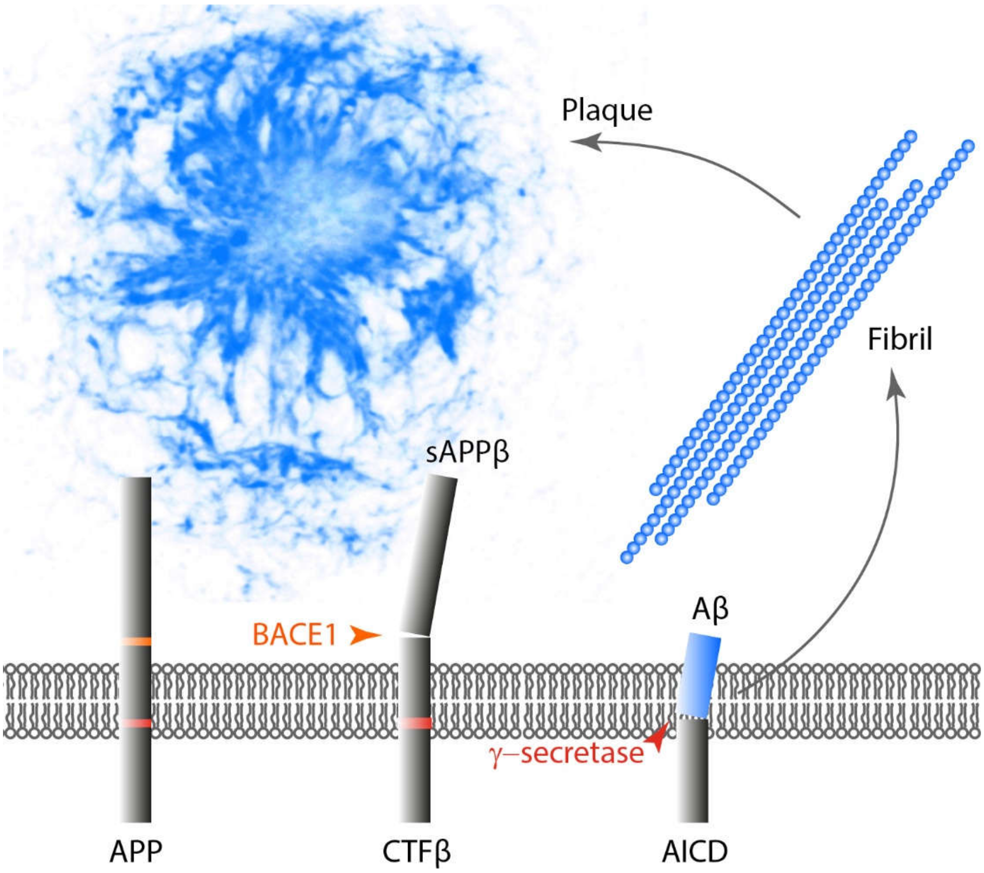

Figure 2. Illustration of the amyloid cascade hypothesis. Proteolytic cleavage by BACE1 initiates amyloidogenic processing of APP and generates CTFβ and sAPPβ which is released into the extracellular space. CTFβ is further processed by γ-secretase, resulting in the formation of Aβ and AICD. Aβ and in particular the Aβ42 variant, is prone to aggregation, which results in the formation of Aβ fibrils and ultimately plaques.

1.2 BACE1

BACE1 is an aspartate endopeptidase and catalyzes the initial and rate-limiting step of amyloidogenic processing of APP to form the toxic β-amyloid peptide (Aβ). Therefore, BACE1 is one of the primary therapeutic targets to lower the cerebral Aβ level in AD patients. The central role of BACE1 in processing of APP was discovered for the first time in 1999 by five different research groups simultaneously (160–164). In these studies, a second aspartate-endopeptidase (BACE2) was identified with 64% amino acid sequence homology. Both endopeptidases can be detected in diverse tissues, but BACE1 is mainly produced in the brain (162,164,165). Also, BACE1 but not BACE2 is the relevant β-secretase *in vivo* for the processing of APP (166). The catalytic domain of BACE1 enzyme has two characteristic (DT/SGS/T) motifs similar to the pepsin family of aspartate proteases (167). However, in contrast to this family of proteases, BACE1 is a type I transmembrane protein. The C-terminus reaches into the cytosol and the N-terminus which contains the active center is located on the luminal side.

1.2.1 Physiological function

Within the plasma membrane, BACE1 localizes to lipid rafts (168) and specific lipids in these cholesterol-rich microdomains can promote activity of BACE1 (168). Intracellularly BACE1 localizes to diverse subcellular organelles. BACE1 is initially synthesized as an inactive pro-enzyme and is converted into the active form in the trans-Golgi network (169,170). The transport of BACE1 in the endosomal-lysosomal system or incorporation into lipid rafts is regulated through phosphorylation and palmitoylation (171,172). The enzyme has maximal catalytical activity at low pH (pH 4.5 – 6.0) in the acidic lumen of the trans-Golgi network and endosomes (173). Previous studies have shown that BACE1 and APP interact in endosomes (173) and the application of compounds that increase endosomal pH effectively inhibit Aβ production (174). Thus, the majority of APP processing takes place in endosomes. The past decade has revealed numerous substrates of BACE1, including 33 neuronal proteins. Thus, BACE1 is one of the most important sheddases in the nervous system (175). The substrates can be divided according to their physiological function into two different categories. The first group are proteins with a synaptic function. The other group are proteins that interact with the extracellular matrix of astrocytes and oligodendrocytes and thereby regulate growth of axons (167).

BACE1$^{-/-}$ mice are viable and fertile. However, due to the important role of BACE1 in synaptic function, *Bace1* gene knockout leads to diverse neurological phenotypes, including impaired learning and memory, epileptic seizures, locomotor hyperactivity and schizophrenia-associated behavioral changes (176–178). Pharmacological inhibition of BACE1 decreases spine turnover and total spine density, which indicates a critical role of BACE1 in structural and functional synaptic plasticity in mice (179,180).

The complex phenotypes of *Bace1*$^{-/-}$ mice are at least partly mediated by the BACE1 substrates Sez-6 (seizure-related gene 6) (181) and the Nav β-subunit (182). Sez-6 is a type 1 membrane protein that localizes to dendrites and is predominantly cleaved by BACE1. Sez-6 knockout mice have reduced spine density and impaired excitability of pyramidal neurons in cortical layer V (181). The structural and functional synaptic plasticity is primarily mediated via BACE1 mediated cleavage of Sez-6 (180).

Epileptic seizures in *Bace1*$^{-/-}$ mice are probably a consequence of reduced processing of the Nav β-subunit, that controls expression and surface localization of sodium channels (183,184). As a result, the density of voltage gated sodium channels is increased in *Bace1*$^{-/-}$ mice which causes increased neuronal excitability and thus increased susceptibility to epileptic seizures.

Among the BACE1 substrates that are involved in regulation of axonal growth, especially the cell adhesion protein CHL1 (close homolog of L1) is well characterized. CHL1 is a type 1 membrane protein that is sequentially cleaved by ADAM8 (A Disintegrin and metalloproteinase domain-containing protein 8) (185) and BACE1 (175). The soluble ectodomain can interact with Neurophilin-

1 und Semaphorin 3A, and thereby influences axonal targeting (186,187). As a result, *Chl1* knockout mice as well as *Bace1*$^{-/-}$ mice have impaired axonal connectivity of hippocampal mossy fibers within the infrapyramidal bundle. Additionally, the total length of the infrapyramidal bundle is reduced by approximately 30% in *Bace1*$^{-/-}$ mice (188). Since the length of the infrapyramidal bundle is correlated with memory performance in mice (189), this might at least in part account for the cognitive deficits in Bace1$^{-/-}$ mice.

Also in the peripheral nervous system, numerous functions of BACE1 have been described. Genetic ablation of the *Bace1* gene causes hypomyelination of nerves in mice (190). This effect is due to reduced proteolytic processing of the BACE1 substrate NRG1 (Neuregulin 1) isoform type III (190), which plays an important role in early postnatal myelination (191). NRG1 type I is also processed by BACE1. Since NRG1 type I has an important function in the formation of muscle spindles, a reduction of NRG1 type I processing causes reduced formation of muscle spindles in *Bace1*$^{-/-}$ mice (192). This effect could be reproduced by pharmacological inhibition of BACE1 in adult wild type mice (192). BACE1 mediated processing of NRG1 type I is not only required for the formation of muscle spindles during their development but also for their maintenance in adulthood. Future clinical trials will reveal whether pharmacological BACE1 inhibition causes a similar phenotype in humans.

1.2.2 Pathophysiology of BACE1 in AD

In the AD brain, amyloid plaques are surrounded by swollen presynaptic dystrophic neurites that are enriched with BACE1 (78,81,193,194). This excessive accumulation of BACE1 might be the reason for the two-fold increased BACE1 levels in brains of AD mice and AD patients compared to healthy individuals (195–200). One possible mechanism for this aberrant localization has been brought up recently by Gowrishankar et al. (77).

According to the hypothesis of this work, Aβ causes microtubule disruption and motor protein mis-localization by an as yet undefined cascade (76,77). Since BACE1 degradation occurs via the lysosomal pathways (201,202) and therefore depends on retrograde transport to the cell body, a local disruption of microtubules and motor protein mis-localization would impair lysosomal maturation. Consequently, BACE1 and other proteins accumulate in peri-plaque dystrophic neurites (76,77). Excessive enrichment of BACE1 in the proximity of plaques might cause a vicious pathogenic cycle (203). According to this hypothesis BACE1 increases local Aβ production at plaques and thereby accelerates amyloid deposition even more.

1.3 Therapeutic approaches

The existing AD drugs are just symptomatic therapies, such as the acetylcholinesterase inhibitors and the N-methyl D-aspartate receptor antagonist memantine. Both cannot stop the progressive neurodegeneration but rather delay progression by about 3 months. Alternatively, epidemiological studies and experiments in transgenic mice have shown that ‘lifestyle’ interventions – such as a healthy diet and physical or cognitive exercise – can reduce the incidence of dementia and dementia-related biochemical changes in the brain (204,205). However, efficacy of current medication is limited to the very early stages of the disease and only provides symptomatic relief.

The amyloid cascade hypothesis has led to the identification of therapeutic targets for treatment or prevention of AD and provides the rationale for the current main focus of the pharmaceutical industry to target Aβ aggregates. The three proteases that are involved in APP processing, namely α-secretase, BACE1 and γ-secretase, are of particular interest, since they can be targeted by small molecule compounds *in vitro* and *in vivo*.

Enhancing processing of APP by α-secretases is protective in the context of AD because the enzymes cleave within the Aβ sequence and thereby prevent the production of Aβ (206,207). However, ablation of many genes that code for α-secretase have turned out to be lethal (206–208). For example, deletion of ADAM10 is lethal in mid-gestation (208). So far, drugs that directly activate α-secretase have not been developed, and thus it is unclear if this strategy is free of adverse side effects and if it might attenuate AD symptoms.

γ-secretase inhibitors decrease Aβ production in human and mouse brains, and chronic administration decreases Aβ deposition in APP mouse models (209–212). However, since γ-secretase cleaves numerous transmembrane proteins, mechanism-based adverse effects pose a major obstacle for the successful clinical development of these compounds. For example, γ-secretase processing of Notch1 is crucial for Notch signaling (213) and deletion of PS1 is embryonically lethal in mice (214,215). γ-secretase modulators alter the profile of Aβ peptides produced by γ-secretase activity *in vitro* and *in vivo* (216,217). Such compounds can selectively reduce the levels of Aβ42 and can be safely administered in the long term (218). However, so far clinical attempts failed to rescue the cognitive decline.

1.3.1 Pharmacological inhibition of BACE1

There are several indications that BACE1 inhibition therapy should be beneficial for the treatment of AD. Discovery of the protective APP point mutation Ala673Thr indicates that life-long reduction of Aβ production by 40% might suffice to prevent AD (219). Additionally, genetic ablation of *Bace1* in transgenic APP overexpressing mice, blocks the production of Aβ and thereby β-amyloid deposition as well as plaque-associated pathology (147,220,221). Initial studies of *Bace1*$^{-/-}$ mice did not detect developmental or behavioral impairments, nor histological alterations (222), which raised the hope that inhibition of BACE1 might be free of adverse effects. Over the course of several years various inhibitors were developed. Initial peptide inhibitors that modelled the active center of BACE1, effectively and specifically inhibited BACE1 activity *in vitro*. However, these compounds were too large to pass the blood brain barrier (223). The development of small-molecule non-peptide inhibitors solved this problem (224) and consequently, several BACE1 inhibitors have entered human clinical trials (225–228). Small-molecule BACE1 inhibitors effectively lower brain Aβ levels (225,229,230) and can reduce plaque burden in mice (231–234). However, two clinical trials have failed so far due to unspecific side effects (6) or lack of efficacy, as documented by the recent failure of the phase 2/3b EPOCH trial of verubecestat (ClinicalTrials.gov identifier NCT01739348). The lack of success may relate to the timing of the intervention. Current trials were performed with mild to moderate dementia cases (235). However, PET (positron emission tomography) studies in combination with amyloid binding radioactive marker Pittsburgh Compound B have shown that in humans, β-amyloid deposition already commences decades before the manifestation of clinical symptoms (1,236–238). Thus, at a stage when amyloid deposition has already reached an asymptote of accumulation, Aβ lowering drugs might have no more impact. Also it is unclear whether at such a late stage Aβ-induced pathology is the main mediator of toxicity or whether other toxic mediators would even persist in the absence of amyloid pathology. The current consensus is that at late stage progressive pathology is already so much advanced that it can not be stopped anymore (239). For future AD therapy with Aβ lowering drugs it is therefore of utmost importance to start therapy at an early stage of β-amyloid pathology (240–242).

1.3.2 Mechanism-based side effects of BACE1 inhibition

Besides optimizing the timing of BACE1 inhibitor treatment, one of the most important prerequisites for successful therapeutic application will be to determine the appropriate BACE1 inhibitor dosage. *Bace1*$^{-/-}$ mice display complex neurological phenotypes, including growth retardation (243), retinal pathology (244), memory deficits (220,221,245), hypomyelination (246,247), seizures (248–250), axon guidance defects (251–253), and schizophrenia-like behaviors (254). The variety of phenotypic alterations in *Bace1*$^{-/-}$ mice indicates that therapeutic BACE1 inhibitor treatment might cause health issues. However, it is unclear whether adverse effects observed in *Bace1*$^{-/-}$ mice also translate to humans. *Bace1*$^{-/-}$ mice completely lack BACE1 enzymatic activity at any developmental stage. Thus, some of the adverse effects might be due to a critical role of BACE1 in development and might not be relevant in adulthood. For example, myelination is an early process that has already completed in adulthood (255) and thus, characteristic hypomyelination in *Bace1*$^{-/-}$ mice clearly is a developmental phenotype. Such reports urge caution against overinterpreting the relevance of *Bace1* deletion data to the outcome of pharmacological inhibition of BACE1. In contrary, formation of muscle spindles is a continuous process that occurs over the whole life span and is affected not only in *Bace1*$^{-/-}$ mice, but also in BACE1 inhibitor treated adult wildtype mice (192). Therefore, this phenotype might also occur in Alzheimer patients (167). Additionally, pharmacological BACE1 inhibition in adult wildtype mice induces rapid and prolonged decrease in spine turnover and spine density after a treatment period of 14 days (179,180). In light of these mechanism-based adverse effects of BACE1 inhibition in mice, it will be critical to minimize BACE1 inhibitor dosage as much as possible. However, there are clear indications that partial inhibition of BACE1 can be therapeutically effective, if the treatment is initiated early enough. Life-long reduction of Aβ levels by 40% results in 5- to 7-fold reduced risk of developing AD (146) and a slight reduction of Aβ levels by 12% in *Bace1*$^{+/-}$ mice reduces total Aβ deposition by 50% in aged mice (256). Thus, moderate inhibition of BACE1 might suffice to effectively reduce Aβ levels and still avoid excessive mechanism-based adverse effects (167). In conclusion, the most challenging question for the clinical development of BACE1 inhibitors concerns the stage of Alzheimer's disease at which to treat for optimum efficacy and the appropriate dosage that balances clinical safety and therapeutic efficacy.

1.4 Intravital microscopy

Two-photon intravital microscopy is an imaging technique that enables to visualize various biological processes in living organisms. The technique proved especially useful for the investigation of neurobiological questions. For example, the technique enabled for the first time to image the structural and functional plasticity of neuronal networks *in vivo* and to correlate it with environmental stimuli. The technical development of intravital microscopy was a result of innovative technical milestones in diverse scientific sectors, such as physics, genetics and biochemistry.

1.4.1 Fluorescence microscopy

Brain tissue consists of small and tightly packed biological structures. By applying serial section scanning microscopy, Kasthuri et al. showed that a 1,500 μm^3 cubic volume of brain tissue (equivalent to a cube of 11.4 µm edge length) contains 193 dendrites, 1407 axons and 1700 synapses (257). Initially, this dense allocation of individual substructures in brain tissue hampered investigating the intricate morphology of neurons. The initial breakthrough was the development of silver staining by Ramón Cajal, because it allowed to selectively visualize separate neurons and their synapses. However, such sparse histochemical labelling requires chemical processing of the specimen and is thereby limited to *post mortem* tissue. The discovery of fluorescence was a key finding that allowed direct visualization of biological structures in living tissue. In 1908, August Köhler was the first to describe a new microscopical method „luminescence microscopy“ (258) which is nowadays known as fluorescence microscopy. Köhler showed that some stainings – so called fluorophores – emit light when excited at a certain wavelength. The spectrum of emitted light is shifted to longer wavelengths as compared to the excitation spectrum. This phenomenon was coined Stokes-shift after the discoverer George Stokes (259) and is illustrated in Figure 3 by a Jabłoński-diagram (260,261).

Upon absorption of a photon of sufficient energy by a chromophore an electron is excited from the lowest-energy ground state to an excited higher-energy state. However, this excited state is energetically unstable causing the electron to return to the initial ground state within 1 to 10 nanoseconds. Spontaneous transition from the first excited state (S1) back to the ground state (S0) with simultaneous emission of a photon is called fluorescence. During this process energy is also released by vibrational relaxation and therefore the emitted photon has lower energy and therefore longer wavelength as compared to the excitation light (Figure 3). Fluorescence microscopy has enabled to directly visualize certain organic compounds due to their intrinsic fluorescence. For example, the autofluorescence of coenzyme nicotinamide adenine dinucleotide (NADH) and nicotinamide adenine dinucleotide phosphate (NADPH) allows to determine the redox state of a cell, since the oxidized versions NAD^+ and $NADP^+$ show reduced fluorescence (262). Additionally, endogenous fluorescence of mitochondrial flavoproteins allows to measure activity of neurons, since flavoproteins have green autofluorescence under aerobic oxidation (263).

While the discovery of fluorescence allowed visualization of biological structures in the living brain it was the development of genetically encoded fluorophores that immensely increased opportunities to investigate biological processes. In 1962, the biochemist Osamu Shimomura and his colleagues isolated the chemiluminescent protein GFP (green fluorescent protein) from the jellyfish *Aequorea victoria* (264). 30 years later the gene for GFP could successfully be cloned and expressed in different species (265–267). For the discovery and development of GFP Osamu Shimomura, Martin Chalfie and Roger Y. Tsien won the nobel prize for chemistry 2008. GFP expression can be applied to investigate localization, interaction and dynamics of diverse proteins. Expression under a specific promoter allows to observe gene activity in individual cells (268). For the *in vivo* analysis of neuronal structures, transgenic mice have been generated that express GFP or spectral variants under control of specific promoters. For example, in the GFP-M mouse, enhanced GFP (eGFP) is expressed by the pan-neuronal promoter Thy-1.2 (269). As a result of random insertion of the transgene in the genome, only specific neuronal groups express the fluorophore. This results in a sparse labelling of individual neurons, similar to a Golgi staining. Another example is the VGLUT1$^{\text{Venus}}$ model which expresses the Vesicular GLUtamate Transporter 1 (VGLUT1), fused to the fluorescent protein Venus under VGLUT1 endogenous promoter (90). This model enables to visualize presynaptic boutons and is described in detail in the following subsection.

Conventional fluorescence microscopy is only partially suited for intravital microscopy of neurons. The high lipid fraction of axonal myelin causes strong scattering of excitation and emission light (270), which limits optical access only to the superficial cortical layer. This shortcoming was substantially improved by the introduction of two-photon microscopy in 1990 by Winfried Denk (271).

1.4.2 *In vivo* two-photon microscopy

The nonlinear optic effect of two-photon (2P) excitation was already postulated in 1931 by Maria Göppert-Mayer (272). Two-photon excitation occurs when two photons coincide quasi-simultaneously on a fluorescent molecule. These photons must have approximately twice the wavelength that is necessary for excitation by a single photon. The probability for non-linear excitation is very low, but increases proportional with the square of light intensity. Therefore, to obtain measurable 2P excitation high photon density in the range of several kW/cm^2 has to be generated. Such high peak power can be obtained with pulsed lasers (**l**ight **a**mplification by **s**timulated **e**mission of **r**adiation). For example titanium-sapphire (Ti:Sa) lasers can generate very short (<100 femtoseconds), intensive light pulses of defined wavelength at a rate of 80 MHz. Since the light is not emitted continuously but in the form of extremely short pulses, a peak power of several 100 kW can be achieved at a low mean power of 2.5 W. This ensures high density of photons without damaging the specimen.

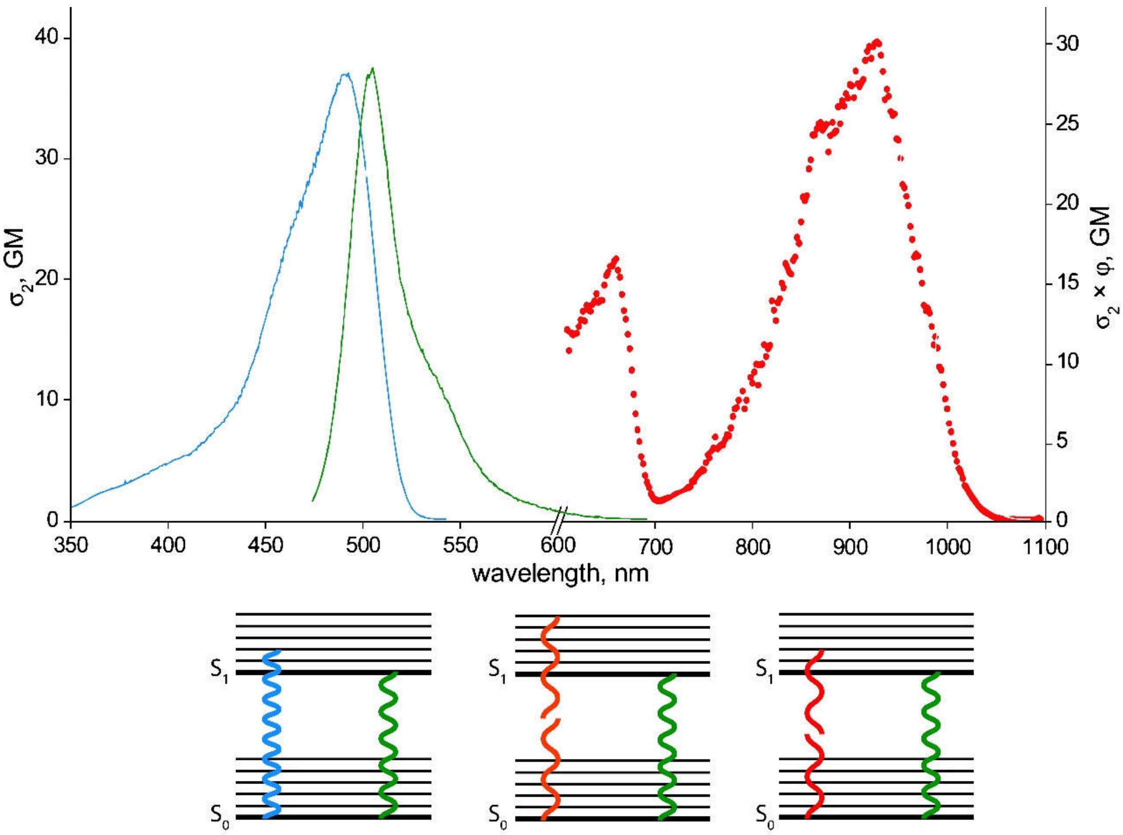

Figure 3. Simplified Jabłoński-diagram for illustration of one-photon versus two-photon exciation for the fluorophore eGFP. For one-photon excitation a single photon (cyan wave) carries sufficient energy to excite the fluorophore to the excited higher-energy state S_1. Upon transition back to the initial ground state S_0, a photon of slightly lower energy as compared to the excitation photon is emitted (green wave). For two-photon excitation, two photons each confer half the energy required for one-photon excitation. This nonlinear optic effect requires the photons to coincide quasi-simultaneously on the fluorophore and requires high photon densities. Since S1 consists of different energy substates, excitation can occur within a range of wavelengths. While the one-photon excitation spectrum usually has one maximum, the two-photon spectrum normally has two maxima. Adapted from Drobizhev et al. (273).

2P microscopy has crucial advantages over conventional laser scanning microscopy. Due to the non-linear optical effect, fluorescence excitation is restricted to the focal spot which provides intrinsic optical sectioning within the axial dimension. In contrast to one-photon excitation – in which the whole light cone is excited – 2P excitation generates no out-of focus excitation. This minimizes photobleaching and phototoxicity. In addition, for 2P excitation photons of longer wavelength and thereby lower energy can be used which is scattered and absorbed less in neuronal tissue and enables deeper penetration up to 800 µm into the brain (271,274).

To gain optical access to the brain of mice a cranial window has to be implanted onto the skull. Different approaches have been described, the thinned skull (275) and the open skull (276) preparation. For the thinned skull method the skull is carefully thinned with a dental drill until only an approximately 20 µm thin transparent layer of skull is left. Such an optical window is limited in size to 0.1 to 0.3 mm^2 and the remaining thin layer of skull causes considerable photon aberration limiting the penetration depth. For chronic imaging over long time periods the preparation has to be repeated due to regrowth of bone. In most cases this is only possible for three to four times, since the skull loses transparency over time.

For the open skull preparation, a circular piece of the skull with a diameter from 3 to 5 mm is completely removed and replaced by a glass window. This preparation allows chronic imaging of brain tissue up to a depth of 800 µm for time periods of up to more than one year (277). This approach is considerably more invasive than the thinned skull procedure and causes activation of microglia and astrocytosis. However, the immune reactions normally subside within 3 to 4 weeks after surgery (276).

1.5 VGLUT1^{Venus} mouse model

VGLUT1^{Venus} mice express the Vesicular GLUtamate Transporter 1, fused to the fluorescent protein Venus under VGLUT1 endogenous promoter (90). VGLUT1 is a transmembrane protein localized in presynaptic vesicles and has the function to uptake glutamate into these vesicles. An average synaptic vesicle (Figure 4a) contains approximately 9 copies of VGLUT1 (278). Hence, in VGLUT1^{Venus} mice all glutamatergic, VGLUT1 positive boutons are fluorescently labeled (Figure 4b). Since the fusion gene replaces VGLUT1 through homologous recombination at the endogenous *vglut1* locus the intensity of emitted fluorescence reflects the amount of VGLUT1 vesicles. VGLUT1^{Venus} mice are viable and fertile. The fusion protein was shown to be fully functional in these mice, since it retains the ability to interact specifically with EndophilinA1 and shows the same glutamate uptake efficacy as WT VGLUT1 (278).

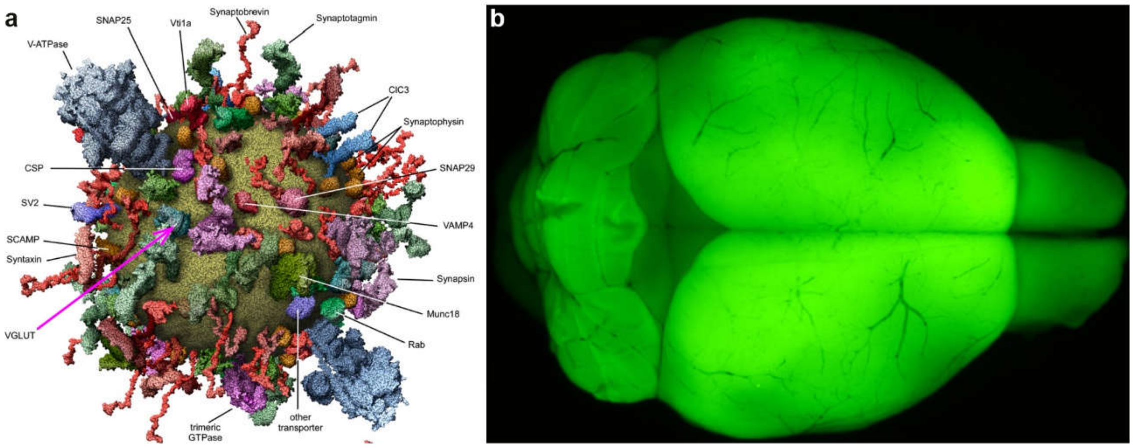
a
SNAP25
Vti1a
Synaptobrevin
Synaptotagmin
V-ATPase
ClC3
Synaptophysin
CSP
SNAP29
SV2
VAMP4
SCAMP
Syntaxin
Synapsin
Munc18
VGLUT
Rab
trimeric GTPase
other transporter
b

Figure 4. Composition of an average vesicle synaptic vesicle. (**a**) An average synaptic vesicle contains approximately 9 copies per vesicle. The magenta arrow highlights VGLUT. Adapted from Takamori et al. (278). (**b**) Overview of VGLUT1^{Venus} fluorescence in PFA-fixed mouse brain. Adapted from Herzog et al. (90).

2. Results

2.1 NB-360 reduces soluble Aβ levels

To assess the efficacy of the BACE1 inhibitor NB-360 (233), APPPS1 mice (89) were fed with food pellet containing NB-360 or vehicle, starting at an age of six weeks. After two weeks of chronic treatment, soluble Aβ40 and Aβ42 levels were determined via ELISA. The age was chosen to obtain brain tissue before initiation of β-amyloid deposition, in order to exclude contamination by deposited fibrillar Aβ. NB-360 treatment reduced soluble Aβ40 and Aβ42 levels in the forebrain by 80% and plasma Aβ40 levels by 70% (Figure 5).

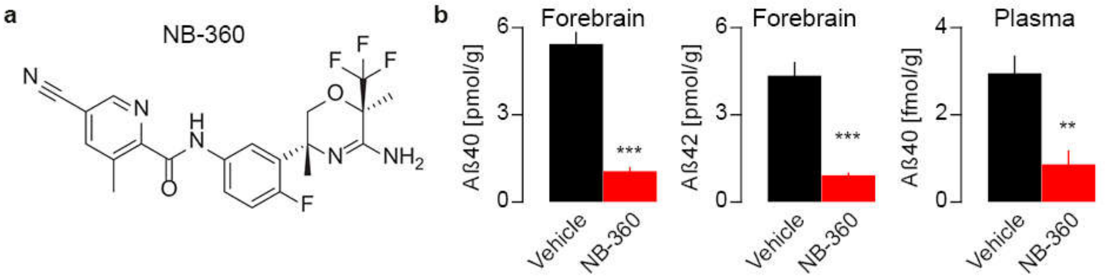

Figure 5. BACE1 inhibition significantly reduces Aβ40 and Aβ42 levels. (**a**) Molecular structure of NB-360. (**b**) In six weeks old mice treated for 14 days *ad libitum* with food pellets containing NB-360 (0.25 g/kg) the levels of Aβ40 and Aβ42 are significantly reduced by 80% in forebrain and by 70% in plasma. Data presented as mean ± SEM with $^{**}p < 0.01$; $^{***}p < 0.001$; $n = 6$; (t-test).

2.2 Concurrent imaging of β-amyloid deposition and synaptic pathology

The question was addressed whether pharmacological interference with Aβ generation beneficially influences amyloid plaque burden and plaque-associated synaptic pathology. For this, chronic *in vivo* two-photon imaging of Methoxy-X04 stained amyloid plaques and glutamatergic boutons was performed in APPPS1xVGLUT1^{Venus} mice (Figure 6a). The somatosensory cortex was imaged weekly from 3 to 7 months of age and NB-360 or vehicle treatment was initiated at 4 months of age (Figure 6b). Individual plaques were tracked in consecutive imaging time points (Figure 6c).

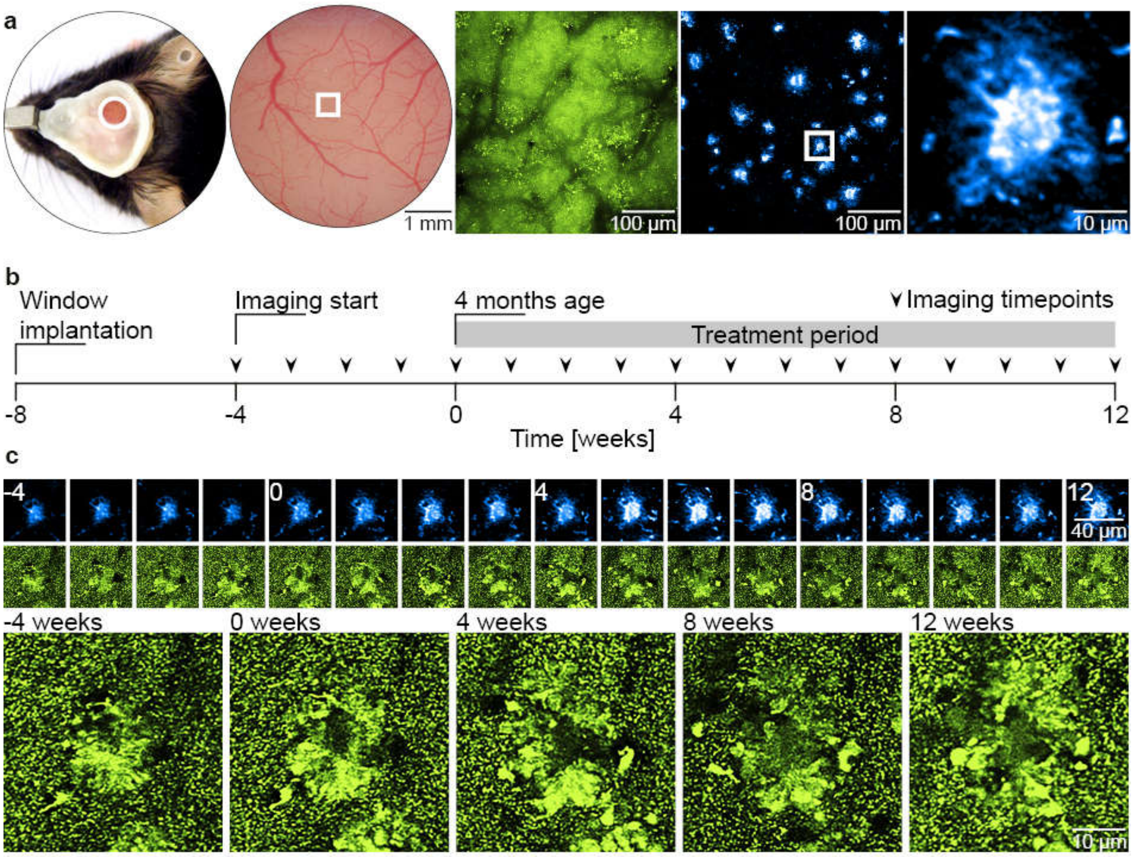
a
1 mm
100 µm
100 µm
10 µm
b
Window implantation
Imaging start
4 months age
Imaging timepoints
Treatment period
-8
-4
0
4
8
12
Time [weeks]
c
-4
0
4
8
12
40 µm
-4 weeks
0 weeks
4 weeks
8 weeks
12 weeks
10 µm

Figure 6. *In vivo* two-photon imaging of plaques and associated synaptic pathology. (**a**) APPPS1xVGLUT1^{Venus} mice were implanted a cranial window to perform chronic *in vivo* two-photon imaging of somatosensory cortex. (**b**) Mice were reimaged repetitively in weekly intervals starting from 3 months of age for up to 16 weeks. After 4 time points of baseline imaging mice were administered BACE1 inhibitor or vehicle food pellet. (**c**) In the same region of interest Methoxy-X04 stained β-amyloid plaques and VGLUT1^{Venus} positive glutamatergic boutons were repetitively imaged.

2.3 BACE1 inhibition slows down β-amyloid deposition

In each mouse approximately 80 plaques were analysed and time point of first appearance and changes in size were quantified over time (Figure 7a). As a result of spherical aberration, plaques seem artificially elongated in axial direction. Thus, for determination of plaque size the largest extension in XY of each individual plaque was determined and – assuming a spherical shape of plaques (279) – the radius was calculated as $radius = \sqrt{area/\pi}$ (Figure 7b, c). Subsequently, growth of individual plaques was quantified as incremental increase of plaque radii per week (Figure 7d).

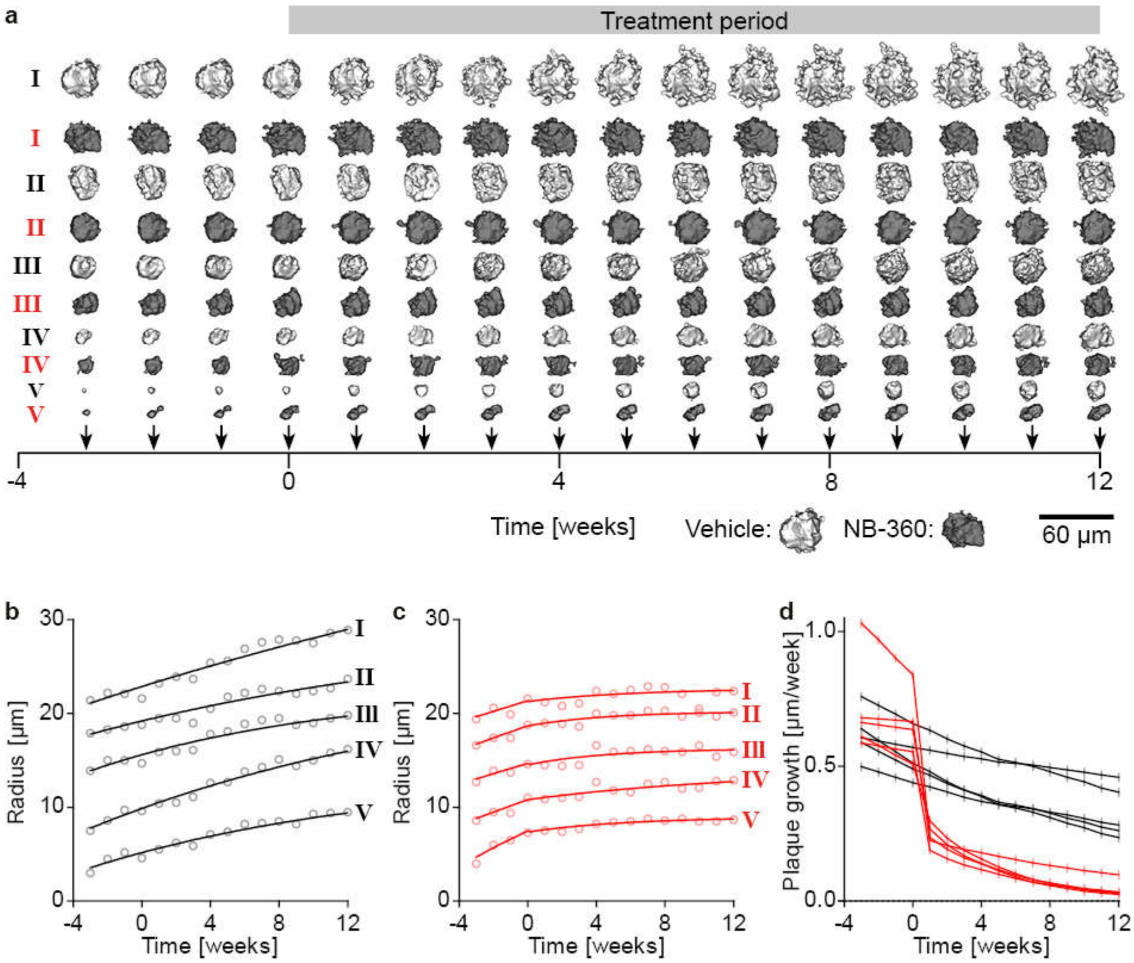

Figure 7. Procedure for determination of plaque growth kinetics. (**a**) Time series of representative 3D rendered plaques of the vehicle (light gray) and NB-360 (dark gray) treated cohorts. Scale bar represents 60 µm. (**b**,**c**) For the same plaques as in (a) the radii at consecutive time points were calculated, fitted with monophasic association functions, and (**d**) growth rates at each time point were derived.

The sum of the volume of all plaques per time point was determined and divided by the total imaged brain volume to obtain the overall β-amyloid burden. In vehicle treated mice the β-amyloid burden increases linearly over the total imaging period at a rate of 0.076% ± 0.015% brain volume occupied by plaques every week (Figure 8a). Pharmacological BACE1 inhibition significantly slowed down β-amyloid deposition by 49%.

2.4 BACE1 inhibition most effectively lowers formation of new plaques

β-amyloid deposition can occur either by adhesion of soluble Aβ to the surface of already existing plaques, resulting in plaque growth or via spontaneous aggregation to form new plaques. These two processes follow different kinetics (277) and have distinct biophysical properties (277,280–282). Therefore, it was important to assess whether BACE1 inhibition affects plaque formation and growth to a different degree.

Over the imaging period, plaque growth slightly decreased with time in both cohorts (Figure 8b). Thus, the imaging period relates to the transition phase of β-amyloid deposition (277), when the plaque surface available for further Aβ accretion, starts to exceed the available levels of soluble Aβ (277,283–285). Apart from the age-dependent decline, BACE1 inhibition reduced plaque growth rates significantly. Between 1 to 10 weeks mean plaque growth was reduced by approximately 52% (values were normalized to week 0, Figure 8b).

To quantify the plaque formation rate, the density of plaques was determined for each time point (Figure 8c) and gain of plaque density with time was calculated. After 8 weeks of BACE1 inhibitor treatment plaque density was reduced by 18.9% (values were normalized to week 0) compared to vehicle treatment. BACE1 inhibition significantly reduced the formation rate of new plaques (Figure 8d). Mean formation rate was decreased by 12-fold between 4 to 8 weeks after treatment.

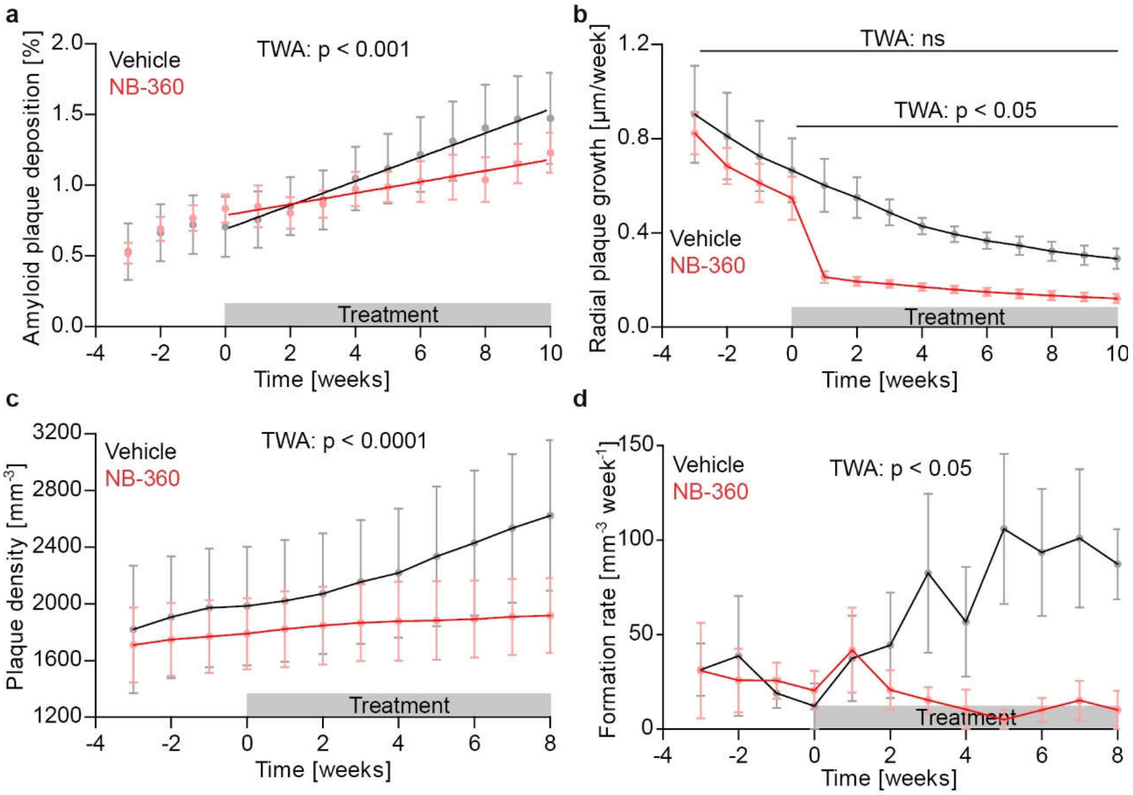

Figure 8. BACE1 inhibition most effectively reduces formation of new plaques. (**a**) Integrated volume fraction of all β-amyloid plaques (TWA: $F_{int}[13] = 3.31$, $p < 0.001$; $F_{time}[13] = 35.07$, $p < 0.0001$). Lines show linear regressions of the data (F-Test, $p < 0.01$). (**b**) Kinetics of mean plaque growth rates (TWA: $F_{int}[30] = 1.80$, $p = 0.010$; $F_{time}[10] = 42.90$, $p < 0.0001$). (**c**) Kinetics of mean plaque density (TWA: $F_{int}[33] = 4.41$, $p < 0.0001$; $F_{time}[11] = 35.28$, $p < 0.0001$), and (**d**) mean rate of newly formed plaques (TWA: $F_{int}[33] = 1.65$, $p = 0.020$; $F_{time}[11] = 2.05$, $p = 0.026$). Data presented as mean ± SEM; n = 5-6.

The combined effect of moderately reduced plaque growth and nearly halted plaque formation should also be apparent from the plaque size distribution. For this, plaques were grouped according to their size, and mean plaque densities were obtained. By comparing plaque size distributions before and at 10 weeks after treatment, a general shift to larger plaque sizes could be detected (Figure 9). Most evidently, small plaques only rarely occur after BACE1 inhibition.

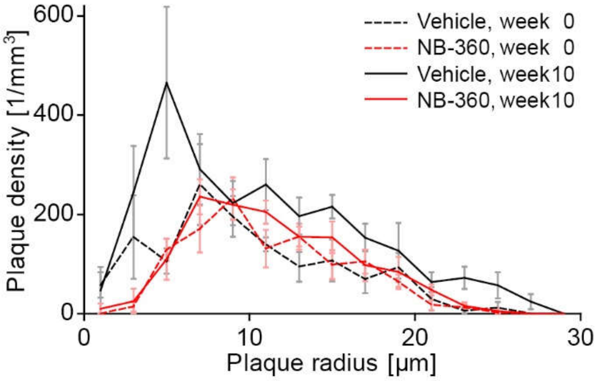

Figure 9. After BACE1 inhibition pre-existing plaques remain smaller and, less small plaques are detected. Frequency distribution of plaque radii at weeks 0 and 10. Reduced plaque formation and growth is reflected in the plaque size distribution as shift to larger radii and lower frequency of small plaque radii. Data presented as mean ± SEM; *n* = 5-6.

2.5 BACE1 inhibition reduces plaque growth irrespective of plaque size

We further tested whether plaques of different size might be differentially affected by BACE1 inhibition. For this we grouped plaques according to their size and obtained mean growth rates for each time point. BACE1 inhibition reduced plaque growth evenly, irrespective of plaque size (Figure 10a). Thus, once plaques had formed they constantly kept growing and did neither shrink nor disappear throughout the period of BACE1 inhibitor treatment.

The volume that β-amyloid plaques occupy only partly reflects their actual pathological impact. With time microglia and astrocytes are recruited to amyloid plaques which causes secondary detrimental effects in the immediate environment of plaques (286,287). Therefore, in the imaged brain volume we measured the distance of each voxel to the closest plaque (Figure 10b). Before treatment initiation the mean distance to closest plaque was approximately 55 µm and the maximal distance was 160 µm (Figure 10c). BACE1 inhibition significantly slowed down the reduction in mean distance (Figure 10d) by 48.5% (-1.03 ± 0.40 µm/week versus -0.50 ± 0.21 µm/week), indicating slower β-amyloid deposition.

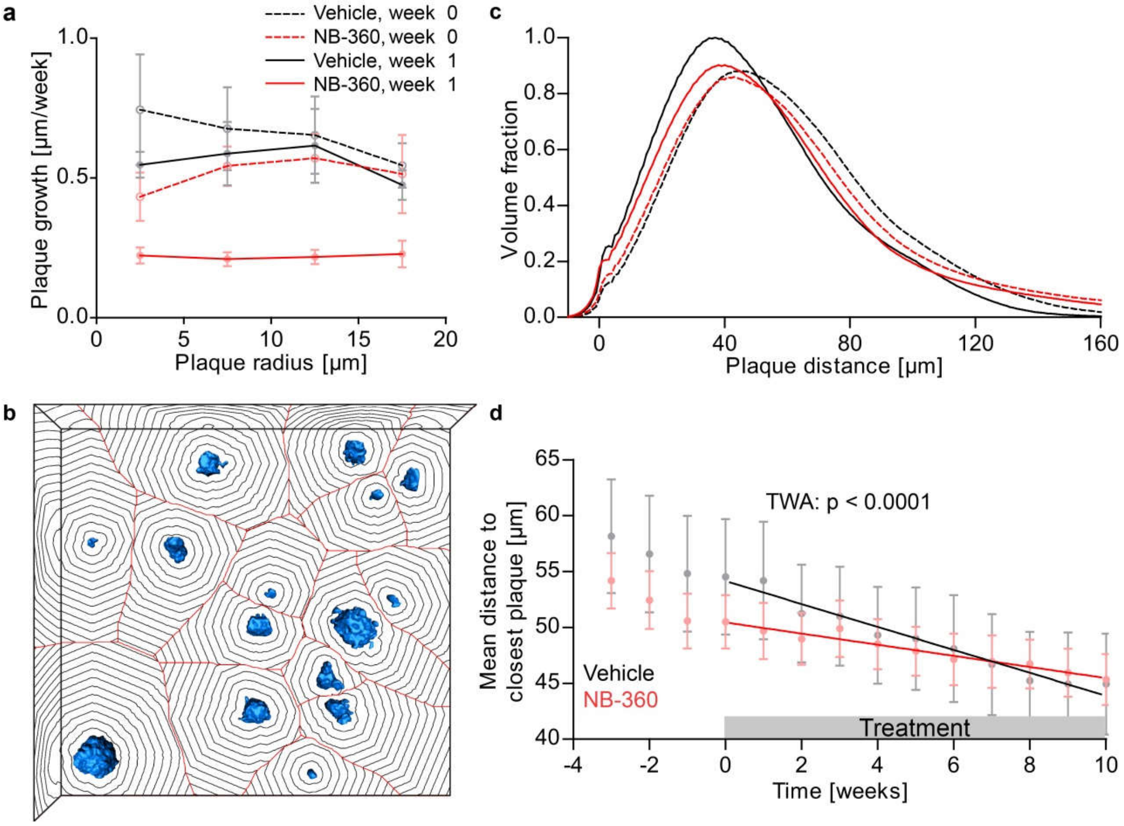

Figure 10. BACE1 inhibition reduces plaque growth independent of plaque size. (**a**) Growth rates of plaques of different radii before and one week after treatment initiation. (**b**) In the imaged brain volume the distance of each voxel to the closest plaque was determined via 3D distance transformation. (**c**) Frequency distribution of the distance of imaged brain volume to the closest plaque surface at weeks 0 and 10. (**d**) Kinetics of mean distance of brain volume to closest plaque (TWA: $F_{int}[13] = 3.90$, $p < 0.0001$; $F_{time}[13] = 41.14$, $p < 0.0001$). Lines show linear regressions of the data (F-Test, $p < 0.05$). Data presented as mean ± SEM; *n* = 5-6.

2.6 Formation of new plaques is enhanced in vicinity to pre-existing plaques

Previously, it was shown that BACE1 accumulates in peri-plaque dystrophic axons (78,81,193,194). Thus, plaques might locally enhance Aβ production (76) and thereby further aggravate β-amyloid deposition. To test this hypothesis and to investigate whether inhibition of BACE1 activity might break this vicious pathogenic cycle, we quantified the mean plaque formation rate close and distant to pre-existing plaques within 1 to 8 weeks after treatment start. In vehicle treated mice, the rate of plaque formation within 0-20 µm distance from pre-existing plaques was 4.2-fold higher as compared to the rate at 80-100 µm distance (Figure 11a and b). At week 10 shorter inter-plaque distances were significantly more frequent (Figure 11c). In BACE1 inhibitor treated mice, plaque formation was globally reduced, but remained 5.4-fold higher in proximity to plaques.

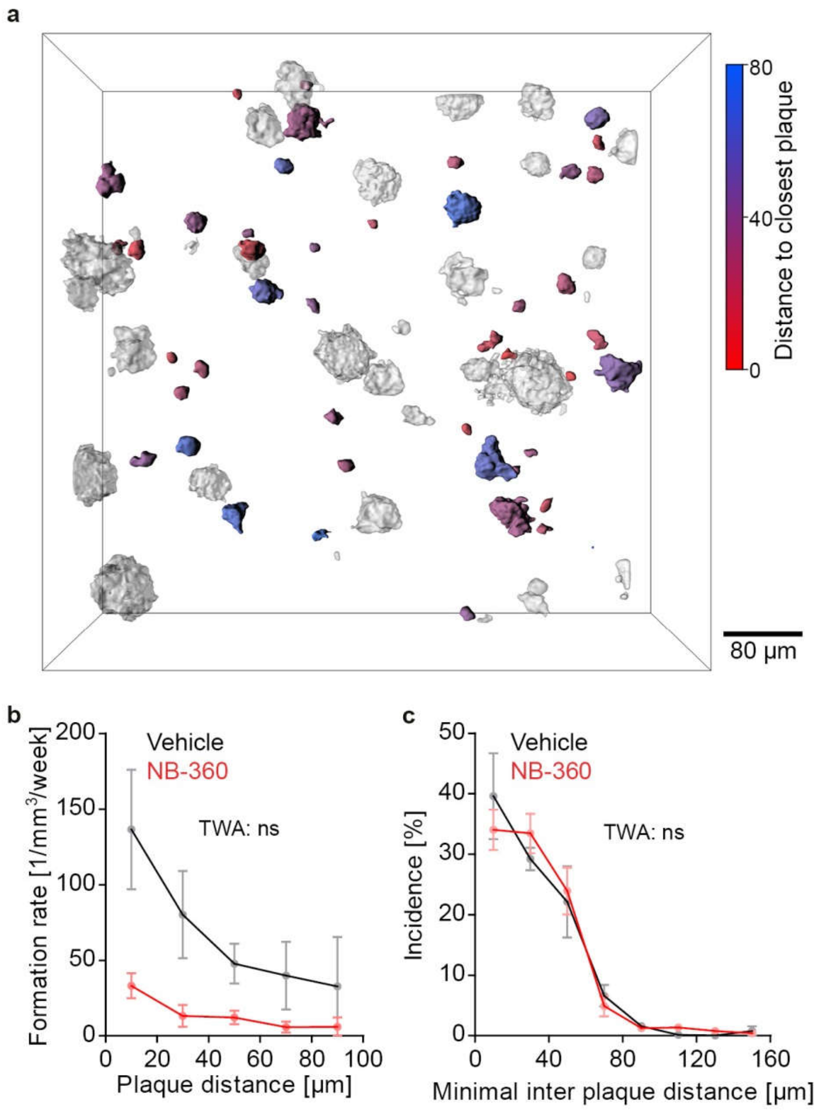

Figure 11. Pre-existing plaques locally enhance further formation of new plaques. (**a**) Representative image of 3D rendered plaques 10 weeks after treatment. The color map indicates the distance of each newly formed plaque to the closest plaque that was already present when the new plaque formed. White plaques were already present from the beginning. (**b**) Mean rate of plaque formation after treatment initiation at varying distances to already existing plaques (TWA: $F_{int}[4] = 2.20$, $p = 0.089$; $F_{treatment}[1] = 8.17$, $p = 0.019$; $F_{distance}[4] = 6.17$, $p < 0.001$). (**c**) Frequency distribution of the minimal distance between each plaque and the closest neighbouring plaque at 10 weeks after treatment (TWA: $F_{int}[7] = 0.46$, $p = 0.863$; $F_{treatment}[1] = 3.27$, $p = 0.104$; $F_{distance}[7] = 52.74$, $p < 0.0001$). Data presented as mean ± SEM; *n* = 5-6.

2.7 BACE1 inhibition fails to prevent BACE1 accumulation in peri-plaque dystrophies

BACE1 distribution was assessed by immunostaining in mice treated for 10 weeks (Figure 12a). Enrichment of BACE1 was detected up to approximately 5 µm from plaque borders (Figure 12b). Local BACE1 accumulation was already evident for small plaques (Figure 12c) and significantly increased with plaque size, reaching a maximum for plaques of 10 µm radius. BACE1 inhibition tended to reduce local accumulation of BACE1 but the effect was not significant (Figure 12c).

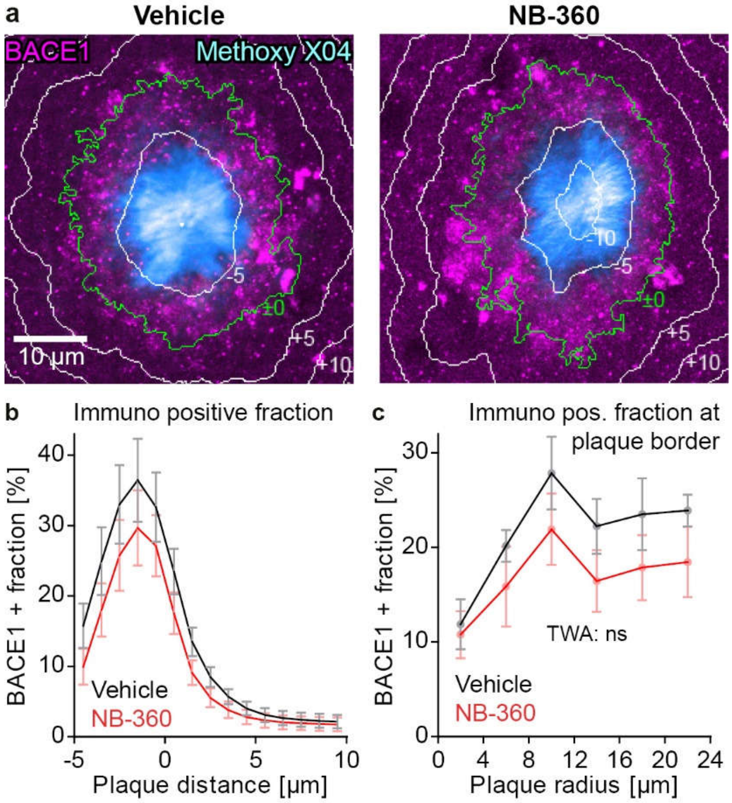

Figure 12. Inhibition of BACE1 activity does not prevent BACE1 accumulation in peri-plaque dystrophies. (**a**) BACE1 immunostainings 10 weeks after treatment onset. The green line depicts the outer plaque border as defined by Methoxy-X04 fluorescence, and white lines indicate 5 µm spaced distance rings from the plaque border. Scale bar represents 10 µm. (**b**) Fraction of BACE1 immuno positive brain volume at varying distances to the closest plaque border for plaques of 10-20 µm radius. (**c**) Mean fraction of BACE1 immuno positive brain volume within 1 µm distance from plaque border for plaques of increasing radii (TWA: $F_{int}[15] = 0.20$, $p = 1.000$; $F_{treatment}[3] = 1.33$, $p = 0.294$; $F_{radius}[5] = 14.04$, $p < 0.0001$). Data presented as mean ± SEM; $n = 5\text{-}6$.

2.8 BACE1 inhibition mitigates progression of presynaptic pathology

The question arose whether the beneficial impact of BACE1 inhibition on β-amyloid deposition would mitigate synaptic pathology. The VGLUT1^{Venus} fluorescence pattern appeared punctate with small sphere-like presynaptic boutons distant from plaques and large swollen axonal dystrophies in proximity to plaques (Figure 13a). Custom-written Matlab cluster analysis was applied for automated morphological segmentation. VGLUT1-positive structures became larger with increasing plaque size and developed within a range of up to 5-10 µm around plaque borders (Figure 13b).

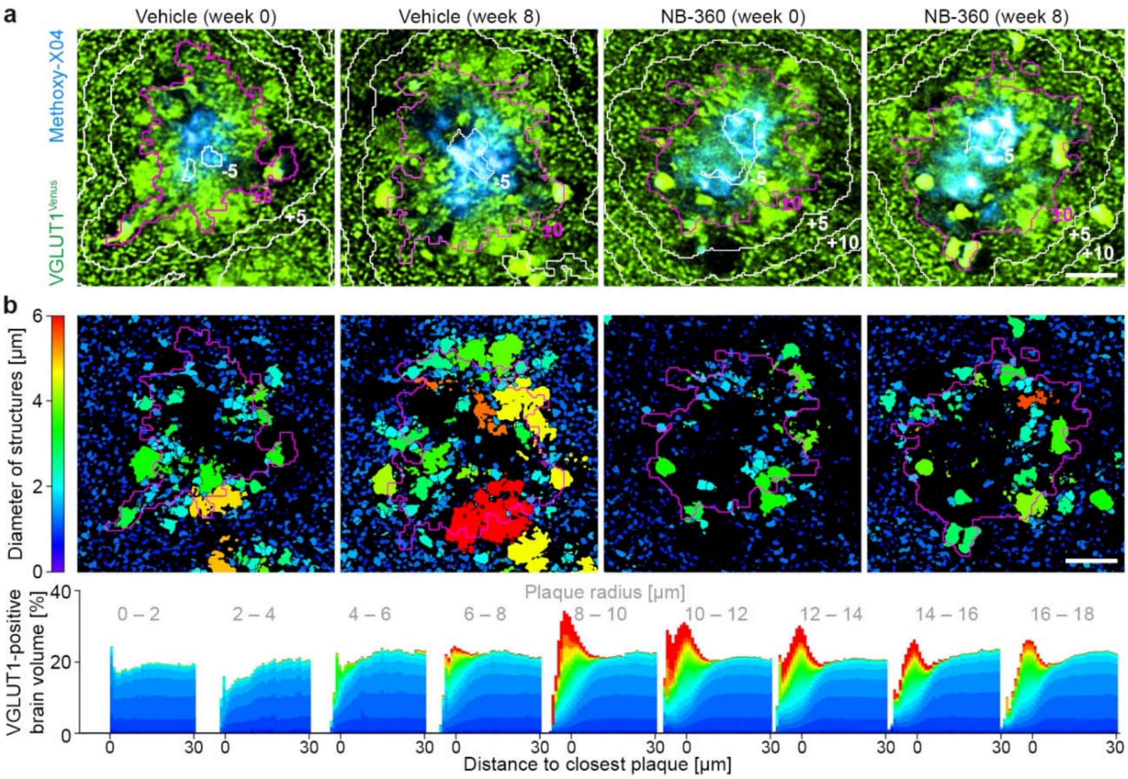
a
Vehicle (week 0)
Vehicle (week 8)
NB-360 (week 0)
NB-360 (week 8)
Methoxy-X04
VGLUT1Venus
-5
±0
+5
+10
b
Diameter of structures [µm]
0
2
4
6
VGLUT1-positive brain volume [%]
0
20
40
Plaque radius [µm]
0 – 2
2 – 4
4 – 6
6 – 8
8 – 10
10 – 12
12 – 14
14 – 16
16 – 18
0
30
Distance to closest plaque [µm]

Figure 13. BACE1 inhibition mitigates progressive axonal pathology. (**a**) VGLUT1$^{\text{Venus}}$ fluorescence micrographs for two plaques before and 8 weeks after treatment. (**b**) Segmentations of the respective images in (A), with color code indicating the minimal diameter of individual VGLUT1-positive structures. Magenta colored lines depict the outer plaque border and white lines indicate 5 µm spaced distance rings from plaque border. The cumulative distributions (below) indicate the proportion change of differently sized VGLUT1-positive structures with distance to closest plaque. Data presented as mean ± SEM.

A previous publication reported that axons with severe plaque-associated dystrophies can develop secondary dystrophies even distant to plaques (288). Consistently, in 6 months old APPPS1xVGLUT1$^{\text{Venus}}$ mice, large VGLUT1-positive structures emerged more frequently even distant (>30 µm) from plaques as compared to wild type VGLUT1^{Venus} mice of same age (Figure 14a). BACE1 inhibition had no evident impact on that specific pathology. According to their diameter, VGLUT1^{Venus}-positive structures were classified either as boutons or axonal dystrophies. A diameter of 2.0 µm was defined as maximal threshold for boutons, since in wild type mice less than 1.0% of VGLUT1-positive structures were larger. Furthermore, a diameter of 2.0 µm also demarked the transition size, at which VGLUT1-positive structures became more abundant in proximity to plaques (Figure 14b). In proximity to plaques the fraction of brain volume occupied by axonal dystrophies depended on plaque size. The corona of axonal dystrophies became denser with increasing plaque radius and was maximal for plaques of 10 µm radius (Figure 14c). BACE1 inhibition tended to reduce the extent of axonal dystrophies at the plaque border, but this effect did not reach statistical significance. However, with time the total amount of plaque-associated axonal dystrophies increased at a 10-fold reduced rate in BACE1 inhibitor treated mice. (Figure 14d).

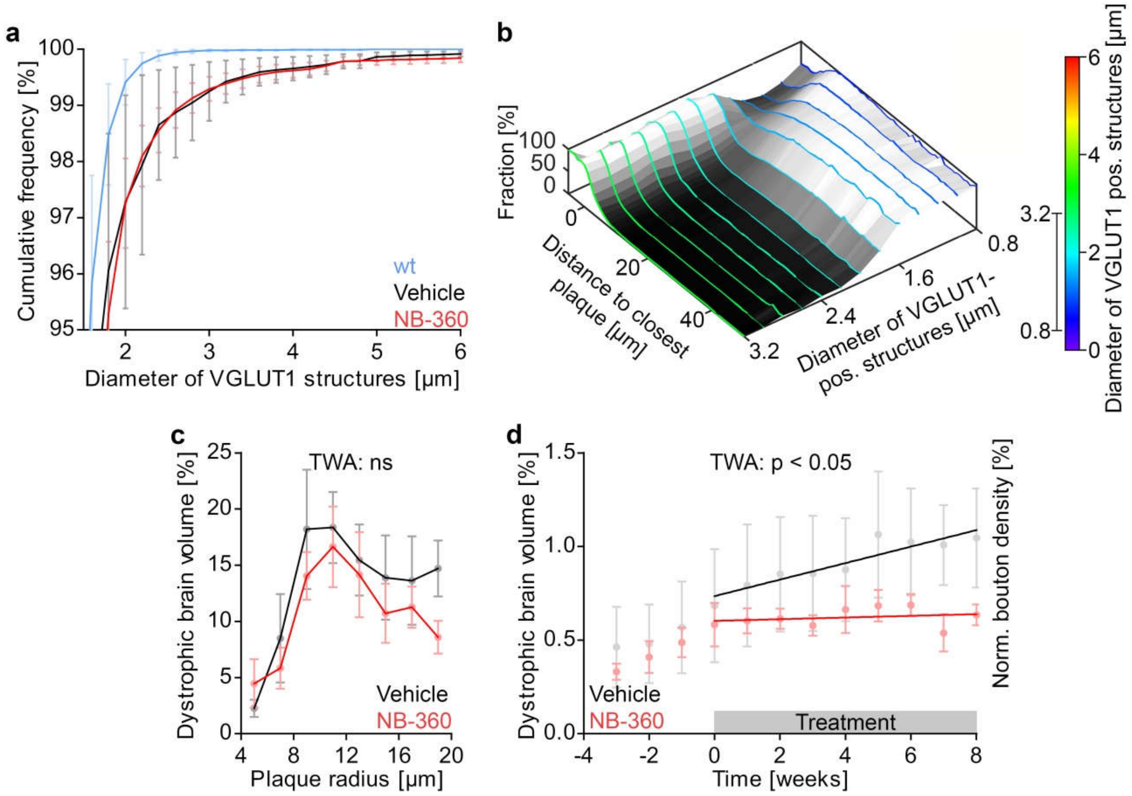

Figure 14. BACE1 inhibition mitigates progression of presynaptic dystrophies. (**a**) Cumulative distribution of VGLUT1-positive brain volume according to the diameter of VGLUT1-positive structures distant (>30 µm) from plaques after 8 weeks of treatment. Age-matched, untreated VGLUT1^{Venus} mice were used as control. (**b**) Normalized distribution of VGLUT1-positive structures of distinct size. Only structures with minimal diameter from 0.8 to 3.2 µm are shown in order to highlight the transition range. Small structures up to 1.8 µm diameter are abundant distant to plaques. Structures of 2.0 µm diameter or higher are abundant in proximity but are reduced distant to plaques (*n* = 10 mice, before treatment onset). (**c**) Fraction of brain volume within 1 µm distance from plaque border occupied by axonal dystrophies (TWA: $F_{int}[7] = 0.43$, $p = 0.882$; $F_{treatment}[1] = 0.94$, $p = 0.360$; $F_{radius}[7] = 6.46$, $p < 0.0001$). (**d**) Total fraction of dystrophic brain volume within 10 µm distance from plaque border (TWA: $F_{int}[11] = 2.29$, $p = 0.016$; $F_{time}[11] = 12.60$, $p < 0.0001$). Lines show linear regressions of the data (F-Test, ns). Data presented as mean ± SEM*;* *n* = 4 vehicle, *n* = 6 NB-360 and *n* = 3 control mice.

2.9 BACE1 inhibition fails to prevent plaque associated bouton loss

The density of boutons locally decreased in proximity to plaques (Figure 15a). This bouton loss became more pronounced with increasing plaque radius, but did not differ between treatment cohorts (Figure 15b). No significant change in bouton density between cohorts was observed over time (Figure 15c).

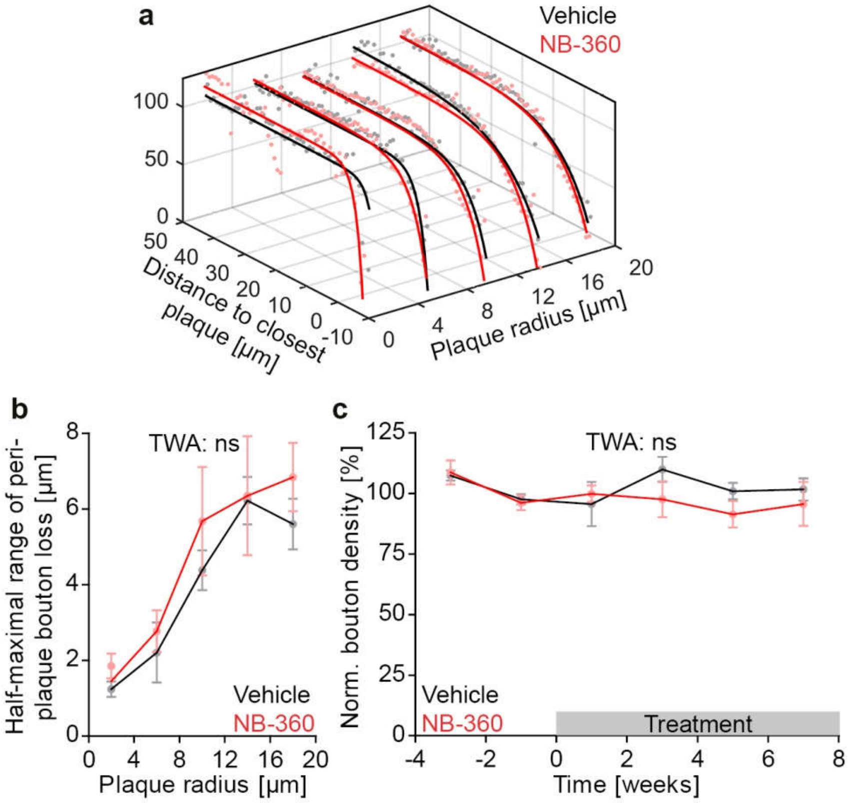

Figure 15. BACE1 inhibition does not prevent plaque-associated bouton loss. (**a**) Quantification of the densities of VGLUT1-positive boutons after treatment onset at varying distances and for plaques of varying radii. Traces were fitted with monophasic association functions to obtain the half-distance. (**b**) Toxic effect of plaques of increasing radii on bouton density, measured as the half-distance of monophasic association fits (TWA: $F_{int}[4] = 0.13$, $p = 0.972$; $F_{treatment}[1] = 1.22$, $p = 0.302$; $F_{radius}[4] = 9.93$, $p < 0.0001$). (**c**) Global bouton densities normalized to time points before treatment ($F_{int}[6] = 0.76$, $p = 0.605$; $F_{time}[6] = 1.95$, $p < 0.0921$). Data presented as mean ± SEM*;* $n = 4\text{-}6$.

3. Discussion

According to the prevailing theory, the amyloid cascade hypothesis, the initial cause for AD is the cerebral accumulation and aggregation of Aβ. Due to the synaptotoxic effect of these Aβ aggregates, synapses are lost and nerve cells degenerate which manifests in progressive cognitive decline (98,289). Based on this hypothesis, in the current study the impact of the Aβ lowering BACE1 inhibitor NB-360 was tested in a transgenic mouse model of AD.

3.1 Amyloid plaque kinetics

At the provided dosage BACE1 inhibitor treatment reduced soluble Aβ levels in APPPS1 mice by 5-fold, plaque growth by 2-fold, and plaque formation by 12-fold. The particularly strong impact of the treatment on the formation of new plaques might have two mechanisms.

i. Nucleation seed formation requires a higher critical Aβ concentration than accretion to already existing β-amyloid fibrils (277,280–282). Thus, reduction of Aβ level decreases the likelihood of new plaque formation more strongly than plaque growth.

ii. Accumulation of BACE1 in peri-plaque dystrophies (78,81,193,194) might enhance local Aβ generation (76). Indeed, our observation of increased plaque formation close to existing plaques, support the notion that Aβ generation is elevated in vicinity of plaques. Additionally, even though BACE1 inhibition effectively reduces BACE1 activity the treatment does not rescue abnormal accumulation of BACE1 in peri-plaque dystrophies.

Therefore, once a plaque has formed, excessive BACE1 accumulation amplifies local Aβ generation even when BACE1 activity is inhibited.

Thus, at a stage when β-amyloid pathology has commenced, these mechanisms aggravate pharmacological intervention to block further Aβ deposition. Consistently, BACE1 inhibition only moderately reduces growth of pre-existing plaques, while plaque formation is almost halted in APPPS1 mice.

3.2 Synaptic Aβ pathology

BACE1 inhibitor treatment reduced the rate of presynaptic dystrophy formation by 10-fold, which indicates a beneficial impact on synaptic toxicity. However, the total density of presynaptic boutons did not significantly differ between treatment cohorts. There are two possible explanations for this discrepancy. In APPPS1 mice bouton loss is restricted to the proximity of plaques and – depending on plaque size – returns to normal density within 5 to 10 µm from plaque border. The BACE1 inhibitor treatment results in 0.5 % reduced β-amyloid deposition compared to vehicle treated APPPS1 mice. For detection of such small changes, the variability of bouton density in different mice is too high. Another explanation would be that the beneficial local impact of the treatment on plaque-associated synaptic pathology is balanced by adverse effects of BACE1 inhibition on synapse density (179,180).

3.3 BACE1 inhibitor dosage

In light of dose-dependent adverse effects of BACE1 inhibition in mice (179,180,290), it is critical to minimize BACE1 inhibitor dosage as much as possible. This particularly applies for preventive treatment that will require life-long drug administration, starting at an age when patients are still healthy and accurate prediction of AD might not always be ensured.

Inhibition of BACE1 seems to be clinically beneficial in the context of elevated BACE1 and Aβ levels in brains of AD patients (195,196,200). However, the unequal distribution of BACE1 poses a major obstacle for pharmacological BACE1 inhibition. An adequate BACE1 inhibitor dosage, necessary to sufficiently inhibit the high BACE1 levels in peri-plaque axonal dystrophies (78,81,193,194), might cause excessive inhibition of physiological BACE1 activity distant to plaques. Conversely, partial BACE1 inhibition to ensure physiological BACE1 activity might prevent potential mechanism-based adverse effects (179,180,290), but might not suffice to break the vicious cycle of self-sustained Aβ generation close to plaques.

The finding of utmost susceptibility of plaque formation in response to BACE1 inhibition, points to a therapeutical strategy that might balance potential adverse effects and sufficiently efficacious reduction of β-amyloid deposition. Such a compromise would be to aim for a BACE1 inhibitor dosage that prevents formation of new plaques rather than aiming for complete arrest of plaque growth. This strategy would be directed at delaying rather than halting the progression of AD at any rate.

Since in human patients Aβ levels are generally lower as compared to APPPS1 mice, it is important to remark that it is possible that a narrow range of BACE1 inhibition dosage exists that is tolerable and still completely halts β-amyloid deposition. However, given the adverse effects in mice this might not be an optimal primary clinical endpoint.

Furthermore, enhanced plaque formation rate in the vicinity of pre-existing plaques might be causative for the characteristic spreading of β-amyloid deposition that typically initiates locally and then gradually disperses into adjoining unaffected brain regions (28–33). This conclusion is in agreement with previous studies, reporting that plaque deposition gradually invades grafted wt tissue in AD mice (291,292). Thus, even if halting plaque growth in humans might turn out to be difficult, it could suffice to abort plaque formation by BACE1 inhibition and thereby prevent further spreading into neighbouring brain regions. For translation of this pharmacological strategy into clinical therapy, it would be necessary to empirically determine the range of BACE1 inhibitor dosage that effectively halts the spreading of β-amyloid deposition into unaffected brain regions, e.g. by PET imaging.

3.4 Timing of pharmacological BACE1 inhibition

The formation of new plaques typically occurs in the initial stage of β-amyloid progression and ultimately reaches a plateau of maximum density (31). In addition, experimental data from mice indicate that towards later stages new plaques rarely form while existing plaques continue to grow (277,279).

In this study only a single dosage was tested at one stage of β-amyloid pathology. However, the key finding of differential impact on plaque formation and growth allows some logical assumptions on the potential outcomes of BACE1 inhibitor treatment applied at different dosages and at different stages of β-amyloid progression (illustrated in Figure 16):

1. For primary prevention treatment, before Aβ accumulation, low BACE1 inhibitor dosage might suffice to restrict Aβ levels below the critical concentration that is required for plaque-seeding. In agreement with this notion, life-long reduction of Aβ levels by 40% results in 5- to 7-fold reduced risk of developing AD (146). Additionally, a slight reduction of Aβ levels by

12% due to heterozygous expression of BACE1 reduces total Aβ deposition by 50% in aged *Bace1*$^{+/-}$ mice (256). Moreover, prophylactic therapy with a γ-secretase inhibitor results in sustained reduction of amyloid plaque pathology in Tg2576 mice (293). The current work and a previous publication (294) indicate, that plaque formation is locally enhanced at plaques and limited up to approximately 50 µm distance from pre-existing plaques. Thus, as long as β-amyloid deposition is still locally confined in the brain, the strategy of halting plaque formation with low BACE1 inhibitor dosage could still apply to suppress further spreading of β-amyloid pathology into yet unaffected parts of the brain.

2. Secondary prevention treatment applies, when substantial parts of the brain are already affected with initial β-amyloid deposition. Under these conditions, β-amyloid deposition might even continue at Aβ levels below the critical concentration for nucleation seed formation. In addition, BACE1 inhibition therapy has to compensate for increased Aβ generation close to plaques. In APPPS1 mice BACE1 inhibitor treatment nearly halts plaque formation and effectively slows down β-amyloid deposition with no sign of compensatory adaptation to the inhibitor over the 2.5 months long treatment period. Even more importantly, the treatment also slows down the progression of plaque-related axonal pathology. While these results imply that β-amyloid pathology can at least be delayed, previous end point studies in other murine AD models indicate that β-amyloid deposition might even be halted completely (233,234).

3. Late-stage treatment in the saturation phase of β-amyloid deposition, might not be sufficient to stop disease progression. Our longitudinal *in vivo* approach shows that in APPPS1 mice, BACE1 inhibition failed to clear plaques that were already present at treatment initiation, and even though

the progression of axonal pathology was slowed down it could not be reverted. This might also explain the recently reported failure of the BACE1 inhibitor verubestat in one clinical late-stage trial for the treatment of AD.

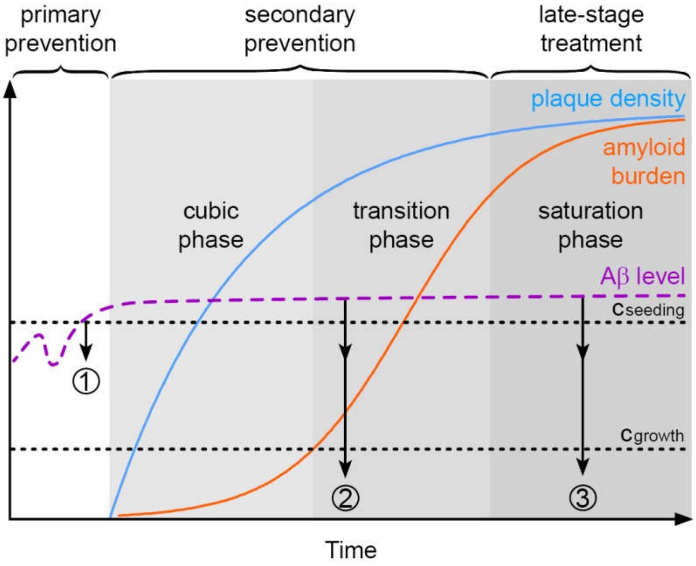
primary prevention
secondary prevention
late-stage treatment
plaque density
amyloid burden
cubic phase
transition phase
saturation phase
Aβ level
cseeding
cgrowth
①
②
③
Time

Figure 16. Hypothetical model on the impact of different therapeutic BACE1 inhibitor approaches on the kinetics of amyloid deposition. The dashed magenta line delineates speculative Aβ levels. Before initial plaque deposition Aβ levels might transiently and locally surpass the critical concentration for plaque formation. Once formed, plaques exacerbate local Aβ-levels via BACE1 accumulation. ① Low BACE1 inhibitor dosage starting already before initial amyloid deposition suffices to suppress Aβ levels constantly below the critical concentration for plaque seeding ($c_{seeding}$). ② After plaque deposition has commenced moderate BACE1 inhibitor doses are required to suppress Aβ levels below $c_{seeding}$ and suppressing plaque growth might only be achievable with high and probably toxic BACE1 inhibitor dosing. ③ In the saturation phase, plaque deposition reaches a plateau with little space for beneficial influence of any BACE1 inhibitor dosage.

3.5 Conclusion

Altogether, the data imply that BACE1 inhibition is most effective if given as early as possible in the progression of β-amyloid pathology. Predictive genetic testing for familial AD would allow to initiate treatment already prophylactically.

However, the majority of AD patients lack predictive genetic markers and β-amyloid deposition is among the earliest pathological alterations in the AD brain (1). Thus, for the majority of AD patients presymptomatic diagnosis will even in future be limited to a stage when first plaques have already formed. Therefore, in this study the effect of BACE1 inhibitor treatment was tested at a stage, when β-amyloid deposition has already commenced but has not yet saturated, as can be deduced from the linear slope of β-amyloid deposition.

The major future challenge will be to identify early AD biomarkers. Indeed, clinical biomarkers have already been determined that enable AD diagnosis several years before symptom onset (1,295), thus paving the way for presymptomatic treatment.

To take advantage of the particular inhibitor susceptibility of plaque formation, treatment should be commenced when β-amyloid deposition is still locally confined in the brain. Thus, a moderate dosage of BACE1 inhibition might suffice to halt or at least delay the progression of β-amyloid pathology to AD. This treatment strategy would ensure moderate suppression of physiological BACE1 function (296) and thus reduces the risk of potential mechanism-based adverse effects (179).

Apart from inhibiting BACE1 activity another therapeutical approach might be to target accumulation of BACE1 at plaques or alleviate the formation of axonal dystrophies. For this, it will be indispensable to understand the pathological mechanisms that cause axonal swelling and subsequent accumulation of BACE1. One possible mechanism has been brought up recently, in which Aβ causes microtubule disruption and motor protein mis-localization (76,77). As a result retrograde transport and thereby maturation of lysosomes is impaired (201,202) which causes BACE1 and other proteins to accumulate in peri-plaque dystrophic neurites (76,77). It would be highly relevant to identify a target within this cascade to interfere with axonal dystrophy formation and thereby BACE1 accumulation. A recent study has shown that swollen axonal varicosities are highly dynamic with strong changes of volume within weeks (297). Consequently, the emergence of peri-plaque axonal dystrophies seems to be reversible within a certain time window. A strategy that would alleviate axonal pathology at plaques in combination with tolerable BACE1 inhibitor dosage might represent an effective future therapeutic approach to interfere with β-amyloid progression.

4. Materials and Methods

4.1 BACE1 inhibitor

NB-360 was synthesized and kindly provided by Novartis. The pharmacologic properties have been characterized previously by Neumann and colleagues (233). Mice were fed *ad libitum* with food pellets containing NB-360 (0.25 g/kg) or control pellet.

4.2 Transgenic mice

All protocols and procedures involving animals were approved and conducted in accordance with the regulations of the Ludwig-Maximilian University and the Government of Upper Bavaria (Aktenzeichen 55.2-1-54-2532-62-12). Heterozygous APPPS1 mice co-express a human APP with the Swedish mutation (KM670/671NL) and a mutated PS1 (L166P) under the neuron-specific Thy1-promoter (89). APPPS1 mice were crossbred with homozygous VGLUT1^{Venus} knock-in mice that express the Vesicular GLUtamate Transporter 1, fused to the fluorescent protein Venus under the endogenous VGLUT1 promoter (90). Non-transgenic APPPS1$^{-/-}$ littermates crossed with homozygous VGLUT1^{Venus} mice served as control. Mice were of both sexes and group-housed under pathogen-free conditions until surgery, after which they were single-housed.

4.3 Statistical Analysis

For statistical analysis, GraphPad Prism 5 (GraftPad Software, San Diego, California) was used. Data were tested for normality using D'Agostino-Pearson omnibus K2 test and Kolmogorov-Smirnov test. Intergroup comparisons were performed using two-tailed unpaired Student's *t*-test. In the longitudinal measurements variables were compared across groups using two-way ANOVA (TWA) and *p* values refer to the test of interaction unless further specified. When treatment effects, genotype effects, time effects, interactions were found, post-hoc analyses were performed using Bonferroni analysis. All results are presented as mean ± SEM unless further specified.

4.4 Plasma and brain homogenization and extraction

Mice were deeply anesthetized with an intraperitoneal injection of ketamine and xylazine (130/10 mg/kg respectively). Blood was collected via cardiac puncture into EDTA tubes (BD microtainer tubes with K2EDTA #365974) on wet ice and was centrifuged at 1500 g for 15min at 4°C. Plasma was obtained from the supernatant and was frozen at -80°C. Brains were isolated, quick-frozen on dry ice and stored at -80°C. Frozen murine forebrains were homogenized in 9 volumes of ice-cold Tris-buffered saline (pH 7.4) containing Complete protease inhibitor cocktail (Roche Diagnostics, Penzberg, Germany) using a Sonifier 450 (Branson) and stored in aliquots at -80°C. Triton X-100 soluble Aβ was extracted by mixing 50 μl 2% Triton X-100 with 50 μl homogenate, incubating for 15 minutes on ice with vortexing, followed by ultracentrifugation at 100000 x g for 15 minutes. The clear supernatant was diluted to a final forebrain dilution of 1:100 and used for analysis.

4.5 Aβ quantification

Six weeks old APPPS1 mice were treated for 2 weeks with vehicle or NB-360-doted food pellets and were sacrificed subsequently to collect blood and brain samples. Aβ40 and 42 were determined in the forebrain and plasma using the electro-chemiluminescence immuno assay kits based on 6E10 from Meso Scale Discovery (Rockville, MD, USA) in either singlet or triplet format. Samples and standards were prepared according to the manufactures protocols.

4.6 Cranial window implantation

A cranial window was implanted over the right cortical hemisphere as previously reported (298,299). To minimize risk of postoperative wound infection, surgical tools were thermically sterilized with a table top steriliser (Fine Science Tools, Heidelberg, Germany). The surgery was performed with a SZ51 stereo microscope (Olympus, Hamburg, Germany) and a KL 1500 LED cold light Schwanenhals lamp (Schott, Mainz, Germany). Mice were anesthetized with an intraperitoneal injection of ketamine/xylazine (130 mg/kg ketamine and 10 mg/kg xylazine in 0,9% NaCl). Anesthesia depth was surveilled by testing the interdigital reflex. After adequate anesthesia was achieved, dexamethason was intraperitoneally administered (6 mg/kg in 0,9% NaCl) as anti-inflammatory to prevent the development of cerebral oedema during trepanation of the skull. Additionally, to circumvent postoperative pain and inflammation, the mice were administered a subcutaneous injection of the analgesic carprophen (7,5 mg/kg in 0,9% NaCl) and the antibiotic cefotaxim (250 mg/kg in 0,9% NaCl). Subsequently, mice were placed on a heating plate (Fine Science Tools, Heidelberg, Germany) to keep body temperature during the surgery constant at 37°C. The mouse head was fixated with a MA-6N holder (Narishige, Tokyo, Japan) and the eyes were protected from dehydration by applying bepanthene ointment. Fur of the skull was disinfected with 70% ethanol and the scalp was removed with a scissor, without damaging the temple muscle. Loose hair at the wound margin was removed with a sterile cotton swab and the periosteum was removed with a scalpel. To reinforce adhesion of dental cement to the skull, a thin layer of Cyano-Veneer liquid glue (Hager und Werken, Duisburg, Germany) was applied on the wound margin and the exposed skull. Subsequently, a circular trepanation of the skull of 5 mm diameter was applied with a C1-Master dental drill (Schick Dental, Schemmerhofen, Germany) above the somatosensory cortex (stereotactic coordinates relative to Bregma: 2 mm caudal und 2,5 mm lateral). Particles of bone were removed with an electric vacuum pump. A drop of PBS was put on the craniotomy to prevent that the cortex dries after opening of the skull. Then the bone was carefully lifted with curved forceps. Slight bleedings were staunched by rinsing with PBS and application of hemostatic gelfoam (Pfizer, New York, USA). Subsequently, a round coverslip of 5 mm diameter (Fine Science Tools, Heidelberg, Germany) was implanted above the craniotomy and PBS was removed with sterile Sugi absorbent swabs (Kettenbach, Eschenburg, Germany). The gap between cover slip and margin of the skull was sealed with histoacryl tissue adhesive (B. Braun Melsungen AG, Melsungen, Germany) and the skull was covered with dental cement (Cyano-Veneer; Hager Werken, Duisburg, Germany). To allow repositioning of the mouse during subsequent imaging sessions a metal bar was attached to the skull and was fixated with dental cement. Until the moment of awakening the animal was placed on a heating pad and was subsequently transferred back to the home cage.

Table 1. Materials for cranial window implantation.

Product	*Manufacturer*
Ketamine 10 %	WDT, Garbsen
Xylazine	Bayer HealthCare, Leverkusen
Dexamethasone	Sigma-Aldrich, Taufkirchen
Rimadyl (active agent Carprofen)	Pfizer, Berlin
Cefotaxim	Pharmore, Ibbenbüren
Isoflurane (Forene)	Abbott, Wiesbaden
Inhalation anaesthetic set Trajan808	Dräger Medical, Lübeck
Gas mask for mice	Custom-made
Heating plate fore mice	FST, Heidelberg
Mouse holder for surgery	Custom-made
Bepanthene	Bayer HealthCare, Leverkusen
Stereo microscope SZ51	Olympus, Hamburg
Table top sterilizer FST 250 Hot Bead Sterilizer	FST, Heidelberg
Drill C1 Master	Schick Dentalgeräte, Schemmerhofen
Drill head	Gebrüder Brasseler, Lemgo
Vacuum suction device	Custom-made
Syringe 1ml	VWR, Ismaning
Cannula 27G/20G	VWR, Ismaning
Ethanol (70%)	Sigma-Aldrich, Taufkirchen
Surgical tools (scissors & forceps)	FST, Heidelberg
Scalpel	Swann-Morton, Sheffield, UK
Cotton swab, sterile	Paul Böttger, Bodenmais
Hemostatic gelfoam	Pfizer, Berlin
Absorbent swabs Sugi, sterile	Kettenbach, Eschenburg
Cover slips (5 mm diameter)	Gerhard Menzel, Braunschweig
Dental adhesive Cyano-Veneer Starter Kit	Hager & Werken, Duisburg
Titanium-bar	Custom-made

4.7 Immunohistochemistry

Deeply anesthetized mice (130/10 mg/kg b.w. ketamine/xylazine i.p. WDT/Bayer Health Care) were perfused with phosphate-buffered saline (PBS) followed by 4% formalin solution. Mouse brains were dissected and post-fixed in 4% formalin for 24 hours. Fixed brains were cut into coronal 50 µm thick sections on a vibratome (VT1000S, Leica). Brain slices were permeabilized for 2 hours with 1% Triton X-100 and 10% normal goat serum (Sigma-Aldrich) in PBS. Slices were then incubated with rabbit polyclonal antibody directed against BACE1 (1:1000; BACe–Cat1) (194) in 0.5 % Triton X-100 for 2 days at 4 °C. Sections were washed in PBS and incubated with the secondary antibody coupled to Alexa633 (anti-rabbit 1/500, Invitrogen) 2 h at RT. To detect amyloid fibrils slices were incubated for 15 min with 10 µg/mL Methoxy-X04 in 50% ethanol and washed three times with 50% ethanol at RT. Sections were finally washed for 5 times 10 min with PBS before mounting them on glass coverslips with fluorescence conserving media (Dako).

4.8 Microscopy

4.8.1 Confocal microscopy

Images were acquired with an inverse LSM 780 confocal microscope (Zeiss) equipped with a 40x/1.4 oil immersion objective. Excitation wavelengths were 405 and 561 nm, emission was collected at 410–580 nm for Methoxy-X04 and 585–735 nm for BACE1. In each mouse brain 3-dimensional 16 bit data stacks of 1024 x 1024 x 100 pixels were acquired from 20 different positions in the somatosensory cortex at a lateral resolution of 0.1 um/pixel and an axial resolution of 0.2 µm/pixel.

4.8.2 Chronic two-photon *in vivo* imaging

In vivo two-photon imaging was started after a recovery period of 3-4 weeks. For amyloid staining Methoxy-X04 (301) was intraperitoneally injected 24 h before imaging at a dose of 0.5 mg/kg body weight. Throughout the imaging sessions, mice were anesthetized with isoflurane (1% in 95% O^2, 5% CO^2, Forene®, Abbott), placed on a heating pad to keep body temperature at 37°C (Fine Science Tools GmbH) and fixed to a custom-made holder using the glued metal plate. *In vivo* two-photon imaging was performed on a LSM 7 MP (Carl Zeiss) equipped with standard photomultiplier detectors and a 20x water-immersion objective (W Plan-Apochromat 20x/1.0 DIC, 1.0 NA, Carl Zeiss). For each mouse, one region of interest was reimaged at a weekly interval. In each imaging session two data stacks were obtained consecutively. To resolve the presynaptic boutons, a high-resolution 3D stack was obtained from the $\text{VGLUT1}^{\text{Venus}}$ fluorescence in cortical layer I at a resolution of 0.08x0.08x0.4 μm^3 and dimensions of 283x283x60 μm^3. Subsequently a larger but less resolved 3D stack was obtained from the Methoxy-X04 fluorescence at a resolution of 0.24x0.24x0.4 μm^3 and dimensions of 425x425x200 μm^3. Methoxy-X04 was excited at 750 nm by a Ti:Sa laser (MaiTai DeepSee, Spectra-Physics) and emission was collected below 485 nm. $\text{VGLUT}^{\text{Venus}}$ was excited at 915 nm and emission was collected from 470 to 550 nm. For both stacks the autofluorescence was recorded simultaneously at an emission range from 590 to 650 nm. In subsequent imaging sessions, the previously imaged volumes were identified by eye using the unique blood vessel pattern. This allowed a precise alignment of the same imaging volumes. The laser intensity was adjusted to keep the emitted fluorescence stable at different depths using the z-correction tool in the microscope control software and also at subsequent imaging sessions. All images were of optimal quality and did not suffer from motion artefacts due to breathing or heart beating of the animal.

Table 2. Imaging settings for acquisition of Methoxy-X04 and VGLUT1^{Venus} fluorescence.

	Methoxy-X04	*VGLUT1Venus*
Excitation wavelength	750 nm	915 nm
Pixel size	1800 x 1800 x 501	3600 x 3600 x 151
Image size	425 µm x 425 µm x 200 µm	283 µm x 283 µm x 60 µm
Resolution	0.24 µm x 0.24 µm x 0.4 µm	0.08 µm x 0.08 µm x 0.4 µm
Pixel dwell time	0.45 µs (no average)	0.45 µs (average 2x)
Emission channels	SP 485 & BP 590-650	SP BP470-550 & BP 590-650

4.9 Data analysis of 3D microscopical data

All data stacks obtained by *in vivo* two-photon microscopy were deconvoluted using AutoQuant (AutoQuantX3, Media Cybernetics). For quantification amyloid plaques, presynaptic boutons, presynaptic dystrophies as well as BACE1 positive dystrophies, the 3D data stacks of fluorescence intensity were analysed using custom-written Matlab software. Initially, local background subtraction was performed to diminish intensity variations among different stacks. Subsequently, a percentile based intensity threshold was applied, and a connected component analysis was used to identify contiguous clusters of voxels. This standard analysis was slightly modified for each of the biological readouts with the detailed analysis described below.

To define **BACE1 positive dystrophies** the 50th percentile of immunofluorescence signal was used as threshold for each image stack. Connected component analysis was applied to identify clusters of contiguous voxels and clusters smaller than 1 µm^3 were excluded.

For data stacks of **VGLUT1$^{\text{Venus}}$ fluorescence** the 75th percentile was used as threshold. Due to the dense arrangement of VGLUT1-positive structures applying that threshold results in a web-like mask of supra-threshold voxels with nearby structures still merging into one another. Therefore, the data was further segmented morphologically by calculating the distance transformation, followed by watershed segmentation along minimal distance ridges. Subsequently, the minimal diameter as well as the distance to the closest plaque was obtained for each segment. To analyse the distribution of minimal diameter of VGLUT1-positive structures as a function of plaque distance and plaque size, the minimal diameter was binned into 0.2 µm steps. Synapse densities in relation to the distance from plaques were fitted using one-phase association curves.

- $Y(d) = Y0 + (Plateau - Y0) * (1 - e^{-K * d})$, with d = distance to closest plaque and Y = bouton density

The half-distance (ln(2) / K) was obtained as a measure for the sphere of toxic influence of plaques on bouton density.

Amyloid plaques were identified applying the 90th percentile on the Methoxy-X04 fluorescence intensity data. Since amyloid burden typically constitutes 1 to 2 % of brain volume in the imaged region of APPPS1 mice, this threshold is intentionally set to a very low level. It allows to obtain the total size of amyloid plaques as opposed to thresholding operations such as using local contrast or half-width intensity that rather detect the dense plaque core. Subsequently, individual amyloid plaques were tracked over time. For this purpose the image data from consecutive time points was loaded as time series in Imaris (Version 7.7.2, Bitplane). Plaque volumes were extracted by 3D-surface-rendering and were semi-automatically tracked over time using the surface tracking module of Imaris. To identify nucleation events, plaques were tracked back to the first time point of appearance and were only assessed when present for at least 3 weeks to warrant unambiguous distinction from background signal. Therefore, quantification of plaque density and formation only include values up to 8 weeks post-treatment even though imaging was performed up to 10 weeks. Correct tracking was manually checked for each amyloid plaque. For reliable determination of the actual size of each amyloid plaque the largest extension in XY was determined and the radius was calculated as $radius = \sqrt{area/\pi}$ assuming a spherical shape of plaques (279). The radii of individual plaques were fitted with a monophasic association function, and the radial growth rate at each time point was obtained by calculating the first derivative of the best fit. All plaques contacting the image border were excluded from the analysis. The distribution of presynaptic boutons, presynaptic dystrophies and BACE1 positive dystrophies was analysed with regards to proximity to the closest amyloid plaque. For this purpose, a quasi euclidean 3D distance transformation was performed to identify the distance of every voxel to the closest plaque border. Distance was calculated at 1 µm resolution from the outer border of plaques into surrounding tissue as well as towards the inside of each plaque. Voxels inside plaques were assigned negative distance from plaque border. To quantify the pathological impact of each plaque separately, the 3D volume was divided into sectors with all voxels closest to a particular plaque constituting the sector of that plaque.

For the correlation of plaque formation rate with plaque distance the distance to the closest already existing plaque was determined for each formation event at the respective time point of formation. For the analysis all plaques formed after treatment onset were pooled and closest plaque distance was binned into 20 µm segments. For the frequency distribution of minimal inter-plaque distance, the distance to the closest plaque was determined for all plaques at week 10, and inter-plaque distance was binned in 20 µm segments.

4.10 Software

Table 3. Software

Program	*Manufacturer*
Adobe Illustrator CS5	Adobe Systems
Adobe Photoshop CS5	Adobe Systems
Adobe Indesign CS5	Adobe Systems
AutoQuant X3	Media Cybernetics
Imaris 7.7.2	Bitplane Imaris
LSM Image Browser 4.2.0	Zeiss
MATLAB 2015b	MathWorks
Microsoft Excel 2010	Microsoft
Microsoft Word 2010	Microsoft
GraphPad PRISM 5	Graphpad Software
Zen 2009	Zeiss

4.11 VGLUT1^{Venus} signal segmentation

Custom-written Matlab cluster analysis was applied for automated morphological segmentation of VGLUT1^{Venus} fluorescence 3D stacks.

```
% VglutGreen: 3D-image of VGLUT1-Venus fluorescence intensity after deconvolution
and background correction
% Exclude: 3D-Mask specifying parts located outside brain
```

```matlab
% Res: Resolution in all three dimensions
% VglutRed: 3D-image of autofluorescence after deconvolution and background correction

function [BoutonList,BoutonIds,Dystrophies2,Dystrophies2Radius,VglutGreen,GRratio]=VglutVenusSegmentation(VglutGreen,Exclude,Res,VglutRed)

Pix=size(VglutGreen).'; % Determine pixel dimension of 3D-image
Um=Pix.*Res; % Determine size in µm of 3D-image

[Threshold]=prctile_2(VglutGreen,75,Exclude==0); % Calculate 75th percentile as threshold for selecting VGLUT1-Venus positive part of 3D-image
clear Exclude;
Mask=VglutGreen>Threshold;

[Mask]=removeIslands_3(Mask,4,[0;0.025],prod(Res(:))); % Excluded voxels that are entirely enclosed by included voxels are detected and included to account for noise
Distance=distanceMat_4(logical(1-Mask),'DistInOut',Res,0.1,1,0,0); % Apply 3D distance transformation to calculate the distance of each voxel to the outer surface of the VGLUT-Venus positive mask
clear Mask;

Watershed=uint8(10)-uint8(Distance); % Voxels that are located more than 1 µm (10 * 0.1 µm) from outer border of VGLUT1-Venus positive mask are set to maximally 1 µm. This is necessary to avoid oversegmentation
Watershed=single(watershed(Watershed,26)); % 3D segmentation of VGLUT1-Venus positive mask. The algoryhtm separates clusters of contiguous voxels along the ridge lines obtained from 3D distance transformation
Watershed(Distance==0)=0;

BW=bwconncomp(logical(Watershed),6); % Detect connected components (clusters)
clear Watershed;
Table=table(cellfun(@numel,BW.PixelIdxList).',BW.PixelIdxList.','VariableNames',{'NumPix','IdxList'});
Table.ID=(1:size(Table,1)).';
Table.Volume=Table.NumPix*prod(Res(1:3)); % calculate Volume in µm^3 of each cluster
Wave1=struct2table(regionprops(BW,'Centroid'));
Table.Centroid=Wave1.Centroid; % calculate center of mass of each cluster
Table.Centroid(:,1:3)=Table.Centroid(:,[2,1,3]);
Table.XYZum(:,1:3)=Table.Centroid.*repmat(Res.',[size(Table,1),1]);
Table.XYZum=Table.XYZum-repmat(Um.'/2,[size(Table,1),1]);

BoutonIds=labelmatrix(BW); % generate 3D image mask assigning each voxel the ID of the cluster that it belongs to
clear BW;

% Calculate maximal area in XY. Due to the strong spherical aberration of two-photon microscopy small VGLUT1-Venus positive structures (synapses) appear as elongated ellipses with approximately 3 times the diameter in axial as compared to lateral direction. Therefore maximal area in XY is used to obtain radius of each cluster
```

```
Wave1=accumarray_8({BoutonIds;repmat(permute(1:Pix(3),[1,3,2]),[Pix(1),Pix(2),1])},
ones(Pix.','uint8'),@sum,'2D');
Table.AreaXY=max(double(Wave1),[],2)*prod(Res(1:2));
Wave1=accumarray_8(BoutonIds,Distance,@max);
Table.DistInMax(Wave1.Roi1,1)=double(Wave1.Value)/10;

% Generate 3D-image in which each voxel is assigned the minimal radius of the
cluster that it belongs to. The minimal radius is the minimal distance value obtained
after 3D distance transformation.
Wave1=uint16(Table.DistInMax*10);
Wave1=Wave1(BoutonIds(BoutonIds>0));
Dystrophies2Radius=BoutonIds;
Dystrophies2Radius(BoutonIds>0)=Wave1;
Dystrophies2Radius=uint16(Dystrophies2Radius);

% Equivalent to the previous definition of "Dystrophies2Radius" another 3D-image is
generated in which each voxels is assigned the maximal volume of the cluster that it
belongs to
Wave1=uint16(ceil(Table.Volume));
Wave1=Wave1(BoutonIds(BoutonIds>0));
Dystrophies2=BoutonIds;
Dystrophies2(BoutonIds>0)=Wave1; Dystrophies2=uint16(Dystrophies2);

% Determine the maximum VGLUT1-Venus intensity value of each cluster
Wave1=accumarray_8(BoutonIds,VglutGreen,@max);
Table.VglutGreenMax(Wave1.Roi1,1)=Wave1.Value;
Table.VglutGreenHWI=uint16(Table.VglutGreenMax/2);

% Use the half-width intensity of each individual cluster to narrow down the size of
each cluster
Wave1=Table.VglutGreenHWI(BoutonIds(BoutonIds>0));
VglutGreenHWIbackground=BoutonIds;
VglutGreenHWIbackground(BoutonIds>0)=Wave1;
VglutGreenHWIbackground=uint16(VglutGreenHWIbackground);
VglutGreenHWIbackground=VglutGreen<VglutGreenHWIbackground;
BoutonIds(VglutGreenHWIbackground==1)=0;
clear VglutGreenHWIbackground;

% After applying half-width intensity to norrow down the total size of VGLUT1-Venus
positive clusters obtain the radius of each cluster from maximal area in lateral
directions.
Wave1=accumarray_8({BoutonIds;repmat(permute(1:Pix(3),[1,3,2]),[Pix(1),Pix(2),1])},
ones(Pix.','uint8'),@sum,'2D');
Table.AreaXYHWI=max(double(Wave1),[],2)*prod(Res(1:2));

% Calculate the minimum value of 3D distance transformation for each cluster
Wave1=accumarray_8(BoutonIds,Distance,@min);
clear Distance;
Table.DistInMin(Wave1.Roi1,1)=double(Wave1.Value)/10;
Table.DistInDiff=Table.DistInMax-Table.DistInMin;
```

```
% Determine the volume of each VGLUT1-Venus positive cluster after applying half-width intensity as limiting criterium.
Wave1=accumarray_8(BoutonIds,ones(Pix.','uint8'),@sum);
Table.VolumeHWI(Wave1.Roi1,1)=double(Wave1.Value)*prod(Res(:));

% For each cluster calculate the mean intensity of VGLUT1-Venus, autofluorescence and the ratio between both (GRratio).
GRratio=uint16(single(VglutGreen)./single(VglutRed)*2000);
IntensityData={'VglutGreen',VglutGreen;'VglutRed',VglutRed;'GRratio',GRratio};
clear VglutRed;
for m=1:size(IntensityData,1)
   Wave1=accumarray_8(BoutonIds,IntensityData{m,2},@mean);
    Table{Wave1.Roi1,[IntensityData{m,1},'Mean']}=Wave1.Value;
end
clear IntensityData;
% Obtain relevant information on VGLUT1-Venus positive clusters as table.
BoutonList=Table(:,{'ID','XYZum','AreaXY','AreaXYHWI','Volume','VolumeHWI','DistInMin','DistInMax','DistInDiff','VglutGreenMax','VglutGreenHWI','VglutGreenMean','VglutRedMean','GRatioMean','Centroid','NumPix'});

% Generate a 3D-image in which each Cluster-ID is assigned a random value between 2 and 256. This allows for visual quality control when monitoring the data in Imaris.
Wave1=find(BoutonIds==0);
BoutonIds=(double(BoutonIds)-floor(double(BoutonIds)/256)*256);
BoutonIds(Wave1)=0;

%% subfunction
% Calculates the percentile for a 3D-image.
% Inside: If necessary a 3D mask of type logical  can be used to limit the calculation to all voxels ascribed the value 1.
function [Result]=prctile_2(Data,Percentiles,Inside)
Data=Data(:);
if exist('Inside')==1
    Inside=Inside(:);
    Data=Data(Inside==1,:);
end
Data=sort(Data);

Ind=round(size(Data,1)*Percentiles/100);
Ind(Ind==0)=1;
if isempty(Data)
    Result=nan(size(Percentiles,1),1);
else
    Result=Data(Ind);
end


%% subfunction
% In a 3D-mask of type logical "Islands" are identified. These are clusters of voxels with value 0 that are entirely enclosed by voxels of value 1.
% MinMaxVolume: can be applied to limit the allowed volume of detected "Islands"
% In the output "Data3D" all detected Islands are set to value 1.
function
[Data3D,Islands]=removeIslands_3(Data3D,Connectivity,MinMaxVolume,Res3D)
Pix=size(Data3D).';
BW=bwconncomp(1-Data3D,Connectivity);

Table=table;
Table.NumPix=cellfun(@numel,BW.PixelIdxList).';
Table.IdxList=BW.PixelIdxList.';
Table.Volume=Table.NumPix*Res3D;
Wave1=struct2table(regionprops(BW,'BoundingBox'));
Table.BoundingBox(:,1:6)=Wave1.BoundingBox;
clear BW;
if exist('MinMaxVolume')==1
    Table=Table(Table.Volume>=MinMaxVolume(1) &
Table.Volume<MinMaxVolume(2),:);
end
Table.BoundingBox(:,1:3)=Table.BoundingBox(:,1:3)+0.5;
Table.BoundingBox(:,4:6)=Table.BoundingBox(:,1:3)+Table.BoundingBox(:,4:6)-1;
Wave1=[1,1,1,Pix.'];
Table.BoundingBox=Table.BoundingBox-repmat(Wave1,[size(Table,1),1]);
if Connectivity==4
    Table.BorderTouch=min(abs(Table.BoundingBox(:,[1,2,4,5])),[],2)==0;
else
    Table.BorderTouch=min(abs(Table.BoundingBox),[],2)==0;
end
Table=Table(Table.BorderTouch==0,:);
Islands=zeros(size(Data3D),'uint8');
Islands(cell2mat(Table.IdxList))=1;
Data3D(Islands==1)=1;

%% subfunction
% Calculates 3D distance transformation with anisotropic resolution
function
[DistInOut,Membership,Dist2Border]=distanceMat_4(Data3D,Output,Res,UmBin,OutC
alc,InCalc,ZeroBin,DistanceBitType)

if exist('ZeroBin','var')==0
    ZeroBin=50;
end
if exist('DistanceBitType','var')==0
    DistanceBitType='uint8';
end
if exist('OutCalc')~=1
    OutCalc=0;
end
if exist('InCalc')~=1
    InCalc=0;
end
if exist('Output')~=1
    Output={'DistInOut';'Membership';'Dist2Border';};
end
```

```
if ischar(Output)
   Output={Output};
end

if exist('UmBin')~=1 || isempty(UmBin)
   UmBin=1;
end
Pix=[size(Data3D,1);size(Data3D,2);size(Data3D,3)];
if exist('Res')~=1
   Res=Um./Pix;
end
if exist('ResCalc')~=1
   ResCalc=min(Res(:));
end
PixCalc=round(Pix.*Res/ResCalc);

Xi=round(linspace(1,Pix(1),PixCalc(1)));
Yi=round(linspace(1,Pix(2),PixCalc(2)));
Zi=round(linspace(1,Pix(3),PixCalc(3)));
Xt=round(linspace(1,PixCalc(1),Pix(1)));
Yt=round(linspace(1,PixCalc(2),Pix(2)));
Zt=round(linspace(1,PixCalc(3),Pix(3)));

Dist2Border=[];
DistInOut=[];
Membership=[];

if strfind1(Output,'Membership',1)
end

cprintf('text','DistanceTransform: ');
Data3D=Data3D(Xi,Yi,Zi);
if OutCalc==1
   if strfind1(Output,'DistInOut',1) && strfind1(Output,'Membership',1)
      [DistInOut,Membership]=bwdist(Data3D,'quasi-euclidean');
   elseif strfind1(Output,'DistInOut',1)
      [DistInOut]=bwdist(Data3D,'quasi-euclidean');
   elseif strfind1(Output,'Membership',1)
      [Membership]=bwdist(Data3D,'quasi-euclidean');
   end
   if strfind1(Output,'DistInOut',1)
      DistInOut=cast(ceil(DistInOut(Xt,Yt,Zt)*ResCalc/UmBin),DistanceBitType); %
convert pixel based distance into µm based distance
   end
   if strfind1(Output,'Membership',1)
      Membership(:)=Data3D(Membership(:));
      Membership=cast(Membership(Xt,Yt,Zt),DistanceBitType);
   end
end
if InCalc==1 && strfind1(Output,'DistInOut',1) % inside
   Data3D=logical(Data3D)==0; % invert so that everything outside plaque is set to 1
   [DistIn]=bwdist(Data3D,'quasi-euclidean'); % make distance transform for inside and
store in Stack
   DistIn=cast(ceil(DistIn(Xt,Yt,Zt)*ResCalc/UmBin),DistanceBitType);
end
clear Data3D;
if strfind1(Output,'DistInOut',1)
   if OutCalc==1 && InCalc==1
      DistInOut=DistInOut+ZeroBin-(DistIn-UmBin);
   elseif OutCalc==1 && InCalc==0
      DistInOut=DistInOut+ZeroBin;
   elseif OutCalc==0 && InCalc==1
      DistInOut=DistIn+ZeroBin;
   end
   clear DistIn;
end
if strfind1(Output,'Dist2Border')
   Dist2Border=zeros(PixCalc(1),PixCalc(2),PixCalc(3),DistanceBitType);
   Dist2Border(1,:,:)=1; Dist2Border(end,:,:)=1; Dist2Border(:,1,:)=1;
Dist2Border(:,end,:)=1; Dist2Border(:,:,1)=1; Dist2Border(:,:,end)=1;
   Dist2Border=bwdist(Dist2Border,'quasi-euclidean'); % make distance transform for
inside and store in Stack
   Dist2Border=(cast((Dist2Border-1)*ResCalc/UmBin,DistanceBitType));
   Dist2Border=Dist2Border(Xt,Yt,Zt,:);
end
cprintf('text','\n');

%% subfunction
% Calculates the function specified in "Function" for all individual rois specified in
"Rois"
function
[Output]=accumarray_8(Rois,Data,Function,OutputFormat,AccumMethod,CountInstan
ces)

if exist('OutputFormat')~=1
   OutputFormat='Table';
end

if istable(Rois)
   Wave1=table;
   for m=1:size(Rois,2)
      Wave1.Data(m,1)={Rois{:,m}};
   end
   Wave1.Name=Rois.Properties.VariableNames.';
   Rois=Wave1;
   clear Wave1;
elseif isnumeric(Rois)
   Wave1=table;
   Wave1.Data(1)={Rois};
   Wave1.Name(1)={'Roi1'};
   Rois=Wave1;
   clear Wave1;
elseif iscell(Rois)
```

```
    Rois=array2table(Rois,'VariableNames',{'Data';'Name'});
end
RoiNumber=size(Rois,1);

for Row=1:size(Rois,1)
    [Rois.Unique{Row},~,Rois.Data{Row}]=unique(Rois.Data{Row});
    Max=max(Rois.Data{Row});
    if Max<=255
        Rois.Data{Row}=uint8(Rois.Data{Row});
    elseif Max<=65535
        Rois.Data{Row}=uint16(Rois.Data{Row});
    elseif Max<=2^32-1
        Rois.Data{Row}=uint32(Rois.Data{Row});
    else
        keyboard;
    end
    Rois.Digits(Row,1)=size(num2str(round(Max)),2);
end

TotalDigits=sum(Rois.Digits);
Pix=size(Rois.Data{1,1}).';
Roi=zeros(Pix.','uint64');

for Row=1:size(Rois,1)
    Roi=Roi+uint64(Rois.Data{Row,1})*10^sum(Rois.Digits(Row+1:end)); % donot use
double, otherwise weird summation problems!!!, rather try uint64
end

if max(Roi(:))==uint64(2^64); keyboard; end;
SparseRoi=Roi;
[UniqueRoi,~,Roi]=unique(Roi);
Rois(:,'Data') = [];
if isempty(Data)
    Data=[]; % in case an empty table is transferred
    Data=[{ones(Pix.','uint8'),'Count'};Data];
elseif isnumeric(Data)
    Data={Data};
elseif istable(Data)
    clear Wave1;
    if exist('CountInstances')==1 && strcmp(CountInstances,'CountInstances')
        Data.CountInstances(:,1)=1;
    end
    for m=1:size(Data,2)
        Wave1(m,1)={Data{:,m}};
    end
    Wave1(:,2)=Data.Properties.VariableNames.';
    Data=Wave1;
    clear Wave1;
end

if size(Data,2)==1
    Data(:,2)=strcat('Value',num2str Array_3((1:size(Data,1)).'));
```

```
end

Data=array2table(Data,'VariableNames',{'Data';'Name'});

if exist('AccumMethod')~=1
    AccumMethod='NonSparse';
end
Output=table;
for Row=1:size(Data,1)
    if strcmp(Data.Name{Row,1},'CountInstances')
        Function=@nansum; % donot set back because is anyways the last Dataset
    end

    if strcmp(AccumMethod,'Sparse')
        keyboard; % attention! zero values in AccumArray are excluded!!!!

AccumArray=accumarray(double(Roi(:)),full(double(Data.Data{Row,1}(:))),[],Function,[]
,true);
        Ind=find(AccumArray);
    elseif strcmp(AccumMethod,'NonSparse')

AccumArray=accumarray(double(Roi(:)),full(double(Data.Data{Row,1}(:))),[],Function);
        Ind=(1:size(AccumArray,1)).';
    end
    if Row==1
        Output.LinRoi=Ind;
        Output{:,Data.Name{Row}}=AccumArray(Ind);
    else
        [~,Wave1]=ismember(Ind,Output.LinRoi);
        ZeroInd=find(Wave1==0);
        Wave1(ZeroInd)=(size(Output,1)+1:1:size(Output,1)+size(ZeroInd,1));
        Output.LinRoi(Wave1,1)=Ind;
        Output{Wave1,Data.Name{Row}}=AccumArray(Ind);
    end
    clear AccumArray;
end

Output.LinRoi=UniqueRoi(Output.LinRoi);
for m=1:RoiNumber
    MinMax=[sum(Rois.Digits(m+1:end))+1;sum(Rois.Digits(m:end))];
    Wave1=getNthNumeric(Output.LinRoi,MinMax);
    Wave1=Rois.Unique{m}(Wave1);
    Output{:,Rois.Name{m}}=Wave1;
end
clear Roi; clear Data;

if strcmp(OutputFormat,'2D')
    keyboard;
    OrigOutput=Output;
    Output=zeros(0,0,'uint32');
    for m=1:max(OrigOutput.Roi2)
        Ind=find(OrigOutput.Roi2==m);
        Output(OrigOutput.Roi1(Ind),m)=OrigOutput.Value(Ind);
    end
end
Output(:,'LinRoi')=[];
```

5. List of Figures

Figure 1. Aβ plaques are surrounded by axonal dystrophies. 6

Figure 2. Illustration of the amyloid cascade hypothesis. 11

Figure 3. Simplified Jabłoński-diagram for illustration of one-photon versus two-photon exciation for the fluorophore eGFP 23

Figure 4. Composition of an average vesicle synaptic vesicle 25

Figure 5. BACE1 inhibition significantly reduces Aβ40 and Aβ42 levels 26

Figure 6. In vivo two-photon imaging of plaques and associated synaptic pathology. 28

Figure 7. Procedure for determination of plaque growth kinetics 29

Figure 8. BACE1 inhibition most effectively reduces formation of new plaques. 31

Figure 9. After BACE1 inhibition pre-existing plaques remain smaller and, less small plaques are detected 32

Figure 10. BACE1 inhibition reduces plaque growth independent of plaque size. 33

Figure 11. Pre-existing plaques locally enhance further formation of new plaques. ... 35

Figure 12. Inhibition of BACE1 activity does not prevent BACE1 accumulation in peri-plaque dystrophies. 37

Figure 13. BACE1 inhibition mitigates progressive axonal pathology. 38

Figure 14. BACE1 inhibition mitigates progression of presynaptic dystrophies. 40

Figure 15. BACE1 inhibition does not prevent plaque-associated bouton loss. 41

Figure 16. Hypothetical model on the impact of different therapeutic BACE1 inhibitor approaches on the kinetics of amyloid deposition. 47

6. List of Tables

Table 1. Materials for cranial window implantation. 54

Table 2. Imaging settings for acquisition of Methoxy-X04 and VGLUT1^{Venus} fluorescence. 57

Table 3. Software 60

7. Reference

1. Bateman RJ, Xiong C, Benzinger TLS, Fagan AM, Goate A, Fox NC, et al. Clinical and Biomarker Changes in Dominantly Inherited Alzheimer's Disease. N Engl J Med. 2012 Aug 30;367(9):795–804.

2. Forsyth E, Ritzline PD. An overview of the etiology, diagnosis, and treatment of Alzheimer disease. Phys Ther. 1998 Dec;78(12):1325–31.

3. Alzheimer's Association. 2016 Alzheimer's disease facts and figures. Alzheimers Dement J Alzheimers Assoc. 2016 Apr;12(4):459–509.

4. Ziegler-Graham K, Brookmeyer R, Johnson E, Arrighi HM. Worldwide variation in the doubling time of Alzheimer's disease incidence rates. Alzheimers Dement J Alzheimers Assoc. 2008 Sep;4(5):316–23.

5. Alois Alzheimer. Über eine eigenartige Erkrankung der Hirnrinde. Allg Z Psychiatr Psych-Gerichtl Med. 1907;64:146–8.

6. Cummings JL, Morstorf T, Zhong K. Alzheimer's disease drug-development pipeline: few candidates, frequent failures. Alzheimers Res Ther. 2014;6(4):37.

7. Weintraub S, Wicklund AH, Salmon DP. The Neuropsychological Profile of Alzheimer Disease. Cold Spring Harb Perspect Med [Internet]. 2012 Apr;2(4). Available from: http://www.ncbi.nlm.nih.gov/pmc/articles/PMC3312395/

8. Selkoe DJ. Alzheimer's disease is a synaptic failure. Science. 2002 Oct 25;298(5594):789–91.

9. Sütterlin S, Hoßmann I, Klingholz R. Demenz-Report. Techn Ber Berl-Inst Für Bevölk Entwickl. 2011 Feb;(1).

10. Dickerson BC, Stoub TR, Shah RC, Sperling RA, Killiany RJ, Albert MS, et al. Alzheimer-signature MRI biomarker predicts AD dementia in cognitively normal adults. Neurology. 2011 Apr 19;76(16):1395–402.

11. Mandelkow EM, Mandelkow E. Tau in Alzheimer's disease. Trends Cell Biol. 1998 Nov;8(11):425–7.

12. Terry RD. Neuropathological changes in Alzheimer disease. Prog Brain Res. 1994;101:383–90.

13. Trojanowski JQ, Lee VM. "Fatal attractions" of proteins. A comprehensive hypothetical mechanism underlying Alzheimer's disease and other neurodegenerative disorders. Ann N Y Acad Sci. 2000;924:62–7.

14. Iqbal K, Grundke-Iqbal I. Neurofibrillary pathology leads to synaptic loss and not the other way around in Alzheimer disease. J Alzheimers Dis JAD. 2002 Jun;4(3):235–8.

15. Beach TG, Walker R, McGeer EG. Patterns of gliosis in Alzheimer's disease and aging cerebrum. Glia. 1989;2(6):420–36.

16. Itagaki S, McGeer PL, Akiyama H, Zhu S, Selkoe D. Relationship of microglia and astrocytes to amyloid deposits of Alzheimer disease. J Neuroimmunol. 1989 Oct;24(3):173–82.

17. Rogers J, Luber-Narod J, Styren SD, Civin WH. Expression of immune system-associated antigens by cells of the human central nervous system: relationship to the pathology of Alzheimer's disease. Neurobiol Aging. 1988 Aug;9(4):339–49.

18. Virchow R. Ueber eine im Gehirn und Rückenmark des Menschen aufgefundene Substanz mit der chemischen Reaction der Cellulose. Arch Für Pathol Anat Physiol Für Klin Med. 1854;6:135–8.

19. Friedreich PDN, Kekulé PDA. Zur Amyloidfrage. Arch Für Pathol Anat Physiol Für Klin Med. 1859;16:50–65.

20. Cruz L, Urbanc B, Buldyrev SV, Christie R, Gómez-Isla T, Havlin S, et al. Aggregation and disaggregation of senile plaques in Alzheimer disease. Proc Natl Acad Sci U S A. 1997 Jul 8;94(14):7612–6.

21. Glenner GG, Wong CW. Alzheimer's disease: initial report of the purification and characterization of a novel cerebrovascular amyloid protein. Biochem Biophys Res Commun. 1984 May 16;120(3):885–90.

22. Masters CL, Simms G, Weinman NA, Multhaup G, McDonald BL, Beyreuther K. Amyloid plaque core protein in Alzheimer disease and Down syndrome. Proc Natl Acad Sci U S A. 1985 Jun;82(12):4245–9.

23. Cummings JL, Vinters HV, Cole GM, Khachaturian ZS. Alzheimer's disease: etiologies, pathophysiology, cognitive reserve, and treatment opportunities. Neurology. 1998 Jul;51(1 Suppl 1):S2-17; discussion S65-67.

24. Rak M, Del Bigio MR, Mai S, Westaway D, Gough K. Dense-core and diffuse Abeta plaques in TgCRND8 mice studied with synchrotron FTIR microspectroscopy. Biopolymers. 2007 Nov;87(4):207–17.

25. Dickson DW. The pathogenesis of senile plaques. J Neuropathol Exp Neurol. 1997 Apr;56(4):321–39.

26. Thal DR, Braak H. [Post-mortem diagnosis of Alzheimer's disease]. Pathol. 2005 May;26(3):201–13.

27. Selkoe DJ. Alzheimer's disease: genes, proteins, and therapy. Physiol Rev. 2001 Apr;81(2):741–66.

28. Blennow K, Zetterberg H, Fagan AM. Fluid biomarkers in Alzheimer disease. Cold Spring Harb Perspect Med. 2012 Sep 1;2(9):a006221.

29. Braak H, Braak E. Alzheimer's disease: striatal amyloid deposits and neurofibrillary changes. J Neuropathol Exp Neurol. 1990 May;49(3):215–24.

30. Braak H, Braak E. Neuropathological stageing of Alzheimer-related changes. Acta Neuropathol (Berl). 1991;82(4):239–59.

31. Braak H, Braak E. Frequency of stages of Alzheimer-related lesions in different age categories. Neurobiol Aging. 1997 Aug;18(4):351–7.

32. Braak H, Tredici KD. Alzheimer's disease: intraneuronal alterations precede insoluble amyloid-β formation. Neurobiol Aging. 2004 Jul 1;25(6):713–8.

33. Thal DR, Rüb U, Orantes M, Braak H. Phases of A beta-deposition in the human brain and its relevance for the development of AD. Neurology. 2002 Jun 25;58(12):1791–800.

34. Arriagada PV, Growdon JH, Hedley-Whyte ET, Hyman BT. Neurofibrillary tangles but not senile plaques parallel duration and severity of Alzheimer's disease. Neurology. 1992 Mar;42(3 Pt 1):631–9.

35. Bierer LM, Hof PR, Purohit DP, Carlin L, Schmeidler J, Davis KL, et al. Neocortical neurofibrillary tangles correlate with dementia severity in Alzheimer's disease. Arch Neurol. 1995 Jan;52(1):81–8.

36. Giannakopoulos P, Herrmann FR, Bussière T, Bouras C, Kövari E, Perl DP, et al. Tangle and neuron numbers, but not amyloid load, predict cognitive status in Alzheimer's disease. Neurology. 2003 May 13;60(9):1495–500.

37. Weingarten MD, Lockwood AH, Hwo SY, Kirschner MW. A protein factor essential for microtubule assembly. Proc Natl Acad Sci U S A. 1975 May;72(5):1858–62.

38. Wischik CM, Novak M, Thøgersen HC, Edwards PC, Runswick MJ, Jakes R, et al. Isolation of a fragment of tau derived from the core of the paired helical filament of Alzheimer disease. Proc Natl Acad Sci U S A. 1988 Jun;85(12):4506–10.

39. Schweers O, Schönbrunn-Hanebeck E, Marx A, Mandelkow E. Structural studies of tau protein and Alzheimer paired helical filaments show no evidence for beta-structure. J Biol Chem. 1994 Sep 30;269(39):24290–7.

40. Cleveland DW, Hwo SY, Kirschner MW. Physical and chemical properties of purified tau factor and the role of tau in microtubule assembly. J Mol Biol. 1977 Oct 25;116(2):227–47.

41. Drubin DG, Kirschner MW. Tau protein function in living cells. J Cell Biol. 1986 Dec;103(6 Pt 2):2739–46.

42. Kar S, Fan J, Smith MJ, Goedert M, Amos LA. Repeat motifs of tau bind to the insides of microtubules in the absence of taxol. EMBO J. 2003 Jan 2;22(1):70–7.

43. Mandelkow EM, Biernat J, Drewes G, Gustke N, Trinczek B, Mandelkow E. Tau domains, phosphorylation, and interactions with microtubules. Neurobiol Aging. 1995 Jun;16(3):355-362; discussion 362-363.

44. Trinczek B, Biernat J, Baumann K, Mandelkow EM, Mandelkow E. Domains of tau protein, differential phosphorylation, and dynamic instability of microtubules. Mol Biol Cell. 1995 Dec;6(12):1887–902.

45. Esmaeli-Azad B, McCarty JH, Feinstein SC. Sense and antisense transfection analysis of tau function: tau influences net microtubule assembly, neurite outgrowth and neuritic stability. J Cell Sci. 1994 Apr;107 (Pt 4):869–79.

46. Litman P, Barg J, Rindzoonski L, Ginzburg I. Subcellular localization of tau mRNA in differentiating neuronal cell culture: implications for neuronal polarity. Neuron. 1993 Apr;10(4):627–38.

47. Ebneth A, Godemann R, Stamer K, Illenberger S, Trinczek B, Mandelkow E. Overexpression of tau protein inhibits kinesin-dependent trafficking of vesicles, mitochondria, and endoplasmic reticulum: implications for Alzheimer’s disease. J Cell Biol. 1998 Nov 2;143(3):777–94.

48. Bancher C, Brunner C, Lassmann H, Budka H, Jellinger K, Wiche G, et al. Accumulation of abnormally phosphorylated tau precedes the formation of neurofibrillary tangles in Alzheimer’s disease. Brain Res. 1989 Jan 16;477(1–2):90–9.

49. Köpke E, Tung YC, Shaikh S, Alonso AC, Iqbal K, Grundke-Iqbal I. Microtubule-associated protein tau. Abnormal phosphorylation of a non-paired helical filament pool in Alzheimer disease. J Biol Chem. 1993 Nov 15;268(32):24374–84.

50. Mandelkow EM, Biernat J, Drewes G, Gustke N, Trinczek B, Mandelkow E. Tau domains, phosphorylation, and interactions with microtubules. Neurobiol Aging. 1995 Jun;16(3):355-362; discussion 362-363.

51. Ebneth A, Godemann R, Stamer K, Illenberger S, Trinczek B, Mandelkow E. Overexpression of tau protein inhibits kinesin-dependent trafficking of vesicles, mitochondria, and endoplasmic reticulum: implications for Alzheimer’s disease. J Cell Biol. 1998 Nov 2;143(3):777–94.

52. Braak F, Braak H, Mandelkow E-M. A sequence of cytoskeleton changes related to the formation of neurofibrillary tangles and neuropil threads. Acta Neuropathol (Berl). 1994 Jun 1;87(6):554–67.

53. Bancher C, Brunner C, Lassmann H, Budka H, Jellinger K, Wiche G, et al. Accumulation of abnormally phosphorylated τ precedes the formation of neurofibrillary tangles in Alzheimer’s disease. Brain Res. 1989 Jan 16;477(1–2):90–9.

54. Carmel G, Mager EM, Binder LI, Kuret J. The structural basis of monoclonal antibody Alz50's selectivity for Alzheimer's disease pathology. J Biol Chem. 1996 Dec 20;271(51):32789–95.

55. Arnold SE, Hyman BT, Flory J, Damasio AR, Van Hoesen GW. The topographical and neuroanatomical distribution of neurofibrillary tangles and neuritic plaques in the cerebral cortex of patients with Alzheimer's disease. Cereb Cortex N Y N 1991. 1991 Feb;1(1):103–16.

56. Su JH, Cummings BJ, Cotman CW. Identification and distribution of axonal dystrophic neurites in Alzheimer's disease. Brain Res. 1993 Oktober;625(2):228–37.

57. Holtzman DM, Morris JC, Goate AM. Alzheimer's disease: the challenge of the second century. Sci Transl Med. 2011 Apr 6;3(77):77sr1.

58. Braak H, Braak E. Neuropathological stageing of Alzheimer-related changes. Acta Neuropathol (Berl). 1991;82(4):239–59.

59. Nelson PT, Alafuzoff I, Bigio EH, Bouras C, Braak H, Cairns NJ, et al. Correlation of Alzheimer disease neuropathologic changes with cognitive status: a review of the literature. J Neuropathol Exp Neurol. 2012 May;71(5):362–81.

60. Huang Y, Mucke L. Alzheimer mechanisms and therapeutic strategies. Cell. 2012 Mar 16;148(6):1204–22.

61. Serrano-Pozo A, Frosch MP, Masliah E, Hyman BT. Neuropathological alterations in Alzheimer disease. Cold Spring Harb Perspect Med. 2011 Sep;1(1):a006189.

62. Hof PR, Cox K, Morrison JH. Quantitative analysis of a vulnerable subset of pyramidal neurons in Alzheimer's disease: I. Superior frontal and inferior temporal cortex. J Comp Neurol. 1990 Nov 1;301(1):44–54.

63. Whitehouse PJ, Price DL, Struble RG, Clark AW, Coyle JT, Delon MR. Alzheimer's disease and senile dementia: loss of neurons in the basal forebrain. Science. 1982 Mar 5;215(4537):1237–9.

64. Gómez-Isla T, Price JL, McKeel DW, Morris JC, Growdon JH, Hyman BT. Profound loss of layer II entorhinal cortex neurons occurs in very mild Alzheimer's disease. J Neurosci Off J Soc Neurosci. 1996 Jul 15;16(14):4491–500.

65. Terry RD, Masliah E, Salmon DP, Butters N, DeTeresa R, Hill R, et al. Physical basis of cognitive alterations in Alzheimer's disease: synapse loss is the major correlate of cognitive impairment. Ann Neurol. 1991 Oct;30(4):572–80.

66. Boncristiano S, Calhoun ME, Howard V, Bondolfi L, Kaeser SA, Wiederhold K-H, et al. Neocortical synaptic bouton number is maintained despite robust amyloid deposition in APP23 transgenic mice. Neurobiol Aging. 2005 May;26(5):607–13.

67. Dong H, Martin MV, Chambers S, Csernansky JG. Spatial relationship between synapse loss and beta-amyloid deposition in Tg2576 mice. J Comp Neurol. 2007 Jan 10;500(2):311–21.

68. Grutzendler J, Helmin K, Tsai J, Gan W-B. Various dendritic abnormalities are associated with fibrillar amyloid deposits in Alzheimer’s disease. Ann N Y Acad Sci. 2007 Feb;1097:30–9.

69. King DL, Arendash GW. Maintained synaptophysin immunoreactivity in Tg2576 transgenic mice during aging: correlations with cognitive impairment. Brain Res. 2002 Feb 1;926(1–2):58–68.

70. Knafo S, Alonso-Nanclares L, Gonzalez-Soriano J, Merino-Serrais P, Fernaud-Espinosa I, Ferrer I, et al. Widespread changes in dendritic spines in a model of Alzheimer’s disease. Cereb Cortex N Y N 1991. 2009 Mar;19(3):586–92.

71. Koffie RM, Meyer-Luehmann M, Hashimoto T, Adams KW, Mielke ML, Garcia-Alloza M, et al. Oligomeric amyloid beta associates with postsynaptic densities and correlates with excitatory synapse loss near senile plaques. Proc Natl Acad Sci U S A. 2009 Mar 10;106(10):4012–7.

72. Spires TL. Dendritic Spine Abnormalities in Amyloid Precursor Protein Transgenic Mice Demonstrated by Gene Transfer and Intravital Multiphoton Microscopy. J Neurosci. 2005 Aug 3;25(31):7278–87.

73. Spires-Jones TL, Meyer-Luehmann M, Osetek JD, Jones PB, Stern EA, Bacskai BJ, et al. Impaired spine stability underlies plaque-related spine loss in an Alzheimer’s disease mouse model. Am J Pathol. 2007 Oct;171(4):1304–11.

74. Tsai J, Grutzendler J, Duff K, Gan W-B. Fibrillar amyloid deposition leads to local synaptic abnormalities and breakage of neuronal branches. Nat Neurosci. 2004 Nov;7(11):1181–3.

75. Selkoe DJ. The molecular pathology of Alzheimer’s disease. Neuron. 1991 Apr;6(4):487–98.

76. Sadleir KR, Kandalepas PC, Buggia-Prévot V, Nicholson DA, Thinakaran G, Vassar R. Presynaptic dystrophic neurites surrounding amyloid plaques are sites of microtubule disruption, BACE1 elevation, and increased Aβ generation in Alzheimer’s disease. Acta Neuropathol (Berl). 2016 Aug;132(2):235–56.

77. Gowrishankar S, Yuan P, Wu Y, Schrag M, Paradise S, Grutzendler J, et al. Massive accumulation of luminal protease-deficient axonal lysosomes at Alzheimer’s disease amyloid plaques. Proc Natl Acad Sci U S A. 2015 Jul 14;112(28):E3699-3708.

78. Kandalepas PC, Sadleir KR, Eimer WA, Zhao J, Nicholson DA, Vassar R. The Alzheimer’s β-secretase BACE1 localizes to normal presynaptic terminals and to dystrophic presynaptic terminals surrounding amyloid plaques. Acta Neuropathol (Berl). 2013 Jul 3;126(3):329–52.

79. Sanchez-Varo R, Trujillo-Estrada L, Sanchez-Mejias E, Torres M, Baglietto-Vargas D, Moreno-Gonzalez I, et al. Abnormal accumulation of autophagic vesicles correlates with axonal and synaptic pathology in young Alzheimer's mice hippocampus. Acta Neuropathol (Berl). 2011 Oct 22;123(1):53–70.

80. Wong PC, Marszalek J, Crawford TO, Xu Z, Hsieh ST, Griffin JW, et al. Increasing neurofilament subunit NF-M expression reduces axonal NF-H, inhibits radial growth, and results in neurofilamentous accumulation in motor neurons. J Cell Biol. 1995 Sep;130(6):1413–22.

81. Zhang X-M, Cai Y, Xiong K, Cai H, Luo X-G, Feng J-C, et al. Beta-secretase-1 elevation in transgenic mouse models of Alzheimer's disease is associated with synaptic/axonal pathology and amyloidogenesis: implications for neuritic plaque development. Eur J Neurosci. 2009 Dec;30(12):2271–83.

82. Grutzendler J, Helmin K, Tsai J, Gan W-B. Various dendritic abnormalities are associated with fibrillar amyloid deposits in Alzheimer's disease. Ann N Y Acad Sci. 2007 Feb;1097:30–9.

83. Nimchinsky EA, Sabatini BL, Svoboda K. Structure and function of dendritic spines. Annu Rev Physiol. 2002;64:313–53.

84. Yuste R, Bonhoeffer T. Morphological changes in dendritic spines associated with long-term synaptic plasticity. Annu Rev Neurosci. 2001;24:1071–89.

85. Yuste R. Dendritic spines and distributed circuits. Neuron. 2011 Sep 8;71(5):772–81.

86. DeKosky ST, Scheff SW. Synapse loss in frontal cortex biopsies in Alzheimer's disease: correlation with cognitive severity. Ann Neurol. 1990 May;27(5):457–64.

87. Scheff SW, DeKosky ST, Price DA. Quantitative assessment of cortical synaptic density in Alzheimer's disease. Neurobiol Aging. 1990 Feb;11(1):29–37.

88. Masliah E, Mallory M, Hansen L, Richard D, Alford M, Terry R. Synaptic and neuritic alterations during the progression of Alzheimer's disease. Neurosci Lett. 1994 Jun 6;174(1):67–72.

89. Radde R, Bolmont T, Kaeser SA, Coomaraswamy J, Lindau D, Stoltze L, et al. Aβ42-driven cerebral amyloidosis in transgenic mice reveals early and robust pathology. EMBO Rep. 2006 Aug 11;7(9):940–6.

90. Herzog E, Nadrigny F, Silm K, Biesemann C, Helling I, Bersot T, et al. In Vivo Imaging of Intersynaptic Vesicle Exchange Using VGLUT1Venus Knock-In Mice. J Neurosci. 2011 Oct 26;31(43):15544–59.

91. Glenner GG, Wong CW. Alzheimer's disease: initial report of the purification and characterization of a novel cerebrovascular amyloid protein. Biochem Biophys Res Commun. 1984 May 16;120(3):885–90.

92. Kang J, Lemaire HG, Unterbeck A, Salbaum JM, Masters CL, Grzeschik KH, et al. The precursor of Alzheimer’s disease amyloid A4 protein resembles a cell-surface receptor. Nature. 1987 Feb 19;325(6106):733–6.

93. Campion D, Dumanchin C, Hannequin D, Dubois B, Belliard S, Puel M, et al. Early-onset autosomal dominant Alzheimer disease: prevalence, genetic heterogeneity, and mutation spectrum. Am J Hum Genet. 1999 Sep;65(3):664–70.

94. Chartier-Harlin MC, Crawford F, Houlden H, Warren A, Hughes D, Fidani L, et al. Early-onset Alzheimer’s disease caused by mutations at codon 717 of the beta-amyloid precursor protein gene. Nature. 1991 Oct 31;353(6347):844–6.

95. Goate A, Chartier-Harlin MC, Mullan M, Brown J, Crawford F, Fidani L, et al. Segregation of a missense mutation in the amyloid precursor protein gene with familial Alzheimer’s disease. Nature. 1991 Feb 21;349(6311):704–6.

96. Nilsberth C, Westlind-Danielsson A, Eckman CB, Condron MM, Axelman K, Forsell C, et al. The “Arctic” APP mutation (E693G) causes Alzheimer’s disease by enhanced Abeta protofibril formation. Nat Neurosci. 2001 Sep;4(9):887–93.

97. Scheuner D, Eckman C, Jensen M, Song X, Citron M, Suzuki N, et al. Secreted amyloid beta-protein similar to that in the senile plaques of Alzheimer’s disease is increased in vivo by the presenilin 1 and 2 and APP mutations linked to familial Alzheimer’s disease. Nat Med. 1996 Aug;2(8):864–70.

98. Hardy JA, Higgins GA. Alzheimer’s disease: the amyloid cascade hypothesis. Science. 1992 Apr 10;256(5054):184–5.

99. Coulson EJ, Paliga K, Beyreuther K, Masters CL. What the evolution of the amyloid protein precursor supergene family tells us about its function. Neurochem Int. 2000 Mar;36(3):175–84.

100. Wasco W, Bupp K, Magendantz M, Gusella JF, Tanzi RE, Solomon F. Identification of a mouse brain cDNA that encodes a protein related to the Alzheimer disease-associated amyloid beta protein precursor. Proc Natl Acad Sci U S A. 1992 Nov 15;89(22):10758–62.

101. Wasco W, Gurubhagavatula S, Paradis MD, Romano DM, Sisodia SS, Hyman BT, et al. Isolation and characterization of APLP2 encoding a homologue of the Alzheimer’s associated amyloid beta protein precursor. Nat Genet. 1993 Sep;5(1):95–100.

102. Goldgaber D, Lerman MI, McBride OW, Saffiotti U, Gajdusek DC. Characterization and chromosomal localization of a cDNA encoding brain amyloid of Alzheimer’s disease. Science. 1987 Feb 20;235(4791):877–80.

103. Robakis NK, Ramakrishna N, Wolfe G, Wisniewski HM. Molecular cloning and characterization of a cDNA encoding the cerebrovascular and the neuritic plaque amyloid peptides. Proc Natl Acad Sci U S A. 1987 Jun;84(12):4190–4.

104. Tanzi RE, Gusella JF, Watkins PC, Bruns GA, St George-Hyslop P, Van Keuren ML, et al. Amyloid beta protein gene: cDNA, mRNA distribution, and genetic linkage near the Alzheimer locus. Science. 1987 Feb 20;235(4791):880–4.

105. Rohan de Silva HA, Jen A, Wickenden C, Jen LS, Wilkinson SL, Patel AJ. Cell-specific expression of beta-amyloid precursor protein isoform mRNAs and proteins in neurons and astrocytes. Brain Res Mol Brain Res. 1997 Jul;47(1–2):147–56.

106. Kirazov E, Kirazov L, Bigl V, Schliebs R. Ontogenetic changes in protein level of amyloid precursor protein (APP) in growth cones and synaptosomes from rat brain and prenatal expression pattern of APP mRNA isoforms in developing rat embryo. Int J Dev Neurosci Off J Int Soc Dev Neurosci. 2001 Jun;19(3):287–96.

107. Koo EH, Sisodia SS, Archer DR, Martin LJ, Weidemann A, Beyreuther K, et al. Precursor of amyloid protein in Alzheimer disease undergoes fast anterograde axonal transport. Proc Natl Acad Sci U S A. 1990 Feb;87(4):1561–5.

108. Schubert W, Prior R, Weidemann A, Dircksen H, Multhaup G, Masters CL, et al. Localization of Alzheimer beta A4 amyloid precursor protein at central and peripheral synaptic sites. Brain Res. 1991 Nov 1;563(1–2):184–94.

109. Shigematsu K, McGeer PL, McGeer EG. Localization of amyloid precursor protein in selective postsynaptic densities of rat cortical neurons. Brain Res. 1992 Oct 2;592(1–2):353–7.

110. Haass C, Kaether C, Thinakaran G, Sisodia S. Trafficking and proteolytic processing of APP. Cold Spring Harb Perspect Med. 2012 May;2(5):a006270.

111. Haass C. Take five--BACE and the gamma-secretase quartet conduct Alzheimer's amyloid beta-peptide generation. EMBO J. 2004 Feb 11;23(3):483–8.

112. Kuhn P-H, Wang H, Dislich B, Colombo A, Zeitschel U, Ellwart JW, et al. ADAM10 is the physiologically relevant, constitutive alpha-secretase of the amyloid precursor protein in primary neurons. EMBO J. 2010 Sep 1;29(17):3020–32.

113. Esch FS, Keim PS, Beattie EC, Blacher RW, Culwell AR, Oltersdorf T, et al. Cleavage of amyloid beta peptide during constitutive processing of its precursor. Science. 1990 Jun 1;248(4959):1122–4.

114. Sisodia SS, Koo EH, Beyreuther K, Unterbeck A, Price DL. Evidence that beta-amyloid protein in Alzheimer's disease is not derived by normal processing. Science. 1990 Apr 27;248(4954):492–5.

115. De Strooper B, Saftig P, Craessaerts K, Vanderstichele H, Guhde G, Annaert W, et al. Deficiency of presenilin-1 inhibits the normal cleavage of amyloid precursor protein. Nature. 1998 Jan 22;391(6665):387–90.

116. Haass C, Selkoe DJ. Cellular processing of beta-amyloid precursor protein and the genesis of amyloid beta-peptide. Cell. 1993 Dec 17;75(6):1039–42.

117. Weidemann A, Paliga K, Dürrwang U, Reinhard FB, Schuckert O, Evin G, et al. Proteolytic processing of the Alzheimer's disease amyloid precursor protein within its cytoplasmic domain by caspase-like proteases. J Biol Chem. 1999 Feb 26;274(9):5823–9.

118. Sisodia SS, Koo EH, Beyreuther K, Unterbeck A, Price DL. Evidence that beta-amyloid protein in Alzheimer's disease is not derived by normal processing. Science. 1990 Apr 27;248(4954):492–5.

119. Seubert P, Oltersdorf T, Lee MG, Barbour R, Blomquist C, Davis DL, et al. Secretion of beta-amyloid precursor protein cleaved at the amino terminus of the beta-amyloid peptide. Nature. 1993 Jan 21;361(6409):260–3.

120. Yamashiro DJ, Maxfield FR. Acidification of endocytic compartments and the intracellular pathways of ligands and receptors. J Cell Biochem. 1984;26(4):231–46.

121. Fukumoto H, Cheung BS, Hyman BT, Irizarry MC. Beta-secretase protein and activity are increased in the neocortex in Alzheimer disease. Arch Neurol. 2002 Sep;59(9):1381–9.

122. De Strooper B. Aph-1, Pen-2, and Nicastrin with Presenilin generate an active gamma-Secretase complex. Neuron. 2003 Apr 10;38(1):9–12.

123. De Strooper B. Aph-1, Pen-2, and Nicastrin with Presenilin generate an active gamma-Secretase complex. Neuron. 2003 Apr 10;38(1):9–12.

124. Shoji M, Golde TE, Ghiso J, Cheung TT, Estus S, Shaffer LM, et al. Production of the Alzheimer amyloid beta protein by normal proteolytic processing. Science. 1992 Oct 2;258(5079):126–9.

125. Wolfe MS, Kopan R. Intramembrane proteolysis: theme and variations. Science. 2004 Aug 20;305(5687):1119–23.

126. Haass C, Selkoe DJ. Cellular processing of beta-amyloid precursor protein and the genesis of amyloid beta-peptide. Cell. 1993 Dec 17;75(6):1039–42.

127. Kakuda N, Funamoto S, Yagishita S, Takami M, Osawa S, Dohmae N, et al. Equimolar production of amyloid beta-protein and amyloid precursor protein intracellular domain from beta-carboxyl-terminal fragment by gamma-secretase. J Biol Chem. 2006 May 26;281(21):14776–86.

128. Szaruga M, Munteanu B, Lismont S, Veugelen S, Horré K, Mercken M, et al. Alzheimer's-Causing Mutations Shift Aβ Length by Destabilizing γ-Secretase-Aβn Interactions. Cell. 2017 Jul 27;170(3):443–456.e14.

129. Sgourakis NG, Yan Y, McCallum S, Wang C, Garcia AE. The Alzheimer's peptides Aβ40 and 42 adopt distinct conformations in water: A combined MD / NMR study. J Mol Biol. 2007 May 18;368(5):1448–57.

130. Jarrett JT, Berger EP, Lansbury PT. The carboxy terminus of the beta amyloid protein is critical for the seeding of amyloid formation: implications for the

pathogenesis of Alzheimer’s disease. Biochemistry (Mosc). 1993 May 11;32(18):4693–7.

131. McGowan E, Pickford F, Kim J, Onstead L, Eriksen J, Yu C, et al. Aβ42 Is Essential for Parenchymal and Vascular Amyloid Deposition in Mice. Neuron. 2005 Jul 21;47(2):191–9.

132. Mann DM, Iwatsubo T, Ihara Y, Cairns NJ, Lantos PL, Bogdanovic N, et al. Predominant deposition of amyloid-beta 42(43) in plaques in cases of Alzheimer’s disease and hereditary cerebral hemorrhage associated with mutations in the amyloid precursor protein gene. Am J Pathol. 1996 Apr;148(4):1257–66.

133. Wang R, Wang B, He W, Zheng H. Wild-type presenilin 1 protects against Alzheimer disease mutation-induced amyloid pathology. J Biol Chem. 2006 Jun 2;281(22):15330–6.

134. Wolfe MS. Inhibition and modulation of gamma-secretase for Alzheimer’s disease. Neurother J Am Soc Exp Neurother. 2008 Jul;5(3):391–8.

135. Hardy J, Selkoe DJ. The amyloid hypothesis of Alzheimer’s disease: progress and problems on the road to therapeutics. Science. 2002 Jul 19;297(5580):353–6.

136. Hardy J, Selkoe DJ. The amyloid hypothesis of Alzheimer’s disease: progress and problems on the road to therapeutics. Science. 2002 Jul 19;297(5580):353–6.

137. Selkoe DJ. The molecular pathology of Alzheimer’s disease. Neuron. 1991 Apr;6(4):487–98.

138. Haass C, Selkoe DJ. Soluble protein oligomers in neurodegeneration: lessons from the Alzheimer’s amyloid beta-peptide. Nat Rev Mol Cell Biol. 2007 Feb;8(2):101–12.

139. Masters CL, Simms G, Weinman NA, Multhaup G, McDonald BL, Beyreuther K. Amyloid plaque core protein in Alzheimer disease and Down syndrome. Proc Natl Acad Sci U S A. 1985 Jun;82(12):4245–9.

140. Olson MI, Shaw CM. Presenile dementia and Alzheimer’s disease in mongolism. Brain J Neurol. 1969 Mar;92(1):147–56.

141. Lai F, Williams RS. A prospective study of Alzheimer disease in Down syndrome. Arch Neurol. 1989 Aug;46(8):849–53.

142. Wisniewski KE, Wisniewski HM, Wen GY. Occurrence of neuropathological changes and dementia of Alzheimer’s disease in Down’s syndrome. Ann Neurol. 1985 Mar;17(3):278–82.

143. Shen J, Kelleher RJ. The presenilin hypothesis of Alzheimer’s disease: evidence for a loss-of-function pathogenic mechanism. Proc Natl Acad Sci U S A. 2007 Jan 9;104(2):403–9.

144. Mullan M, Crawford F, Axelman K, Houlden H, Lilius L, Winblad B, et al. A pathogenic mutation for probable Alzheimer’s disease in the APP gene at the N-terminus of beta-amyloid. Nat Genet. 1992 Aug;1(5):345–7.

145. O’Brien RJ, Wong PC. Amyloid precursor protein processing and Alzheimer’s disease. Annu Rev Neurosci. 2011;34:185–204.

146. Jonsson T, Atwal JK, Steinberg S, Snaedal J, Jonsson PV, Bjornsson S, et al. A mutation in APP protects against Alzheimer’s disease and age-related cognitive decline. Nature. 2012 Aug 2;488(7409):96–9.

147. Luo Y, Bolon B, Kahn S, Bennett BD, Babu-Khan S, Denis P, et al. Mice deficient in BACE1, the Alzheimer’s beta-secretase, have normal phenotype and abolished beta-amyloid generation. Nat Neurosci. 2001 Mar;4(3):231–2.

148. Kim J, Basak JM, Holtzman DM. The role of apolipoprotein E in Alzheimer’s disease. Neuron. 2009 Aug 13;63(3):287–303.

149. Huang Y-WA, Zhou B, Wernig M, Südhof TC. ApoE2, ApoE3, and ApoE4 Differentially Stimulate APP Transcription and Aβ Secretion. Cell. 2017 Jan 26;168(3):427–441.e21.

150. Poorkaj P, Bird TD, Wijsman E, Nemens E, Garruto RM, Anderson L, et al. Tau is a candidate gene for chromosome 17 frontotemporal dementia. Ann Neurol. 1998 Jun;43(6):815–25.

151. Spillantini MG, Bird TD, Ghetti B. Frontotemporal dementia and Parkinsonism linked to chromosome 17: a new group of tauopathies. Brain Pathol Zurich Switz. 1998 Apr;8(2):387–402.

152. Goedert M, Ghetti B, Spillantini MG. Frontotemporal dementia: implications for understanding Alzheimer disease. Cold Spring Harb Perspect Med. 2012 Feb;2(2):a006254.

153. Lewis J, Dickson DW, Lin WL, Chisholm L, Corral A, Jones G, et al. Enhanced neurofibrillary degeneration in transgenic mice expressing mutant tau and APP. Science. 2001 Aug 24;293(5534):1487–91.

154. Nussbaum JM, Schilling S, Cynis H, Silva A, Swanson E, Wangsanut T, et al. Prion-like behaviour and tau-dependent cytotoxicity of pyroglutamylated amyloid-β. Nature. 2012 May 31;485(7400):651–5.

155. Rapoport M, Dawson HN, Binder LI, Vitek MP, Ferreira A. Tau is essential to beta -amyloid-induced neurotoxicity. Proc Natl Acad Sci U S A. 2002 Apr 30;99(9):6364–9.

156. Roberson ED, Scearce-Levie K, Palop JJ, Yan F, Cheng IH, Wu T, et al. Reducing endogenous tau ameliorates amyloid beta-induced deficits in an Alzheimer’s disease mouse model. Science. 2007 May 4;316(5825):750–4.

157. Mairet-Coello G, Courchet J, Pieraut S, Courchet V, Maximov A, Polleux F. The CAMKK2-AMPK kinase pathway mediates the synaptotoxic effects of Aβ oligomers through Tau phosphorylation. Neuron. 2013 Apr 10;78(1):94–108.

158. Ittner LM, Götz J. Amyloid-β and tau--a toxic pas de deux in Alzheimer's disease. Nat Rev Neurosci. 2011 Feb;12(2):65–72.

159. Ittner LM, Ke YD, Delerue F, Bi M, Gladbach A, van Eersel J, et al. Dendritic function of tau mediates amyloid-beta toxicity in Alzheimer's disease mouse models. Cell. 2010 Aug 6;142(3):387–97.

160. Hussain I, Powell D, Howlett DR, Tew DG, Meek TD, Chapman C, et al. Identification of a novel aspartic protease (Asp 2) as beta-secretase. Mol Cell Neurosci. 1999 Dec;14(6):419–27.

161. Sinha S, Anderson JP, Barbour R, Basi GS, Caccavello R, Davis D, et al. Purification and cloning of amyloid precursor protein beta-secretase from human brain. Nature. 1999 Dec 2;402(6761):537–40.

162. Vassar R, Bennett BD, Babu-Khan S, Kahn S, Mendiaz EA, Denis P, et al. β-Secretase Cleavage of Alzheimer's Amyloid Precursor Protein by the Transmembrane Aspartic Protease BACE. Science. 1999 Oct 22;286(5440):735–41.

163. Yan R, Bienkowski MJ, Shuck ME, Miao H, Tory MC, Pauley AM, et al. Membrane-anchored aspartyl protease with Alzheimer's disease beta-secretase activity. Nature. 1999 Dec 2;402(6761):533–7.

164. Lin X, Koelsch G, Wu S, Downs D, Dashti A, Tang J. Human aspartic protease memapsin 2 cleaves the beta-secretase site of beta-amyloid precursor protein. Proc Natl Acad Sci U S A. 2000 Feb 15;97(4):1456–60.

165. Bennett BD, Babu-Khan S, Loeloff R, Louis JC, Curran E, Citron M, et al. Expression analysis of BACE2 in brain and peripheral tissues. J Biol Chem. 2000 Jul 7;275(27):20647–51.

166. Vassar R, Kovacs DM, Yan R, Wong PC. The β-Secretase Enzyme BACE in Health and Alzheimer's Disease: Regulation, Cell Biology, Function, and Therapeutic Potential. J Neurosci. 2009 Oct 14;29(41):12787–94.

167. Vassar R, Kuhn P-H, Haass C, Kennedy ME, Rajendran L, Wong PC, et al. Function, therapeutic potential and cell biology of BACE proteases: current status and future prospects. J Neurochem. 2014 Jul;130(1):4–28.

168. Kalvodova L, Kahya N, Schwille P, Ehehalt R, Verkade P, Drechsel D, et al. Lipids as modulators of proteolytic activity of BACE: involvement of cholesterol, glycosphingolipids, and anionic phospholipids in vitro. J Biol Chem. 2005 Nov 4;280(44):36815–23.

169. Bennett BD, Denis P, Haniu M, Teplow DB, Kahn S, Louis JC, et al. A furin-like convertase mediates propeptide cleavage of BACE, the Alzheimer's beta - secretase. J Biol Chem. 2000 Dec 1;275(48):37712–7.

170. Benjannet S, Elagoz A, Wickham L, Mamarbachi M, Munzer JS, Basak A, et al. Post-translational processing of beta-secretase (beta-amyloid-converting enzyme) and its ectodomain shedding. The pro- and transmembrane/cytosolic domains affect its cellular activity and amyloid-beta production. J Biol Chem. 2001 Apr 6;276(14):10879–87.

171. Vetrivel KS, Meckler X, Chen Y, Nguyen PD, Seidah NG, Vassar R, et al. Alzheimer disease Abeta production in the absence of S-palmitoylation-dependent targeting of BACE1 to lipid rafts. J Biol Chem. 2009 Feb 6;284(6):3793–803.

172. Pastorino L, Ikin AF, Nairn AC, Pursnani A, Buxbaum JD. The carboxyl-terminus of BACE contains a sorting signal that regulates BACE trafficking but not the formation of total A(beta). Mol Cell Neurosci. 2002 Feb;19(2):175–85.

173. Kinoshita A, Fukumoto H, Shah T, Whelan CM, Irizarry MC, Hyman BT. Demonstration by FRET of BACE interaction with the amyloid precursor protein at the cell surface and in early endosomes. J Cell Sci. 2003 Aug 15;116(Pt 16):3339–46.

174. Mitterreiter S, Page RM, Kamp F, Hopson J, Winkler E, Ha H-R, et al. Bepridil and amiodarone simultaneously target the Alzheimer’s disease beta- and gamma-secretase via distinct mechanisms. J Neurosci Off J Soc Neurosci. 2010 Jun 30;30(26):8974–83.

175. Kuhn P-H, Koroniak K, Hogl S, Colombo A, Zeitschel U, Willem M, et al. Secretome protein enrichment identifies physiological BACE1 protease substrates in neurons. EMBO J. 2012 Jun 22;31(14):3157–68.

176. Savonenko AV, Melnikova T, Laird FM, Stewart K-A, Price DL, Wong PC. Alteration of BACE1-dependent NRG1/ErbB4 signaling and schizophrenia-like phenotypes in BACE1-null mice. Proc Natl Acad Sci U S A. 2008 Apr 8;105(14):5585–90.

177. Hitt BD, Jaramillo TC, Chetkovich DM, Vassar R. BACE1-/- mice exhibit seizure activity that does not correlate with sodium channel level or axonal localization. Mol Neurodegener. 2010 Aug 23;5:31.

178. Laird FM, Cai H, Savonenko AV, Farah MH, He K, Melnikova T, et al. BACE1, a major determinant of selective vulnerability of the brain to amyloid-beta amyloidogenesis, is essential for cognitive, emotional, and synaptic functions. J Neurosci Off J Soc Neurosci. 2005 Dec 14;25(50):11693–709.

179. Filser S, Ovsepian SV, Masana M, Blazquez-Llorca L, Brandt Elvang A, Volbracht C, et al. Pharmacological Inhibition of BACE1 Impairs Synaptic Plasticity and Cognitive Functions. Biol Psychiatry. 2015 Apr;77(8):729–39.

180. Zhu K, Xiang X, Filser S, Marinković P, Dorostkar MM, Crux S, et al. Beta-Site Amyloid Precursor Protein Cleaving Enzyme 1 Inhibition Impairs Synaptic Plasticity via Seizure Protein 6. Biol Psychiatry. 2016 Dec 26;

181. Gunnersen JM, Kim MH, Fuller SJ, De Silva M, Britto JM, Hammond VE, et al. Sez-6 Proteins Affect Dendritic Arborization Patterns and Excitability of Cortical Pyramidal Neurons. Neuron. 2007 Nov;56(4):621–39.

182. Kim DY, Gersbacher MT, Inquimbert P, Kovacs DM. Reduced sodium channel Na(v)1.1 levels in BACE1-null mice. J Biol Chem. 2011 Mar 11;286(10):8106–16.

183. Hu X, Zhou X, He W, Yang J, Xiong W, Wong P, et al. BACE1 deficiency causes altered neuronal activity and neurodegeneration. J Neurosci Off J Soc Neurosci. 2010 Jun 30;30(26):8819–29.

184. Kim DY, Carey BW, Wang H, Ingano LAM, Binshtok AM, Wertz MH, et al. BACE1 regulates voltage-gated sodium channels and neuronal activity. Nat Cell Biol. 2007 Jul;9(7):755–64.

185. Naus S, Richter M, Wildeboer D, Moss M, Schachner M, Bartsch JW. Ectodomain shedding of the neural recognition molecule CHL1 by the metalloprotease-disintegrin ADAM8 promotes neurite outgrowth and suppresses neuronal cell death. J Biol Chem. 2004 Apr 16;279(16):16083–90.

186. Montag-Sallaz M, Schachner M, Montag D. Misguided axonal projections, neural cell adhesion molecule 180 mRNA upregulation, and altered behavior in mice deficient for the close homolog of L1. Mol Cell Biol. 2002 Nov;22(22):7967–81.

187. Heyden A, Angenstein F, Sallaz M, Seidenbecher C, Montag D. Abnormal axonal guidance and brain anatomy in mouse mutants for the cell recognition molecules close homolog of L1 and NgCAM-related cell adhesion molecule. Neuroscience. 2008 Jul 31;155(1):221–33.

188. Hitt B, Riordan SM, Kukreja L, Eimer WA, Rajapaksha TW, Vassar R. β-Site Amyloid Precursor Protein (APP)-cleaving Enzyme 1 (BACE1)-deficient Mice Exhibit a Close Homolog of L1 (CHL1) Loss-of-function Phenotype Involving Axon Guidance Defects. J Biol Chem. 2012 Sep 17;287(46):38408–25.

189. Crusio WE, Schwegler H. Learning spatial orientation tasks in the radial-maze and structural variation in the hippocampus in inbred mice. Behav Brain Funct BBF. 2005 Apr 22;1(1):3.

190. Willem M, Garratt AN, Novak B, Citron M, Kaufmann S, Rittger A, et al. Control of peripheral nerve myelination by the beta-secretase BACE1. Science. 2006 Oct 27;314(5799):664–6.

191. Birchmeier C, Nave K-A. Neuregulin-1, a key axonal signal that drives Schwann cell growth and differentiation. Glia. 2008 Nov 1;56(14):1491–7.

192. Cheret C, Willem M, Fricker FR, Wende H, Wulf-Goldenberg A, Tahirovic S, et al. Bace1 and Neuregulin-1 cooperate to control formation and maintenance of muscle spindles. EMBO J. 2013 Jul 17;32(14):2015–28.

193. Deng M, He W, Tan Y, Han H, Hu X, Xia K, et al. Increased Expression of Reticulon 3 in Neurons Leads to Reduced Axonal Transport of β Site Amyloid Precursor Protein-cleaving Enzyme 1. J Biol Chem. 2013 Oct 18;288(42):30236–45.

194. Zhao J, Fu Y, Yasvoina M, Shao P, Hitt B, O'Connor T, et al. Beta-site amyloid precursor protein cleaving enzyme 1 levels become elevated in neurons around amyloid plaques: implications for Alzheimer's disease pathogenesis. J Neurosci Off J Soc Neurosci. 2007 Apr 4;27(14):3639–49.

195. Fukumoto H, Cheung BS, Hyman BT, Irizarry MC. Beta-secretase protein and activity are increased in the neocortex in Alzheimer disease. Arch Neurol. 2002 Sep;59(9):1381–9.

196. Fukumoto H, Rosene DL, Moss MB, Raju S, Hyman BT, Irizarry MC. Beta-secretase activity increases with aging in human, monkey, and mouse brain. Am J Pathol. 2004 Feb;164(2):719–25.

197. Holsinger RMD, McLean CA, Beyreuther K, Masters CL, Evin G. Increased expression of the amyloid precursor beta-secretase in Alzheimer's disease. Ann Neurol. 2002 Jun;51(6):783–6.

198. Li R, Lindholm K, Yang L-B, Yue X, Citron M, Yan R, et al. Amyloid beta peptide load is correlated with increased beta-secretase activity in sporadic Alzheimer's disease patients. Proc Natl Acad Sci U S A. 2004 Mar 9;101(10):3632–7.

199. Tyler SJ, Dawbarn D, Wilcock GK, Allen SJ. alpha- and beta-secretase: profound changes in Alzheimer's disease. Biochem Biophys Res Commun. 2002 Dec 6;299(3):373–6.

200. Yang L-B, Lindholm K, Yan R, Citron M, Xia W, Yang X-L, et al. Elevated beta-secretase expression and enzymatic activity detected in sporadic Alzheimer disease. Nat Med. 2003 Jan;9(1):3–4.

201. Tesco G, Koh YH, Kang EL, Cameron AN, Das S, Sena-Esteves M, et al. Depletion of GGA3 stabilizes BACE and enhances beta-secretase activity. Neuron. 2007 Jun 7;54(5):721–37.

202. Kang EL, Cameron AN, Piazza F, Walker KR, Tesco G. Ubiquitin regulates GGA3-mediated degradation of BACE1. J Biol Chem. 2010 Jul 30;285(31):24108–19.

203. Torres M, Jimenez S, Sanchez-Varo R, Navarro V, Trujillo-Estrada L, Sanchez-Mejias E, et al. Defective lysosomal proteolysis and axonal transport are early pathogenic events that worsen with age leading to increased APP metabolism and synaptic Abeta in transgenic APP/PS1 hippocampus. Mol Neurodegener. 2012;7:59.

204. Knopman DS. Mediterranean diet and late-life cognitive impairment: a taste of benefit. JAMA. 2009 Aug 12;302(6):686–7.

205. Lazarov O, Robinson J, Tang Y-P, Hairston IS, Korade-Mirnics Z, Lee VM-Y, et al. Environmental enrichment reduces Abeta levels and amyloid deposition in transgenic mice. Cell. 2005 Mar 11;120(5):701–13.

206. Hung AY, Haass C, Nitsch RM, Qiu WQ, Citron M, Wurtman RJ, et al. Activation of protein kinase C inhibits cellular production of the amyloid beta-protein. J Biol Chem. 1993 Nov 5;268(31):22959–62.

207. Skovronsky DM, Moore DB, Milla ME, Doms RW, Lee VM. Protein kinase C-dependent alpha-secretase competes with beta-secretase for cleavage of amyloid-beta precursor protein in the trans-golgi network. J Biol Chem. 2000 Jan 28;275(4):2568–75.

208. Hartmann D, de Strooper B, Serneels L, Craessaerts K, Herreman A, Annaert W, et al. The disintegrin/metalloprotease ADAM 10 is essential for Notch signalling but not for alpha-secretase activity in fibroblasts. Hum Mol Genet. 2002 Oct 1;11(21):2615–24.

209. Abramowski D, Wiederhold K-H, Furrer U, Jaton A-L, Neuenschwander A, Runser M-J, et al. Dynamics of Abeta turnover and deposition in different beta-amyloid precursor protein transgenic mouse models following gamma-secretase inhibition. J Pharmacol Exp Ther. 2008 Nov;327(2):411–24.

210. Bateman RJ, Siemers ER, Mawuenyega KG, Wen G, Browning KR, Sigurdson WC, et al. A gamma-secretase inhibitor decreases amyloid-beta production in the central nervous system. Ann Neurol. 2009 Jul;66(1):48–54.

211. Dovey HF, John V, Anderson JP, Chen LZ, de Saint Andrieu P, Fang LY, et al. Functional gamma-secretase inhibitors reduce beta-amyloid peptide levels in brain. J Neurochem. 2001 Jan;76(1):173–81.

212. Siemers ER, Dean RA, Friedrich S, Ferguson-Sells L, Gonzales C, Farlow MR, et al. Safety, tolerability, and effects on plasma and cerebrospinal fluid amyloid-beta after inhibition of gamma-secretase. Clin Neuropharmacol. 2007 Dec;30(6):317–25.

213. De Strooper B, Annaert W, Cupers P, Saftig P, Craessaerts K, Mumm JS, et al. A presenilin-1-dependent gamma-secretase-like protease mediates release of Notch intracellular domain. Nature. 1999 Apr 8;398(6727):518–22.

214. Shen J, Bronson RT, Chen DF, Xia W, Selkoe DJ, Tonegawa S. Skeletal and CNS defects in Presenilin-1-deficient mice. Cell. 1997 May 16;89(4):629–39.

215. Wong PC, Zheng H, Chen H, Becher MW, Sirinathsinghji DJ, Trumbauer ME, et al. Presenilin 1 is required for Notch1 and Dll1 expression in the paraxial mesoderm. Nature. 1997 May 15;387(6630):288–92.

216. Kukar T, Golde TE. Possible mechanisms of action of NSAIDs and related compounds that modulate gamma-secretase cleavage. Curr Top Med Chem. 2008;8(1):47–53.

217. Weggen S, Eriksen JL, Das P, Sagi SA, Wang R, Pietrzik CU, et al. A subset of NSAIDs lower amyloidogenic Abeta42 independently of cyclooxygenase activity. Nature. 2001 Nov 8;414(6860):212–6.

218. Green RC, Schneider LS, Amato DA, Beelen AP, Wilcock G, Swabb EA, et al. Effect of tarenflurbil on cognitive decline and activities of daily living in patients with mild Alzheimer disease: a randomized controlled trial. JAMA. 2009 Dec 16;302(23):2557–64.

219. Jonsson T, Atwal JK, Steinberg S, Snaedal J, Jonsson PV, Bjornsson S, et al. A mutation in APP protects against Alzheimer's disease and age-related cognitive decline. Nature. 2012 Aug 2;488(7409):96–9.

220. Laird FM, Cai H, Savonenko AV, Farah MH, He K, Melnikova T, et al. BACE1, a major determinant of selective vulnerability of the brain to amyloid-beta amyloidogenesis, is essential for cognitive, emotional, and synaptic functions. J Neurosci Off J Soc Neurosci. 2005 Dec 14;25(50):11693–709.

221. Ohno M, Sametsky EA, Younkin LH, Oakley H, Younkin SG, Citron M, et al. BACE1 deficiency rescues memory deficits and cholinergic dysfunction in a mouse model of Alzheimer's disease. Neuron. 2004 Jan 8;41(1):27–33.

222. Luo Y, Bolon B, Kahn S, Bennett BD, Babu-Khan S, Denis P, et al. Mice deficient in BACE1, the Alzheimer's beta-secretase, have normal phenotype and abolished beta-amyloid generation. Nat Neurosci. 2001 Mar;4(3):231–2.

223. Hong L, Turner RT, Koelsch G, Shin D, Ghosh AK, Tang J. Crystal structure of memapsin 2 (beta-secretase) in complex with an inhibitor OM00-3. Biochemistry (Mosc). 2002 Sep 10;41(36):10963–7.

224. May PC, Dean RA, Lowe SL, Martenyi F, Sheehan SM, Boggs LN, et al. Robust central reduction of amyloid-β in humans with an orally available, non-peptidic β-secretase inhibitor. J Neurosci Off J Soc Neurosci. 2011 Nov 16;31(46):16507–16.

225. May PC, Dean RA, Lowe SL, Martenyi F, Sheehan SM, Boggs LN, et al. Robust central reduction of amyloid-β in humans with an orally available, non-peptidic β-secretase inhibitor. J Neurosci Off J Soc Neurosci. 2011 Nov 16;31(46):16507–16.

226. Wang H, Li R, Shen Y. β-Secretase: its biology as a therapeutic target in diseases. Trends Pharmacol Sci. 2013 Apr;34(4):215–25.

227. Yan R, Vassar R. Targeting the β secretase BACE1 for Alzheimer's disease therapy. Lancet Neurol. 2014 Mar;13(3):319–29.

228. Yuan J, Venkatraman S, Zheng Y, McKeever BM, Dillard LW, Singh SB. Structure-based design of β-site APP cleaving enzyme 1 (BACE1) inhibitors for the treatment of Alzheimer's disease. J Med Chem. 2013 Jun 13;56(11):4156–80.

229. May PC, Willis BA, Lowe SL, Dean RA, Monk SA, Cocke PJ, et al. The potent BACE1 inhibitor LY2886721 elicits robust central Aβ pharmacodynamic responses in mice, dogs, and humans. J Neurosci Off J Soc Neurosci. 2015 Jan 21;35(3):1199–210.

230. Kennedy ME, Stamford AW, Chen X, Cox K, Cumming JN, Dockendorf MF, et al. The BACE1 inhibitor verubecestat (MK-8931) reduces CNS β-amyloid in animal models and in Alzheimer's disease patients. Sci Transl Med. 2016 Nov 2;8(363):363ra150-363ra150.

231. Bacioglu M, Maia LF, Preische O, Schelle J, Apel A, Kaeser SA, et al. Neurofilament Light Chain in Blood and CSF as Marker of Disease Progression in Mouse Models and in Neurodegenerative Diseases. Neuron. 2016 Jun 9;

232. Jacobsen H, Ozmen L, Caruso A, Narquizian R, Hilpert H, Jacobsen B, et al. Combined Treatment with a BACE Inhibitor and Anti-Aβ Antibody Gantenerumab Enhances Amyloid Reduction in APPLondon Mice. J Neurosci. 2014 Aug 27;34(35):11621–30.

233. Neumann U, Rueeger H, Machauer R, Veenstra SJ, Lueoend RM, Tintelnot-Blomley M, et al. A novel BACE inhibitor NB-360 shows a superior pharmacological profile and robust reduction of amyloid-β and neuroinflammation in APP transgenic mice. Mol Neurodegener [Internet]. 2015 Dec [cited 2016 Apr 11];10(1). Available from: http://www.molecularneurodegeneration.com/content/10/1/44

234. Thakker DR, Sankaranarayanan S, Weatherspoon MR, Harrison J, Pierdomenico M, Heisel JM, et al. Centrally Delivered BACE1 Inhibitor Activates Microglia, and Reverses Amyloid Pathology and Cognitive Deficit in Aged Tg2576 Mice. J Neurosci. 2015 Apr 29;35(17):6931–6.

235. Tarawneh R, Holtzman DM. The clinical problem of symptomatic Alzheimer disease and mild cognitive impairment. Cold Spring Harb Perspect Med. 2012 May;2(5):a006148.

236. Hsiao K, Chapman P, Nilsen S, Eckman C, Harigaya Y, Younkin S, et al. Correlative memory deficits, Abeta elevation, and amyloid plaques in transgenic mice. Science. 1996 Oct 4;274(5284):99–102.

237. Villemagne VL, Burnham S, Bourgeat P, Brown B, Ellis KA, Salvado O, et al. Amyloid β deposition, neurodegeneration, and cognitive decline in sporadic Alzheimer's disease: a prospective cohort study. Lancet Neurol. 2013 Apr;12(4):357–67.

238. Yau W-YW, Tudorascu DL, McDade EM, Ikonomovic S, James JA, Minhas D, et al. Longitudinal assessment of neuroimaging and clinical markers in autosomal dominant Alzheimer's disease: a prospective cohort study. Lancet Neurol. 2015 Aug;14(8):804–13.

239. Selkoe DJ. Resolving controversies on the path to Alzheimer's therapeutics. Nat Med. 2011 Sep;17(9):1060–5.

240. Callaway E. Alzheimer’s drugs take a new tack. Nature. 2012 Sep 6;489(7414):13–4.

241. Garber K. Genentech’s Alzheimer’s antibody trial to study disease prevention. Nat Biotechnol. 2012 Aug;30(8):731–2.

242. Mullard A. Sting of Alzheimer’s failures offset by upcoming prevention trials. Nat Rev Drug Discov. 2012 Sep;11(9):657–60.

243. Dominguez D, Tournoy J, Hartmann D, Huth T, Cryns K, Deforce S, et al. Phenotypic and biochemical analyses of BACE1- and BACE2-deficient mice. J Biol Chem. 2005 Sep 2;280(35):30797–806.

244. Cai J, Qi X, Kociok N, Skosyrski S, Emilio A, Ruan Q, et al. β-Secretase (BACE1) inhibition causes retinal pathology by vascular dysregulation and accumulation of age pigment. EMBO Mol Med. 2012 Sep;4(9):980–91.

245. Ohno M, Cole SL, Yasvoina M, Zhao J, Citron M, Berry R, et al. BACE1 gene deletion prevents neuron loss and memory deficits in 5XFAD APP/PS1 transgenic mice. Neurobiol Dis. 2007 Apr;26(1):134–45.

246. Hu X, Hicks CW, He W, Wong P, Macklin WB, Trapp BD, et al. Bace1 modulates myelination in the central and peripheral nervous system. Nat Neurosci. 2006 Dec;9(12):1520–5.

247. Willem M, Garratt AN, Novak B, Citron M, Kaufmann S, Rittger A, et al. Control of peripheral nerve myelination by the beta-secretase BACE1. Science. 2006 Oct 27;314(5799):664–6.

248. Hitt BD, Jaramillo TC, Chetkovich DM, Vassar R. BACE1-/- mice exhibit seizure activity that does not correlate with sodium channel level or axonal localization. Mol Neurodegener. 2010;5:31.

249. Hu X, Zhou X, He W, Yang J, Xiong W, Wong P, et al. BACE1 deficiency causes altered neuronal activity and neurodegeneration. J Neurosci Off J Soc Neurosci. 2010 Jun 30;30(26):8819–29.

250. Kobayashi D, Zeller M, Cole T, Buttini M, McConlogue L, Sinha S, et al. BACE1 gene deletion: impact on behavioral function in a model of Alzheimer’s disease. Neurobiol Aging. 2008 Jun;29(6):861–73.

251. Cao L, Rickenbacher GT, Rodriguez S, Moulia TW, Albers MW. The precision of axon targeting of mouse olfactory sensory neurons requires the BACE1 protease. Sci Rep [Internet]. 2012 Jan 20 [cited 2014 Jan 20];2. Available from: http://www.nature.com/doifinder/10.1038/srep00231

252. Hitt B, Riordan SM, Kukreja L, Eimer WA, Rajapaksha TW, Vassar R. β-Site amyloid precursor protein (APP)-cleaving enzyme 1 (BACE1)-deficient mice exhibit a close homolog of L1 (CHL1) loss-of-function phenotype involving axon guidance defects. J Biol Chem. 2012 Nov 9;287(46):38408–25.

253. Rajapaksha TW, Eimer WA, Bozza TC, Vassar R. The Alzheimer's β-secretase enzyme BACE1 is required for accurate axon guidance of olfactory sensory neurons and normal glomerulus formation in the olfactory bulb. Mol Neurodegener. 2011;6:88.

254. Savonenko AV, Melnikova T, Laird FM, Stewart K-A, Price DL, Wong PC. Alteration of BACE1-dependent NRG1/ErbB4 signaling and schizophrenia-like phenotypes in BACE1-null mice. Proc Natl Acad Sci U S A. 2008 Apr 8;105(14):5585–90.

255. Salzer JL. Axonal regulation of Schwann cell ensheathment and myelination. J Peripher Nerv Syst JPNS. 2012 Dec;17 Suppl 3:14–9.

256. McConlogue L, Buttini M, Anderson JP, Brigham EF, Chen KS, Freedman SB, et al. Partial reduction of BACE1 has dramatic effects on Alzheimer plaque and synaptic pathology in APP Transgenic Mice. J Biol Chem. 2007 Sep 7;282(36):26326–34.

257. Kasthuri N, Hayworth KJ, Berger DR, Schalek RL, Conchello JA, Knowles-Barley S, et al. Saturated Reconstruction of a Volume of Neocortex. Cell. 2015 Jul 30;162(3):648–61.

258. Köhler A. Mikrophotographische Untersuchungen mit ultraviolettem Licht. 1904;21:129-165; 273-304.

259. Stokes GG. On the Change of Refrangibility of Light. Philos Trans R Soc Lond. 1852 Jan 1;142:463–562.

260. Jablonski A. Uber den Mechanismus der Photolumineszenz von Farbstoffphosphoren. Z Phys. 1935;94:38–44.

261. Jablonski A. Efficiency of anti-Stokes fluorescence in dyes. 1933;131:839–40.

262. Chance B, Cohen P, Jobsis F, Schoener B. Intracellular oxidation-reduction states in vivo. Science. 1962 Aug 17;137(3529):499–508.

263. Shibuki K, Hishida R, Murakami H, Kudoh M, Kawaguchi T, Watanabe M, et al. Dynamic imaging of somatosensory cortical activity in the rat visualized by flavoprotein autofluorescence. J Physiol. 2003 Jun 15;549(Pt 3):919–27.

264. Shimomura O, Johnson FH, Saiga Y. Extraction, purification and properties of aequorin, a bioluminescent protein from the luminous hydromedusan, Aequorea. J Cell Comp Physiol. 1962 Jun;59:223–39.

265. Prasher DC, Eckenrode VK, Ward WW, Prendergast FG, Cormier MJ. Primary structure of the Aequorea victoria green-fluorescent protein. Gene. 1992 Feb 15;111(2):229–33.

266. Chalfie M, Tu Y, Euskirchen G, Ward WW, Prasher DC. Green fluorescent protein as a marker for gene expression. Science. 1994 Feb 11;263(5148):802–5.

267. Inouye S, Tsuji FI. Aequorea green fluorescent protein. Expression of the gene and fluorescence characteristics of the recombinant protein. FEBS Lett. 1994 Mar 21;341(2–3):277–80.

268. Chudakov DM, Matz MV, Lukyanov S, Lukyanov KA. Fluorescent proteins and their applications in imaging living cells and tissues. Physiol Rev. 2010 Jul;90(3):1103–63.

269. Feng G, Mellor RH, Bernstein M, Keller-Peck C, Nguyen QT, Wallace M, et al. Imaging neuronal subsets in transgenic mice expressing multiple spectral variants of GFP. Neuron. 2000 Oct;28(1):41–51.

270. Jacques SL. Optical properties of biological tissues: a review. Phys Med Biol. 2013 Jun 7;58(11):R37-61.

271. Denk W, Strickler JH, Webb WW. Two-photon laser scanning fluorescence microscopy. Science. 1990 Apr 6;248(4951):73–6.

272. Göppert-Mayer M. Über Elementarakte mit zwei Quantensprüngen. Ann Phys. 1931 Jan 1;401(3):273–94.

273. Drobizhev M, Makarov NS, Tillo SE, Hughes TE, Rebane A. Two-photon absorption properties of fluorescent proteins. Nat Methods. 2011 Apr 28;8(5):393–9.

274. Helmchen F, Denk W. Deep tissue two-photon microscopy. Nat Methods. 2005 Dec;2(12):932–40.

275. Yang G, Pan F, Parkhurst CN, Grutzendler J, Gan W-B. Thinned-skull cranial window technique for long-term imaging of the cortex in live mice. Nat Protoc. 2010 Feb;5(2):201–8.

276. Holtmaat A, Bonhoeffer T, Chow DK, Chuckowree J, De Paola V, Hofer SB, et al. Long-term, high-resolution imaging in the mouse neocortex through a chronic cranial window. Nat Protoc. 2009;4(8):1128–44.

277. Burgold S, Filser S, Dorostkar MM, Schmidt B, Herms J. In vivo imaging reveals sigmoidal growth kinetic of β-amyloid plaques. Acta Neuropathol Commun. 2014;2(1):1.

278. Takamori S, Holt M, Stenius K, Lemke EA, Grønborg M, Riedel D, et al. Molecular Anatomy of a Trafficking Organelle. Cell. 2006 Nov 17;127(4):831–46.

279. Hefendehl JK, Wegenast-Braun BM, Liebig C, Eicke D, Milford D, Calhoun ME, et al. Long-Term In Vivo Imaging of -Amyloid Plaque Appearance and Growth in a Mouse Model of Cerebral -Amyloidosis. J Neurosci. 2011 Jan 12;31(2):624–9.

280. Harper JD, Lansbury PT. Models of amyloid seeding in Alzheimer's disease and scrapie: mechanistic truths and physiological consequences of the time-dependent solubility of amyloid proteins. Annu Rev Biochem. 1997;66:385–407.

281. Hellstrand E, Boland B, Walsh DM, Linse S. Amyloid β-protein aggregation produces highly reproducible kinetic data and occurs by a two-phase process. ACS Chem Neurosci. 2010 Jan 20;1(1):13–8.

282. Jarrett JT, Lansbury PT. Seeding “one-dimensional crystallization” of amyloid: a pathogenic mechanism in Alzheimer’s disease and scrapie? Cell. 1993 Jun 18;73(6):1055–8.

283. Bittner T, Burgold S, Dorostkar MM, Fuhrmann M, Wegenast-Braun BM, Schmidt B, et al. Amyloid plaque formation precedes dendritic spine loss. Acta Neuropathol (Berl). 2012 Sep 21;124(6):797–807.

284. Burgold S, Bittner T, Dorostkar MM, Kieser D, Fuhrmann M, Mitteregger G, et al. In vivo multiphoton imaging reveals gradual growth of newborn amyloid plaques over weeks. Acta Neuropathol (Berl). 2010 Dec 7;121(3):327–35.

285. Yan P, Bero AW, Cirrito JR, Xiao Q, Hu X, Wang Y, et al. Characterizing the appearance and growth of amyloid plaques in APP/PS1 mice. J Neurosci Off J Soc Neurosci. 2009 Aug 26;29(34):10706–14.

286. Fuhrmann M, Bittner T, Jung CKE, Burgold S, Page RM, Mitteregger G, et al. Microglial Cx3cr1 knockout prevents neuron loss in a mouse model of Alzheimer’s disease. Nat Neurosci. 2010 Apr 1;13(4):411–3.

287. Jung CKE, Keppler K, Steinbach S, Blazquez-Llorca L, Herms J. Fibrillar amyloid plaque formation precedes microglial activation. PloS One. 2015;10(3):e0119768.

288. Adalbert R, Nogradi A, Babetto E, Janeckova L, Walker SA, Kerschensteiner M, et al. Severely dystrophic axons at amyloid plaques remain continuous and connected to viable cell bodies. Brain. 2008 Jun 20;132(2):402–16.

289. Selkoe DJ. Alzheimer’s disease is a synaptic failure. Science. 2002 Oct 25;298(5594):789–91.

290. Cheret C, Willem M, Fricker FR, Wende H, Wulf-Goldenberg A, Tahirovic S, et al. Bace1 and Neuregulin-1 cooperate to control formation and maintenance of muscle spindles. EMBO J. 2013 Jul 17;32(14):2015–28.

291. Meyer-Luehmann M, Stalder M, Herzig MC, Kaeser SA, Kohler E, Pfeifer M, et al. Extracellular amyloid formation and associated pathology in neural grafts. Nat Neurosci. 2003 Apr;6(4):370–7.

292. Meyer-Luehmann M, Coomaraswamy J, Bolmont T, Kaeser S, Schaefer C, Kilger E, et al. Exogenous induction of cerebral beta-amyloidogenesis is governed by agent and host. Science. 2006 Sep 22;313(5794):1781–4.

293. Das P, Verbeeck C, Minter L, Chakrabarty P, Felsenstein K, Kukar T, et al. Transient pharmacologic lowering of Aβ production prior to deposition results in sustained reduction of amyloid plaque pathology. Mol Neurodegener. 2012 Aug 14;7:39.

294. McCarter JF, Liebscher S, Bachhuber T, Abou-Ajram C, Hübener M, Hyman BT, et al. Clustering of plaques contributes to plaque growth in a mouse model of Alzheimer's disease. Acta Neuropathol (Berl). 2013 Aug;126(2):179–88.

295. Suárez-Calvet M, Araque Caballero MÁ, Kleinberger G, Bateman RJ, Fagan AM, Morris JC, et al. Early changes in CSF sTREM2 in dominantly inherited Alzheimer's disease occur after amyloid deposition and neuronal injury. Sci Transl Med. 2016 Dec 14;8(369):369ra178.

296. Kuhn P-H, Koroniak K, Hogl S, Colombo A, Zeitschel U, Willem M, et al. Secretome protein enrichment identifies physiological BACE1 protease substrates in neurons. EMBO J. 2012 Jun 22;31(14):3157–68.

297. Blazquez-Llorca L, Valero-Freitag S, Rodrigues EF, Merchán-Pérez Á, Rodríguez JR, Dorostkar MM, et al. High plasticity of axonal pathology in Alzheimer's disease mouse models. Acta Neuropathol Commun. 2017 Feb 7;5(1):14.

298. Fuhrmann M, Mitteregger G, Kretzschmar H, Herms J. Dendritic pathology in prion disease starts at the synaptic spine. J Neurosci Off J Soc Neurosci. 2007 Jun 6;27(23):6224–33.

299. Holtmaat A, Bonhoeffer T, Chow DK, Chuckowree J, De Paola V, Hofer SB, et al. Long-term, high-resolution imaging in the mouse neocortex through a chronic cranial window. Nat Protoc. 2009;4(8):1128–44.

300. Bacioglu M, Maia LF, Preische O, Schelle J, Apel A, Kaeser SA, et al. Neurofilament Light Chain in Blood and CSF as Marker of Disease Progression in Mouse Models and in Neurodegenerative Diseases. Neuron. 2016 Jul 6;91(1):56–66.

301. Klunk WE, Bacskai BJ, Mathis CA, Kajdasz ST, McLellan ME, Frosch MP, et al. Imaging Abeta plaques in living transgenic mice with multiphoton microscopy and methoxy-X04, a systemically administered Congo red derivative. J Neuropathol Exp Neurol. 2002 Sep;61(9):797–805.

8. Abbreviations

°C	degree celcius
µg	microgram
µL	microliter
µm	micrometer
Aβ	amyloid-β peptide
AD	Alzheimer's disease
ADAM10	a disintegrin and metalloproteinase domain-containing protein 10
AICD	amyloid precursor protein intracellular domain
ANOVA	analysis of variance
ApoE4	Apolipoprotein E4
APP	amyloid precurser protein
BACE1	Beta site amyloid precursor protein cleaving enzyme 1
CHL1	close homolog of L1
CNS	central nervous system
3D	three-dimensional
et al.	and others
GFP	green fluorescent protein
h	hour
Hz	Hertz
i.p.	intraperitoneal
kg	kilogramm
LSM	laser scanning microscope
LTP	long-term potentiation
M	molar
MAP	mitogen-activated protein
mg	milligram
min	minute
mL	milliliter

MRI	magnetic resonance imaging
NADH	nicotinamide adenine dinucleotide
NMDA	N-Methyl-D-Aspartat
2P	two-photon
PBS	phosphate buffered saline
PFA	paraformaldehyde
ROI	region of interest
s	second
SEM	standard error of the mean
Sez-6	seizure-related gene 6
Thy1	thymocyte antigen 1; CD90
TWA	two-way ANOVA
VGLUT1	vesicular glutamate transporter 1
W	watt
WT	wild type

9. Curriculum Vitae

Name	Finn Peters
Address	Feodor-Lynen-Str. 17, 81377 Munich, Germany
Date of birth	09.01.1983
E-Mail	finn.peters@med.uni-muenchen.de

Professional Academic Experience

2012-2017	**PhD student** at the German Center for Neurodegenerative Diseases (DZNE), Munich, Germany. **Doctoral thesis**: ‘Pharmacological BACE1 inhibitor treatment during early progression of β-amyloid pathology maximizes therapeutic efficacy‘; Prof. Jochen Herms, Ludwig-Maximilians University Munich, Germany.
2010-2012	**Research assistant**: Prof. Peter Seeburg, MPI for medical research, Department of Neurobiology, Heidelberg, Germany.

Academic Education

2006-2010	**Diploma**: ’Biochemistry’, Free University of Berlin, Germany. **Diploma thesis**: ‘Analysis of neuronal effector proteins of Drosophila Rab5 and Rab11‘; Prof. Claudia Miech and Prof. Volker Haucke, Institute for Chemistry and Biochemistry, Free University of Berlin, Germany.

2005-2006	**Bachelor of Science**: ’Biochemistry’, Université Denis Diderot, Paris, France.
2003-2005	**Intermediate diploma**: ’Biochemistry’, University Hamburg, Germany.

Civile Service

2002-2003	Young Men's Christian Association (YMCA), Hamburg, Germany.

School Education

2002	Secondary school leaving examination (’Abitur’), Max Brauer Schule, Hamburg, Germany.

IT Skills

Graphing	GraphPad Prism, Adobe Illustrator
Imaging	ZEN (advanced), Imaris (advanced)
Presentation	MS Office (advanced), Adobe Indesign (advanced)
Coding	Matlab (advanced), Igor Pro, Visual Basic

Languages

German	Native language
English	Fluent
French	Good working knowledge

Professional Training

06.2010	Course in Basics of Laboratory Animal Science according to FELASA (Category B), University Heidelberg, Deutschland.

Teaching

04.2010 **Teaching assistant:** ‘*In vivo* two-photon imaging‘,German Center for Neurodegenerative Diseases (DZNE), Munich, Germany.

2008 **Teaching assistant:** ‘*Introductory course Biochemistry*‘,Institute for Chemistry and Biochemistry, Free University of Berlin, Germany.

Congress Participation

2017 **Oral presentation**: ‘Pharmacological inhibition of BACE1 reduces amyloid and presynaptic pathology in transgenic Alzheimer mice.‘ Alzheimer’s & Parkinson’s Diseases Congress - AD/PDTM, 2017, Vienna, Austria.

2016 **Poster presentation**: ‘Pharmacological inhibition of BACE1 reduces amyloid and presynaptic pathology in transgenic Alzheimer mice.‘ Kloster Seeon meeting on BACE proteases in health and disease, near Munich, Germany.

2013 **Oral presentation**: ‘Long-term in vivo imaging of presynaptic pathology in transgenic Alzheimer mice.‘ SfN annual meeting, 2013, San Diego, USA.

Congress Hosting

2012 ‘2nd Heidelberg Forum For Young Life Scientists‘, Heidelberg, Germany.

Children

2016	Jan Lion Asmussen, Munich, Germany.
2013	Max Anders Asmussen, Munich, Germany.

10. List of Publications

1. M. Brendel, C. Focke, T. Blume, **F. Peters**, M. Deussing, F. Probst, A. Jaworska, F. Overhoff, N. Albert, S. Lindner, B. von Ungern-Sternberg, P. Bartenstein, C. Haass, G. Kleinberger, J. Herms, A. Rominger, Time Courses of Cortical Glucose Metabolism and Microglial Activity Across the Life-Span of Wild-Type Mice: A PET Study, *J. Nucl. Med. Off. Publ. Soc. Nucl. Med.* (2017), doi:10.2967/jnumed.117.195107.

2. S. Blumenstock, E. F. Rodrigues, **F. Peters**, L. Blazquez-Llorca, F. Schmidt, A. Giese, J. Herms, Seeding and transgenic overexpression of alpha-synuclein triggers dendritic spine pathology in the neocortex, *EMBO Mol. Med.* **9**, 716–731 (2017).

3. C. Zou, E. Montagna, Y. Shi, **F. Peters**, L. Blazquez-Llorca, S. Shi, S. Filser, M. M. Dorostkar, J. Herms, Intraneuronal APP and extracellular Aβ independently cause dendritic spine pathology in transgenic mouse models of Alzheimer's disease, *Acta Neuropathol. (Berl.)* **129**, 909–920 (2015).

Manuscripts in preparation

Peters F, Rodrigues E, Salihoglu H, Herzog E, Blume T, Filser S, Dorostkar M, Shimshek D, Brose N, Neumann U, Herms J. " Pharmacological BACE1 inhibitor treatment during early progression of β amyloid pathology maximizes therapeutic efficacy."

Marinković P, Blumenstock S, Goldstein P, Korzhova V, Knebl A, **Peters F**, Stancu IC, Dewachter I and Herms J. "In vivo imaging reveals reduced activity of neuronal cicuits in the mouse tauopathy model."

Blumenstock S, Angelo MF, **Peters F**, Crux S, Herzog E and Herms J. “Local synaptic translation is reduced in tissue overexpressing alpha-synuclein. Blumenstock S, Marinković P, Goldstein P, Korzhova V, Peters F, Sun F, Sgobio C and Herms J.”

Rodrigues E, **Peters F**, Blazquez-Llorca L, Shimshek D, Neumann U, Herms J. “BACE1 inhibitor treatment rescues β-amyloid plaque associated axonal pathology.”

Salihoglu H, **Peters F**, Rodrigues E, Herzog E, Blume T, Filser S, Dorostkar M, Shimshek D, Brose N, Neumann U, Herms J. “Partial reduction of tau reduces alzheimer plaque in APP transgenic mice.”

11. Acknowledgements

I would like to thank Prof. Jochen Herms, for his continous support of this project, his confidential supervision and many critical discussions. I particularly want to acknowledge the trustful working atmosphere that allowed me to raise two children during the doctoral thesis.

Furthermore, I want to cordially thank Prof. Rainer Uhl who readily agreed to represent this dissertation at the faculty for biology. Special thanks also to Prof. Anja Horn-Bochtler for her interest in this work and the time and effort for preparing the second assessment of this dissertation.

During my doctoral thesis I had the possibility to collaborate with many distinguished scientists. I want to emphasize the collaboration with Novartis and would like to thank Dr. Ulf Neumann for the excellent collaborative work. I want to thank Dr. Severin Filser for his tremendous help on the manuscript, scientific advice and many years of friendship. I am very grateful to Hazal Salihoglu and Tanja Blume who contributed valuable experimental data to finish the project and to Dr. Etienne Herzog and Prof. Nils Brose for allowing me to work with their VGLUT1$^{\text{Venus}}$ mouse model.

I also would like to thank Dr. Steffen Burgold and Dr. Carmelo Sgobio for their scientific advice and all people who proof-read this dissertation, in particular my friend Dr. Wilhelm Ching. I furthermore want to acknowledge the excellent technical support provided by Nadine Hoffmann, Eric Grießinger, Sarah Hanselka, Katharina Bayer and Sonja Steinbach, and I thank all collegues from the animal facility for their commitment and help. For the enjoyable atmoshpere

in the lab I want to thank all current and former colleagues from the ZNP and the AG Herms.

I dedicate this work to my wife Marie Asmussen who always encouraged me in my scientific work. Thank you for two wonderful children!